

A sub-millimeter Mapping Survey of Herbig AeBe Stars

Göran Sandell¹, David A. Weintraub²,

and

Murad Hamidouche¹

Goran.H.Sandell@nasa.gov

mhamidouche@sofia.usra.edu

david.a.weintraub@vanderbilt.edu

ABSTRACT

We have acquired sub-millimeter observations of 33 fields containing 37 Herbig Ae/Be (HAEBE) stars or potential HAEBE stars, including SCUBA maps of all but two of these stars. Nine target stars show extended dust emission. The other 18 are unresolved, suggesting that the dust envelopes or disks around these stars are less than a few arcseconds in angular size. In several cases we find that the strongest sub-millimeter emission originates from younger, heavily embedded sources rather than from the HAEBE star, which means that previous models must be viewed with caution. These new data, in combination with far-infrared flux measurements available in the literature, yield SEDs from far-infrared to millimeter wavelengths for all the observed objects. Isothermal fits to these SEDs demonstrate excellent fits, in most cases, to the flux densities longward of 100 μm . We find that a smaller proportion of B-type stars than A and F-type stars are surrounded by circumstellar disks, suggesting that disks around B stars dissipate on shorter time scales than those around later spectral types. Our models also reveal that the mass of the circumstellar material and the value of β are correlated, with low masses corresponding to low values of β . Since low

¹ SOFIA-USRA, NASA Ames Research Center, Mail Stop N211-3, Building N211/Rm. 249, Moffett Field, CA 94035, U.S.A.

²Department of Physics & Astronomy, Vanderbilt University, P.O. Box 1807 Station B, Nashville, TN 37235, U.S.A.

values of β imply large grain sizes, our results suggest that a large fraction of the mass in low-beta sources is locked up in very large grains. Several of the isolated HAEBE stars have disks with very flat sub-millimeter SEDs. These disks may be on the verge of forming planetary systems.

Subject headings: ISM: clouds – (Stars:) circumstellar matter – Stars:formation – Stars: pre-main sequence – Stars: variables: T Tauri, Herbig Ae/Be – Submillimeter: stars

1. Introduction

Herbig Ae/Be (HAEBE) stars are very young, intermediate mass ($2 - 8 M_{\odot}$) pre-main-sequence stars (Herbig 1960; Strom et al. 1972; Finkenzeller & Mundt 1984; Hillenbrand et al. 1992; Thé, de Winter and Pérez 1994). Since Herbig first established criteria for membership in this class, our understanding and consequently our classification rules for HAEBE stars have changed somewhat to include some stars of slightly later spectral class and others that do not illuminate reflection nebulae, including "isolated" HAEBE stars. At visible wavelengths, spectra of HAEBE stars often include broad emission lines that show rapid variability while at longer wavelengths HAEBE stars often are associated with infrared and far-infrared excesses and millimeter wavelength line emission. These properties are very strongly associated with circumstellar gas and dust at a wide range of temperatures. Most workers in the field now accept that the bulk of the circumstellar gas and dust around many, if not most of these stars, is found in fairly massive ($\sim 0.01 M_{\odot}$) circumstellar disks (Hamidouche et al. 2006; Eisner et al. 2003; Meeus et al. 2001; Natta et al. 2001; Natta, Grinin, & Mannings 2000; Hillenbrand et al. 1992). HAEBE stars are the progenitors of Vega like stars. Probing the circumstellar disks of HAEBE stars is important to investigate the likelihood of planet formation around intermediate mass stars. Accretion disks around the more massive Herbig Be stars also are important in understanding the formation of massive stars. In addition, it is possible that accretion plays a role in generating X-ray emission in HAEBE stars (Hamidouche et al. 2008).

Hillenbrand et al. (1992) suggested a classification scheme for HAEBE stars akin to that used for T Tauri stars. Using the slope of a star's spectral energy distribution in the near to mid-infrared, stars with large infrared excesses and spectral slopes with $\lambda F_{\lambda} \sim \lambda^{-4/3}$ were assigned to Group I; these stars presumably have geometrically flat, optically thick circumstellar disks and may have optically thin inner disks. Group II stars have flat or rising spectra and were interpreted to have disk systems surrounded by gas and dust envelopes. Finally, Group III HAEBE stars have very small infrared excesses and appear to have only

gaseous emission from any residual circumstellar disk or envelope.

The spectral energy distribution, which is composed of high spatial resolution optical and near-infrared observations combined with much lower spatial resolution *Infrared Space Observatory* (ISO), *Infrared Astronomy Satellite* (IRAS), and ground-based sub-millimeter continuum data may, however, be incorrect, if the far-infrared and sub-millimeter emission seen toward these stars is dominated by emission from extended reflection nebulae or nearby embedded protostars. If this is the case, which it can be, especially for B stars, see e.g., Henning et al. (1998, 1994); Sandell and Weintraub (1994a); Aspin, Sandell & Weintraub (1994) and the results from this paper, then the disk and envelope models for these HAEBE stars must be re-examined based on higher resolution observations.

In this paper, we present high spatial resolution 850 μm and 450 μm maps of HAEBE stars that enable us to examine what fraction of the long wavelength emission that has always been assumed to be part of the spectral energy distributions for these stars is associated with the stars and whether some of the emission originates from the surrounding cloud and/or invisible nearby young objects.

2. Observations

Almost all of the sub-millimeter observations reported in this paper have been obtained with SCUBA on JCMT¹, Mauna Kea, Hawaii. Some of the observations were carried out by us in August 2001; others have been retrieved from the JCMT archive at the CADC². We also present a few observations obtained using the single element bolometer UKT14 on JCMT (Sandell and Weintraub 1994b).

SCUBA (Holland et al. 1999) has 37 bolometers in the long and 91 in the short wavelength array separated by approximately two beam widths in a hexagonal pattern. The field of view of both arrays is $\sim 2'3$. Both arrays can be used simultaneously by means of a dichroic beamsplitter. The long wavelength array is optimized for 850 μm and the short wavelength array for 450 μm , but one can also choose to observe at 750 μm and 350 μm for the long and short wavelength array, respectively, with slightly reduced sensitivity. The 750/350 μm filter

¹The JCMT is operated by the Joint Astronomy Centre, on behalf of the UK Particle Physics and Astronomy Research Council, the Netherlands Organization for Scientific Research, and the Canadian National Research Council.

²Guest User, Canadian Astronomy Data Center, which is operated by the Dominion Astrophysical Observatory for the National Research Council of Canada's Herzberg Institute of Astrophysics

combination is no longer supported, but it was used in 1997 and 1998 and we have retrieved and reduced some 750 μm and 350 μm from this time period. The measured Half Power Beam Width (HPBW) is 14".5 and 7".8 for 850 μm and 450 μm , respectively, for standard jiggle-map observing in stable night time conditions. For the 750/350 μm filter combination, we measured HPBWs of 12".9 for 750 μm and 6".5 for 350 μm , respectively.

For sources with angular sizes less than or about equal to the field of view, the preferred observing mode is to use the long and short wavelength filter combination in jiggle-map mode. Larger emission regions have to be observed in scan-map mode. In jiggle map mode, the spacings between the bolometers are filled in by performing a jiggle pattern with the chopping secondary, while the secondary is chopping with a frequency of 7.8125 Hz. To completely sample both arrays, one needs to sample 64 positions with the array, while only 16 jiggle positions are needed if only one of the arrays is used. The default time for each jiggle step is 1 sec for standard observing. Each 64-point jiggle pattern is done in a set of four, 16-point jiggles, each followed by a nod of the telescope into the other beam. In scan-map mode the array is tilted relative to the scan direction to ensure full sampling over the array with the telescope is scanning with a rate of 24" s⁻¹ while chopping with a frequency of 7.8125 Hz. Each scan is overlapped by about half the array. The typical scan-map mode at JCMT is a basket weaving technique first suggested by Emerson (1995) where one can scan the source in an arbitrary angle, but chop in two orthogonal directions (fixed in equatorial coordinates) and restore the dual beam map in the Fourier space after converting the dual beam maps to equatorial coordinates. The standard setup for SCUBA is to use six maps, three of which are made while chopping in RA with three different chop throws and three while chopping in Dec. also with three different chop throws. The chop throws are chosen to so that the final map is sensitive to most spatial frequencies. Scan-maps never go as deep as jiggle-maps, because the restoration process results in baseline uncertainties and sky noise and even small pointing errors cause additional restoration noise (Sandell, Jessop and Jenness 2001). However, for compact sources well above the noise level of the map, this is not a problem, since one can always subtract or filter out the background emission.

The majority of the data presented in this paper have been obtained in jiggle-map mode, typically with a 120" chop in azimuth or at a fixed position angle in order to avoid chopping onto extended emission. A few compact isolated sources have been observed with shorter chop throws, but not less than 80". Most HAEBE stars are known to illuminate large reflection nebulae or are located in extended molecular cloud complexes; these sources have been observed in scan-map mode. A few stars — HD 200775 in NGC 7023, and CoD-42° 11721 — have been observed in both scan-map and jiggle-map modes. For these regions both jiggle and scan-maps agree within errors with each other. The absolute pointing of SCUBA

is typically checked on blazars or calibrators near the target object before and after each map or set of maps. This enables us, in the data reduction stage, to correct for possible pointing drifts that may occur between the start and end of a map. Some of the maps retrieved from the archive did not have such frequent pointing observations. In these cases we have used the closest pointing observation to correct the pointing for the target star and then used the target star or another suitable point source in the map to correct for possible pointing drifts during the observations. The absolute pointing accuracy is expected to be better than $2''$. The sub-millimeter opacity was determined from sky dips at $850\ \mu\text{m}$ and/or derived from *CSO tau*, the sky dip meter located at CSO, which provides opacity information every 10 minutes at $\lambda = 1.3\ \text{mm}$. Two data sets were reduced from SCUBA in photometry mode. The reduction of these data sets is essentially similar, although we only obtain a total flux density, i.e., no information about whether the source is compact or extended.

All the data have been flux calibrated from maps of Mars, Uranus or Neptune or from maps of the SCUBA secondary calibrator sources HL Tau, OH231.8+4.2, IRC+10216, RAFGL 618 and RAFGL 2688 (Sandell 1994, 1998; Jenness et al. 2002) typically observed several times during a night. If sufficient calibration information was not available for a night, we have derived flux calibration from nearby nights with similar weather conditions. A complete list of the HAEBE stars observed in this survey is given in Table 1.

The data were reduced in a standard way using SURF (Jenness and Lightfoot 1999; Sandell, Jessop and Jenness 2001) and STARLINK imaging software, i.e., we flat fielded, extinction corrected, sky subtracted, despiked, and calibrated the images in Jy beam^{-1} . We then pointing-corrected each scan for any drift in pointing between each pointing observation and added the data together to determine the most likely sub-millimeter position at $850\ \mu\text{m}$. Once we had derived a source position this way, we then applied small additional RA and Dec corrections to each scan (shift and add) to sharpen the final image to this position. Both despiking and sky subtraction can be done in several different ways depending on the amount of data and what observing mode was used for collecting the data (Sandell, Jessop and Jenness 2001). We generally followed the advice given in Sandell, Jessop and Jenness (2001) or tried several different ways in order to find the optimal way to ensure good data quality.

All our maps were converted to FITS files and exported to MIRIAD (Sault, Teuben and Wright 1995) for further analysis. In order to correct for the error lobe contribution, especially at $450\ \mu\text{m}$, we have deconvolved all the maps using CLEAN and a circular model beam even though the beam is generally somewhat elliptical, i.e., broadened in the chop direction. However, for large data sets sky rotation will circularize the average beam profile anyway. Since our data set spans a variety of observing conditions and several observing seasons the beam size and error lobe contribution varies significantly from data set to data set. At $450\ \mu\text{m}$ the HPBW

can vary due to seeing conditions and changes in the surface by as much as $1''$. The error beam is even more sensitive to thermal gradients over the telescope. Especially in the early evening and during daytime, the $450\ \mu\text{m}$ error beam can change due to these thermal gradients (Sandell, JCMT internal report). We find that the $450\ \mu\text{m}$ HPBW varied by as much as $1''$ and occasionally more due to all these factors.

For jigglemaps we measured HPBW at $850\ \mu\text{m}$ in the range $14''.3 - 15''.5$, but most of our maps in good stable night time conditions agree with the nominal value of $14''.5$. At $450\ \mu\text{m}$ the nominal HPBW is $7''.8$. For scan maps a typical HPBW at $850\ \mu\text{m}$ is $\sim 15''$, while it is $\sim 8''.5$ at $450\ \mu\text{m}$. For jiggle-maps our model beam is composed of three symmetric Gaussians: a main beam, a near-error lobe, and an extended, low amplitude, far-error lobe. For scan maps we only use a two component model, i.e., a main beam and a near-error beam. At $850\ \mu\text{m}$ the compact near-error beam has a HPBW of $\sim 40'' - 55''$ with an amplitude of $1 - 2\%$ of the beam peak and an extended error lobe with a HPBW $\geq 100''$ and an amplitude of $\sim 0.1\%$ of the maximum. Because the amplitude of the extended error lobe is so small at $850\ \mu\text{m}$, we can ignore it. At $450\ \mu\text{m}$ we find the near-error beam to have a HPBW in the range $25'' - 34''$ with an amplitude $3 - 7\%$ of the beam peak, i.e., much larger variations than those we see at $850\ \mu\text{m}$. The extended error lobe for jiggle-maps at $450\ \mu\text{m}$ has a HPBW of $\sim 120''$ and an amplitude of $\leq 1\%$.

In almost all cases, we have restored our CLEAN images back to $14''$ resolution at $850\ \mu\text{m}$ and to $8''$ resolution at $450\ \mu\text{m}$. In a few cases, where the signal-to-noise is marginal, we have restored the maps back to a resolution ($15'' - 16''$ for $850\ \mu\text{m}$; $10'' - 12''$ for $450\ \mu\text{m}$) which improves the signal-to-noise without degrading the resolution too much. Then, using the task IMFIT in MIRIAD, we fit a two-component elliptical Gaussian, one for the HAEBE star, and one for the surrounding cloud core. The fit of the cloud core is mainly used to provide a good subtraction of the extended emission and is not used to estimate the flux density of the surrounding cloud. For blended sources like LkH α 198 and LkH α 198 mm we used constrained fits with multiple components, increasing the uncertainty in the derived parameters. The results of these Gaussian fits for the detected HAEBE stars are given in Table 2a. Note that the quoted flux densities are background corrected flux densities, i.e., the surrounding cloud emission has been subtracted before we computed the integrated flux density. Additional sub-millimeter photometric measurements with UKT14 are presented in Table 2b. Limits for non-detections, all $3\text{-}\sigma$ upper limits, are given in Table 2c.

3. Archive *Spitzer* observations

We searched the *Spitzer* archive for all MIPS 24 and 70 μm observations of our target stars and retrieved and analyzed all photometric (image) data. A few stars were covered by the c2d legacy project (Evans II et al. 2003). For these stars we retrieved the results from the IRSA General Catalog Query Engine, Gator (<http://irsa.ipac.caltech.edu/applications/Gator/>). If the MIPS pbcd-data appeared to be of good quality, we extracted photometry with Mopex, which was developed by the *Spitzer* Science center; otherwise we first reduced the images from the Archive BCD-data using Apex, another software package developed by the *Spitzer* Science center. The results of the *Spitzer* MIPS photometry are given in Table 3.

4. Analysis

We fit the observed total fluxes with a simple graybody fit, see e.g., Sandell (2000); Sandell and Weintraub (2001). For “isolated” HAEBE stars, i.e., stars for which we do not see any emission from the surrounding cloud or from nearby sources, we make use of IRAS, ISO or KAO far infrared data longward of 60 μm in addition to our own sub-millimeter data. In a few cases, where we have no 100 μm data or where there is a clear excess at 100 μm , we assume a dust temperature or explore a plausible range in dust temperature. The fits for these stars are shown in Figure 1 and Figure 2.

For confused regions, i.e., where nearby sources or strong emission from the surrounding cloud core are present, we do not use the far-infrared data, because we have no way to accurately partition the contribution of each component to the far infrared flux measured in a much larger beam. In these cases we also assume a plausible dust temperature based on all the available information we have for these sources.. Since we have measured the source size (Table 2a), we constrain the size and only fit for the dust emissivity, β , the dust temperature, T_d (if we have far infrared flux density measurements), and the dust optical depth at 850 μm . To derive masses we assume standard Hildebrand opacities ($\kappa_{1200\text{GHz}} = 0.1 \text{ cm}^2 \text{ g}^{-1}$) and a gas-to-dust ratio of 100 (Hildebrand 1983). The results of the graybody fits are given in Table 4. In the same table we also list the spectral index of the dust emission α ($F_\nu \propto \nu^\alpha$), after subtraction of free-free emission, which was derived by least-squares fitting all millimeter and sub-millimeter data for each source. For optically thin dust in the Rayleigh-Jeans regime, the spectral index, $\alpha = \beta + 2$, where β is the dust emissivity index.

5. Results

All maps of the sources listed in Table 1, except one, show emission in the SCUBA field of view, although the observed emission is not always associated with the HAEBE stars. Early B stars are luminous enough to heat up their surrounding clouds and, with the exception of the very distant HAEBE star V431 Sct (MWC 300), invariably show extended cloud emission. This is the only field where we see no emission at all. We have only detected three HAEBE stars of spectral type early B or late O. The failure to detect early type stars does not, however, mean that massive stars do not form disks; rather, in this sample it appears to be a selection effect. When Herbig Be stars are bright enough to illuminate reflection nebulae, they may already have freed themselves from the cloud cores in which they were formed, i.e., they are already close to the main sequence and appear to have dispersed the disks with which they were born.

5.1. Isolated HAEBE stars

Isolated HAEBE stars have the same characteristics as “classical” HAEBE stars, i.e., they are often located near, but not in star forming regions, they have $H\alpha$ in emission, IR excesses due to thermal emission from dust, but differ from them due to the absence of nebulosities (Grinin et al. 1991). The absence of nebulosities suggests that these stars on the average are older than “classical” HAEBE stars, because they have already freed themselves from the clouds in which they were born. At least three (HD 135344 B, HD 141569, and HD 169142), possibly more of our isolated HAEBE stars are transition objects (Najita, Strom & Muzerolle 2007). These are stars which show significant disk evolution. The transition disks are characterized by an inner gap, which is still gas rich but contains very little dust, and a cold outer disk. Due to the inner gap they have very little near-infrared excess, but they have strong mid- and far-infrared excess due to the outer disk.

Meeus et al. (2001) did ISO spectroscopy of 14 isolated HAEBE stars and separated them into two groups based on their infrared SEDs: group I and group II. For group I the infrared to sub-millimeter continuum could be modeled by a power-law and a blackbody, suggesting that stars of this group have optically thick and geometrically thin disks (power-law component) and an optically thin flared region (black body component). Group II objects only needed a power-law to fit their continuum, which Meeus et al. (2001) suggested indicates that they are more evolved stars with partially optically thin inner disks protecting the outer disk from flaring. We have sub-millimeter data on many of the stars observed by Meeus et al. (2001). Observations of several of them made with millimeter arrays confirm that the infrared excess is due to circumstellar disks (Mannings, Koerner, & Sargent 1997;

Mannings & Sargent 1997, 2000; Natta et al. 2004; Hamidouche et al. 2006; Isella et al. 2007). In the millimeter and sub-millimeter regime there is very little difference, if any, between Meeus et al. group I and group II objects.

MWC 480 (HD 31648) is a bright, isolated Ae star in the Taurus-Auriga complex with a Hipparchos parallax distance of 131 pc (van den Ancker et al. 1998). It has a spectral class of A3 - A5 Ve and an age of 4 - 8 Myr (Simon, Dutrey & Guilloteau 2000; Piétu et al. 2006; Piétu, Dutrey & Guilloteau 2007). The star has never been searched for free-free emission, but if it has free-free emission, it is presumably weak. It has been extensively studied with mm-arrays and is surrounded by a large circumstellar disk in Keplerian rotation (Mannings & Sargent 1997; Simon, Dutrey & Guilloteau 2000; Piétu et al. 2006; Piétu, Dutrey & Guilloteau 2007; Hughes et al. 2008a). The disk is well resolved both in CO and continuum. At 1.4 mm Hamidouche et al. (2006) find a disk size of $0''.8 \times 0''.7$ at a P.A. of $143^\circ \pm 5^\circ$, while the CO disk is much larger with a diameter of $\sim 8''$ at a P.A. of $\sim 150^\circ$ (Simon, Dutrey & Guilloteau 2000; Piétu, Dutrey & Guilloteau 2007). Both continuum and CO images give a similar inclination angle for the disk, $i = 37^\circ$ (Hamidouche et al. 2006; Piétu, Dutrey & Guilloteau 2007). Even though the disk is quite large, it is not seen in coronagraphic near-infrared images (Augereau et al. 2001). Piétu, Dutrey & Guilloteau (2007) derive $\sim 1.8 M_\odot$ for the mass of the central star from analysis of the Keplerian rotation of the disk in the $J = 1 \rightarrow 0$ and $J = 2 \rightarrow 1$ transitions of CO and its isotopomers as well as from $\text{HCO}^+ J = 1 \rightarrow 0$. The derived mass would suggest that the star is of spectral type A5.

Our SCUBA observations (Table 2a, Figure 3) resolve the disk around MWC 480 both at 850 and 450 μm . Our observations show an emission feature extending to the south from the disk. This emission is nearly at the same P.A. as the observed jet-like emission by Hamidouche et al. (2006) and could therefore be real. Our isothermal graybody fit to the millimeter and 100 μm data predict a cold dust disk, $T_d \sim 28$ K and a dust emissivity index, $\beta \sim 0.8$ (Table 4). As we can see from Figure 1 the dust emissivity is well constrained, but the fit underestimates the observed flux densities at 60 μm , which suggests that one needs a warm dust component as well in order to explain the 60 μm emission.

HD 34282 is of spectral type A3 Ve (Mora et al. 2001; Mérim et al. 2004) with an age of 6.4 Myr. It has no detectable free-free emission (Natta et al. 2004). Its disk was resolved at 1.3 mm with the IRAM Plateau de Bure interferometer (PdB) with a size of $1''.7 \times 0''.9$ (Piétu, Dutrey & Kahane 2003). They find from imaging the disk in CO $J = 2 \rightarrow 1$ that the disk is in Keplerian rotation and seen at an inclination of $56^\circ \pm 3^\circ$. Based on the dynamical mass they argue that the previously reported distance estimate, from Hipparcos parallax observations, 160 ± 42 pc (van den Ancker et al. 1998) must be in error and that the most

likely distance is 400 pc. The detailed modeling of the stellar parameters by Mérim et al. (2004) gives 348 pc, We will therefore use the distance 350 pc. The disk was also imaged with the OVRO interferometer by Mannings & Sargent (2000) in the continuum at 2.6 mm and by Natta et al. (2004) with the PbB interferometer at 3.2 and 1.3 mm. The observed continuum fluxes agree well with the results of Piétu, Dutrey & Kahane (2003).

We find the star to be unresolved at 850 μm and 450 μm (Table 2a). These SCUBA data have also been published by Sheret, Dent & Wyatt (2004), who get somewhat discrepant results at 450 μm . In this analysis we use our results. The star was included in the CO J = 3 \rightarrow 2 single dish JCMT survey by Dent et al. (2005) and shows a CO profile similar to what was observed with the PbB interferometer, confirming that this is an isolated HAEBE star. Since the star appears compact in both single dish, coronagraphic imaging (Doering et al. 2007) and aperture synthesis observations, we combined all millimeter and sub-millimeter data in our isothermal modeling. The dust emissivity we derive, $\beta = 1.29$, is very similar to what Piétu, Dutrey & Kahane (2003) derived from their detailed modeling. However, in this case we find the dust emission to be marginally optically thick at 850 μm , $\tau_{850} \sim 0.2$, and we get a slightly higher mass, 0.18 M_{\odot} (Table 4), than Piétu, Dutrey & Kahane. The mass of the disk is much higher than we find for any other isolated Ae star.

HD 35187 is a visual binary star with a separation of 1''38 in Taurus at a distance of 150 pc (Dunkin & Crawford 1998). Dunkin & Crawford found the stars have spectral types of A2 V (HD 35187 B) and A7 V (HD 35187 A). Only HD 35187 B shows H α in emission and has an infrared excess, suggesting it is surrounded by an accretion disk. The age of the system is ~ 10 Myr.

HD 35187 was detected at 1.1 mm and 800 μm by Sylvester et al. (1996) with the single pixel bolometer UKT14 on JCMT. It is a relatively strong radio source with a flux density of 1 mJy at 3.6 cm (Natta et al. 2004). Natta et al. (2004) imaged the star in continuum with the VLA at 7 mm and with the PbB interferometer at 3.6 and 1.3 mm. Most of the emission at 7 mm is due to free-free emission. The free-free emission is still significant at 3.6 mm, but at 1.3 mm and shorter wavelengths the emission is dominated by dust emission.

Our 850 and 450 μm SCUBA maps show an unresolved point source. These SCUBA maps were previously published by Sheret, Dent & Wyatt (2004). We have reduced them independently and find somewhat higher flux densities (16% and 27% at 850 μm and 450 μm , respectively) than Sheret, Dent & Wyatt, but in good agreement with other published data on this star. A graybody isothermal fit to all (sub-)millimeter data and the IRAS 100 μm data point (Figure 1) gives a dust temperature of 44 K and a dust emissivity index, $\beta = 0.87$. The mass of the disk is relatively low, 0.002 M_{\odot} (Table 4).

HD 36112 is an isolated HAEBE star located in the outskirts of the Taurus-Auriga complex. Chapillon et al. (2008) adopted a distance of 140 pc, arguing that the star is likely to be at the same distance as the Taurus-Auriga complex. Beskrovnaya et al. (1999) classified it as A8 Ve with an age of 5 - 10 Myrs. A three component fit to low resolution UV spectra give a spectral class of A7 IIIe, with an age of 4.4 Myr and a distance of 200 pc (Blondel & Tjin A Djie 2006). The latter agrees with the Hipparcos parallax distance (van den Ancker et al. 1998). We assume 200 pc.

The star has not been detected in free-free emission at centimeter wavelengths. It was first observed by Mannings & Sargent (1997) with the OVRO array in continuum at 2.7 mm and in the ^{13}CO $J = 1 \rightarrow 0$ line. The dust disk was unresolved in continuum and barely detected in ^{13}CO . Follow-up observations with the OVRO array (Mannings & Sargent 2000) observed the star in continuum at 1.3 mm, but did not resolve it. Chapillon et al. (2008) observed the star with the IRAM PdB interferometer in continuum at 3.4 mm, 2.6 mm, and 1.3 mm, as well as the ^{12}CO $J = 2 \rightarrow 1$ and $1 \rightarrow 0$ transitions. They resolve the disk in continuum at 1.3 and 2.6 mm with a size of $\sim 1''$ (150 AU), and find the disk slightly more extended in CO ($r \sim 250$ AU). Dent et al. (2005) detected the disk in the CO $J = 3 \rightarrow 2$ line emission. By modeling the CO profile they found the disk to be almost face-on with an inclination $< 10^\circ$ and deduced an outer radius of 170 ± 30 AU. Their results agree quite well with the far better constrained modeling by Chapillon et al., who determine a disk inclination of $16^\circ - 18^\circ$ from their CO observations.

We do not resolve the dust emission, which agrees well with the the PdB results. A graybody fit to all (sub-)millimeter and FIR data to 100 μm , including ISO data from Elia et al. (2005), give a dust emissivity index, $\beta = 1.25$, a dust temperature of 43 K, and a disk mass of 0.014 M_\odot . Our deduced dust emissivity is slightly higher, but well constrained by our fit (Figure 1), and our disk mass is a factor of two lower than what was found by Chapillon et al. (2008). They derived a dust emissivity index, $\beta = 1.0 \pm 0.15$, and a disk mass of 0.027 M_\odot .

HD 135344 B is an isolated F4 Ve star (Dunkin, Barlow, & Ryan 1997; Grady et al. 2009) in the Sco OB 2 - 3 association at a distance of ~ 140 pc (Coulson & Walther 1995; van Boekel et al. 2005). The star has been extensively studied from X-rays to millimeter wavelengths (Grady et al. 2009, and references therein). It has strong millimeter and far-infrared excesses (Walker & Wolstencroft 1988; Coulson & Walther 1995; Sylvester et al. 1996), and Grady et al. (2009) conclude that is definitely a PMS star with an age of ~ 8 Myr. As deduced both from modeling (Dent et al. 2005; Brown et al. 2007) and direct imaging in the mid-infrared and in the sub-millimeter (Pontoppidan et al. 2008; Brown et al. 2009), the disk is seen approximately face-on and has a large inner gap. The star therefore has a tran-

sitional disk, where the inner disk is largely free of dust. Yet the disk appears surprisingly gas rich (Dent et al. 2005).

The star is well studied in the (sub-)millimeter wavelength regime. Both Coulson & Walther (1995) and Sylvester et al. (1996) obtained photometry of the star with UKT14 on JCMT, Walker & Butner (1995) observed it at Caltech sub-millimeter Observatory (CSO) at 1.3 mm and 800 μm , and Brown et al. (2009) imaged it with high spatial resolution with the Smithsonian Submillimeter Array (SMA) at 880 μm . Brown et al. resolved the dust disk with a radius of $\sim 0''.9$ (125 AU) and found an inner hole with an outer radius of 39 AU. We have deep images with SCUBA at 850 μm and 450 μm , which show that the disk is unresolved in an $8''$ beam (Table 2a). This is consistent with the observed size ($1''.8$) at 880 μm (Brown et al. 2009), although our observed flux density is $\sim 50\%$ higher than what Brown et al. find in their high spatial resolution SMA observations, suggesting they may filter out some of the extended emission. Our isothermal graybody fit, including all millimeter, sub-millimeter as well as the IRAS 100 μm flux densities gives a dust emissivity index, $\beta = 1.38$, and a dust temperature of 32 K. We did not include the ISO 200 μm flux density (Walker & Heinrichsen 2000), because it appears anomalously low compared to all the sub-millimeter and IRAS data. We derive a much lower dust temperature than Coulson & Walther (1995), because they fitted the SED with a blackbody. As with all evolved disks, however, the graybody fit to the millimeter and sub-millimeter data underestimate the flux densities shortward of 100 μm , which require a warm dust component as well. If we assume normal gas-to-dust ratio, we get a disk mass of 0.025 M_\odot (Table 4).

HD 141569 is a nearby, isolated A0 Ve/B9.5 Ve star, which is the primary member of a triple system in the outskirts of the Sco-Cen system with an age of 3 - 5 Myrs (Dunkin, Barlow, & Ryan 1997; Weinberger et al. 2000). Mérin et al. (2004) determined a more precise age for the primary by fitting surface gravity, metallicity and effective temperature to high resolution spectra and photometry. They find an age of 4.7 Myr, a spectral type of B9.5 Ve and a distance of 108 pc, which agrees within errors with the Hipparchos distance, 99 pc. Coronagraphic imaging in the near-infrared (Augereau et al. 1999; Weinberger et al. 1999) shows a large ($r \sim 400$ AU), slightly asymmetric dust disk with depression (gap) at 250 AU and a 30 AU inner hole (Marsh et al. 2002). The disk has also been resolved in the mid-infrared (Fisher et al. 2000; Marsh et al. 2002) with a size of $2''.2$ at 10 μm . HD 141569 is often referred to as a debris disk; however, Dent et al. (2005) detected CO $J = 3 \rightarrow 2$, and all debris disks are gas poor. The only supposed debris disk star known to have a molecular gas disk is 49 Ceti (Hughes et al. 2008b), and it is quite possible that the disk surrounding 49 Ceti is primordial, rather than a debris disk. In addition *Spitzer* IRS spectra also show that HD 141569 has strong PAH emission (Sloan et al. 2005; Keller et al. 2008), which is not seen in debris disks. Furthermore, at an age of only 5 Myr, HD 141569 is likely too young to

be a debris disk star. Thus, its youth, the presence of a gas in the disk, and the detection of PAH emission from the disk all strongly suggest that HD 141569 has a primordial transition disk, not a debris disk.

For this star the the SCUBA data presented in Table 2a were obtained in photometry mode and are based on the same data that were published by Sheret, Dent & Wyatt (2004). The flux densities that we obtain agree quite well with those of Sheret, Dent & Wyatt. The star was also observed by SCUBA at 1.35 mm by Sylvester, Dunkin & Barlow (2001) and at CSO and IRAM at 1.3 mm by (Walker & Butner 1995), but the latter have poor signal-to-noise and have not been used in our analysis. The star was observed in photometry mode by *Spitzer* MIPS at 24, 70, and 160 μm . The photometry at 24 and 70 μm is given in Table 3 and agrees with results by Weinberger (private communication). The MIPS images only show emission from HD 141569 and no emission is seen from the companions. Our graybody fit severely underestimates the observed flux at 100 and 70 μm , suggesting that the disk must have a warm dust component as well. The temperature of the cold outer disk is therefore uncertain. In Table 4 we give the results for an assumed dust temperature of 40 K, which results in a β index of 0.5 and a disk mass of $9 \times 10^{-5} M_{\odot}$. Because we assumed a temperature rather than derived it, this results in much higher uncertainties for the dust emissivity and disk mass. By varying the temperature from 25 – 70 K, we find that varies by less than ± 0.2 , while the mass could be off by a factor of two.

HD 142666 is located in the Sco OB2-2 association at a distance of 145 pc (van Boekel et al. 2005). It has a spectral type of A8 Ve (Dunkin, Barlow, & Ryan 1997; Mora et al. 2001; van Boekel et al. 2005; Guimarães et al. 2006) with an estimated age > 10 Myr (Natta et al. 2004). It was not detected in free-free emission at 3.6 cm (Natta et al. 2004). It was included in the ISO survey by Meeus et al. (2001) where it was classified as a group IIa object, i.e. a star having an optically thick disk in the FIR. The disk was detected in the CO J = 3 \rightarrow 2 survey by (Dent et al. 2005). Even though the CO emission is clearly detected, the signal-to-noise is poor and Dent et al. fitted it with a single broad line predicting that the disk is seen nearly face-on ($i = 18 \pm 5^{\circ}$) and a radius of 45 AU, which would suggest a disk size $< 1''$.

The star was observed with a 7-channel bolometer array on IRAM at 1.2 mm (Bockelée-Morvan et al. 1994) and with UKT14 on JCMT at wavelengths from 2 mm to 450 μm (van der Veen et al. 1994; Sylvester et al. 1996). These observations were all photometric observations. HD 142666 was also observed with the IRAM PdB interferometer in continuum at 3.3, 3.1, and 1.2 mm. Although Natta et al. (2004) give no size information, the 1.2 mm flux density from PbB appears somewhat low compared to single dish photometry, suggesting that the disk could be extended. The disk is unresolved in our SCUBA images at 850 μm , although at 450 μm

we obtain a size of $2''.2$. Since the size is not verified at $850\ \mu\text{m}$, we consider this an upper limit. Far infrared flux densities observed with ISO (Elia et al. 2005) appear overestimated when compared to IRAS data, and we have not included them in our analysis. If we only use the (sub-)millimeter observations and the IRAS $100\ \mu\text{m}$ flux density, our graybody fit gives a relatively low dust emissivity, $\beta = 0.72$ for a dust temperature of 31 K. The isothermal fit cannot reproduce flux density at $60\ \mu\text{m}$ (Figure 1). To fit the millimeter and far-infrared SED we need a warm dust component as well, which is true for most isolated HAEBEs.

HD 144432 is a binary star with a late type companion in the Sco OB2-2 association at a distance of ~ 145 pc (Pérez et al. 2004). The spectral type is somewhat uncertain. Dunkin, Barlow, & Ryan (1997) classified it as A9/F0 Ve, while Pérez et al. (2004) and Blondel & Tjin A Djie (2006) assign it a spectral stype A8 Ve or A9 IIIe with an age of 6.5 - 6.8 Myr. It was included in the ISO survey of isolated HAEBE stars (Meeus et al. 2001), where it was classified as group IIa object. It was detected at 1.2 mm by Bockelée-Morvan et al. (1994) and at 1.3 mm and $800\ \mu\text{m}$ by Sylvester et al. (1996).

We have only SCUBA photometry of this star (Table 2a). A graybody fit to all (sub-)millimeter and IRAS $100\ \mu\text{m}$ data give $\beta = 0.59$ and a disk mass of $0.002\ M_{\odot}$. The fit greatly underestimates the flux density at $60\ \mu\text{m}$ (Figure 2), suggesting that we need a warm dust component as well.

HD 150193 is located in Ophiuchus at a distance of ~ 150 pc. Mora et al. (2001) classified it as an A2 IVe star, while Blondel & Tjin A Djie (2006) found it to have a spectral type A3 IIIe from analysis of UV-spectra. Elias (1978) classified it as A0. It is a visual binary with a separation of $1''.1$ (Reipurth & Zinnecker 1993). The companion is quite faint. Carmona, van der Ancker & Henning (2007) find the secondary to be a T Tauri star with a spectral type F9Ve. Carmona, van der Ancker & Henning (2007) find a common age for the binary system of ~ 10 Myr. The star was not detected in the CO $J = 3 \rightarrow 2$ survey by Dent et al. (2005), confirming that it is an isolated HAEBE star, which is not associated with any molecular cloud. It also appears to have a gas-poor disk. HD 150193 is associated with faint free-free emission, $0.2\ \text{mJy}$ at $3.6\ \text{cm}$ (Skinner, Brown, & Stewart 1993; Natta et al. 2004), almost certainly originating from a thermal wind.

The star has strong infrared excess (Elias 1978) and was first detected in sub-millimeter continuum at 800 and $450\ \mu\text{m}$ with the single pixel bolometer UKT14 on JCMT by Jensen, Mathieu & Fuller (1996). It was imaged with the OVRO interferometer in the $2.6\ \text{mm}$ dust continuum and in the CO $J = 1 \rightarrow 0$ line (Mannings & Sargent 1997), who found the dust continuum to be unresolved and did not detect the disk in CO. It was also imaged by Natta et al. (2004) with the VLA at $7\ \text{mm}$ in their study of evolved dust disks in HAEBE stars. We report SCUBA observations at $850\ \mu\text{m}$ (Table 2a), which show an unresolved point-source. The star was

also imaged by *Spitzer* MIPS, which show an isolated point source at $70\ \mu\text{m}$ (Table 3). It was not detected by IRAS at $100\ \mu\text{m}$, but at $60\ \mu\text{m}$ the IRAS flux density is more than twice as large as what we see with MIPS at $70\ \mu\text{m}$ suggesting that IRAS picked up some extended emission in its much larger beam. Fitting an isothermal graybody disk model to all available millimeter and sub-millimeter data and the MIPS $70\ \mu\text{m}$ data point indicates that the disk is marginally optically thick at $850\ \mu\text{m}$ ($\tau \sim 0.2$) with a temperature of 44 K (Table 4) and a mass of $0.002\ M_{\odot}$. The dust emissivity we derive, $\beta = 0.65$, is lower than what Natta et al. (2004) found ($\beta = 1.0 - 1.6$) from their more limited sampling of the SED. Figure 2 shows that our fit is reasonably well constrained with an uncertainty in β of ± 0.2 .

KK Oph is in the outskirts of the Ophiuchi cloud complex. It was classified as A8 Vev by Mora et al. (2001), while Blondel & Tjin A Djie (2006) classify it as a A5 Ve, with a range A5 - A7 Ve from modeling UV spectra and photometry. It is a binary with a separation of $1''.5$ (Pirzkal et al. 1997). The secondary is a T Tauri star with a spectral type G6 Ve (Carmona, van der Ancker & Henning 2007). The distance is not well determined, but Blondel & Tjin A Djie (2006) quote $< 250\ \text{pc}$ from Wallenquist (1937), while Leinert et al. (2004) estimate the distance to be $160 \pm 30\ \text{pc}$, which we adopted in this paper. Blondel & Tjin A Djie estimate an age of $\sim 7.9\ \text{Myr}$, which agrees well with Carmona, van der Ancker & Henning (2007) who find an age of 7 Myr. Even though *Spitzer* MIPS archive images at 24 and $70\ \mu\text{m}$ do not show any sign of nebulosity or cloud emission around the star, the flux density observed by MIPS at $70\ \mu\text{m}$ is rather faint when compared to the IRAS $60\ \mu\text{m}$ flux density. The MIPS flux density at $70\ \mu\text{m}$, even without color correction, is only $2.88 \pm 0.02\ \text{Jy}$, while the ADDSCAN IRAS flux density at $60\ \mu\text{m}$ is $6.7 \pm 0.7\ \text{Jy}$ (Hillenbrand et al. 1992). Since both IRAS and *Spitzer* produce well calibrated data, it would appear that the much broader IRAS beam picks up some extended emission around the star. The star has weak free-free emission, $0.25\ \text{mJy}$ at $3.6\ \text{cm}$ (Skinner, Brown, & Stewart 1993).

KK Oph was detected $1.3\ \text{mm}$ by (Hillenbrand et al. 1992) with broad beam photometry, but there are no other published (sub-)millimeter observations. We obtained $800\ \mu\text{m}$ photometry with UKT14 (Table 2b) and mapped it with SCUBA at $850\ \mu\text{m}$. We find KK Oph to be faint and unresolved (Table 2a). For KK Oph, we derive a fairly typical mass of $0.002\ M_{\odot}$ and a rather shallow β index, 0.74; however, the β index is not well constrained, since we only have data covering a narrow wavelength regime.

HD 163296 is an early A star at a distance of $122\ \text{pc}$ and with an age of $\sim 4\ \text{Myr}$ (Table 1). The star is isolated, i.e., there is no sign of the molecular cloud in which the star was presumably formed (Dent et al. 2005). However, Grady et al. (2000) show that HD 163296 is still an active Ae star, suggesting that there are still some remnants left of the

cloud out of which it was formed. Single-dish observations of HD 163296 show strong dust emission at millimeter and sub-millimeter wavelengths (Hillenbrand et al. 1992; Mannings 1994; Henning et al. 1994, 1998). The star is very faint in free-free emission (Natta et al. 2004). Therefore, the millimeter emission is completely dominated by thermal emission from dust. Isella et al. (2007) have observed HD 163296 in continuum with the SMA at 870 μm , with PdB at 1.3 mm and 2.8 mm, and with the VLA at 7 mm. They resolve the disk at all wavelengths except 7 mm, where the VLA is less sensitive or has resolved out the cold, extended, outer part of the disk. At 870 μm they derive a disk size of $3''.6 \times 2''.6$. They also imaged the disk in emission from several molecular lines. From the ^{12}CO $J = 3 \rightarrow 2$ and ^{12}CO $J = 2 \rightarrow 1$ lines, they deduce that the velocity pattern is well fitted with a Keplerian disk with an inclination angle $46^\circ \pm 4^\circ$ and a stellar mass of $2.6 M_\odot$, while Grady et al. (2000) found an inclination angle of $\sim 60^\circ \pm 5^\circ$ from their coronagraphic imaging of the reflected light from the disk. The radius of the disk observed in CO, ~ 540 AU, is much larger than in continuum, ~ 200 AU; such a behavior can be explained by an exponential falloff of the surface density at large radii (Hughes et al. 2008a).

We find HD 163296 to be extended and well resolved at both 850 and 450 μm (Table 2a; Figure 4). Although there are many observations of HD 163296 in the JCMT archive, very few of the observations were done in good sky conditions with sufficient calibration observations to enable us to obtain well-calibrated data sets with good beam characterization. We retained only three data sets taken in engineering time in 2004 and 2005. Even though we find the dust emission around HD 163296 to be slightly elliptical, the elongation is not large enough to permit us to determine the position angle of the disk with high accuracy at either 850 or 450 μm . For our 450 μm data sets, where the HPBW is $\sim 8''$, we created a model beam by rotating the measured beam profiles to the average position angle of each map of HD 163296, since the beam is always somewhat elongated in the chop direction (see Section 2). We added the three rotated beam profiles together to form a beam profile which best approximates the beam of the coadded 450 μm map. After cleaning the 450 μm map with this model beam, we find a FWHM = $4''.6 \times 3''.2$, P.A. = $-13^\circ \pm 27^\circ$, with an uncertainty of $\sim 1''$ (Table 2a). The size of the 450 μm disk is slightly larger than what Isella et al. (2007) determined from their 870 μm SMA observations, but both results agree well within observational errors. The total flux densities derived by Isella et al. also agree very well with single dish results at 1.3 mm and 870 μm , confirming that the aperture synthesis observation have recovered all the continuum emission from the disk. We can therefore use both interferometric data and single dish data to determine the emissivity index, β , and disk mass. An isothermal graybody fit to these data gives $T = 28$ K and $\beta = 0.94$. By assuming a gas-to-dust mass ratio of 100, we deduce a disk mass $\sim 0.065 M_\odot$. The graybody fit underestimates the IRAS flux density at 60 μm , suggesting that there is

an additional contribution from warm dust at $60\ \mu\text{m}$, although its contribution to the disk mass is negligible. Our results are very consistent with the results of Isella et al. (2007). These studies indicate that some grain growth has already occurred in the HD 163296 disk.

HD 169142 was classified as A5 Ve (Dunkin, Barlow, & Ryan 1997; van Boekel et al. 2005), A7Ve (Blondel & Tjin A Djie 2006) and as A9 III/IVe (Guimarães et al. 2006; Vieira et al. 2003). Here we adopt the spectral class A7 Ve, which is based on fitting low resolution UV spectra with a three component model, the stellar photosphere, an optically thick accretion disk, and a boundary layer between the disk and the star. The analysis of Blondel & Tjin A Djie (2006) indicate that the disk is seen approximately face-on, which agrees with other findings (see below) and predicts a distance of 150 pc and an age of ~ 12 Myr. This distance agrees very well with the distance of 145 pc derived by van Boekel et al. (2005), which we have adopted here. Dent et al. (2006) did not detect any free-free emission at 3.6 cm, although the flux density they observed at 7 mm appears anomalously high and is most likely due to free-free emission or a radio flare (see below). It was included in the ISO survey of isolated HAEBEs (Meeus et al. 2001) and classified as a Ib type HAEBE star. HD 169142 shows a narrow emission line in CO (Dent et al. 2005) and in [OI] at $6300\ \text{\AA}$ (Acke et al. 2005), suggesting that the disk must be seen nearly face-on. Meeus et al. (2010) modeled the disk including new *Herschel* data, and found that in order to explain the weak $10\ \mu\text{m}$ excess emission, the disk must have a gap, i.e. it appears to be a transition disk.

In the (sub-)millimeter the disk was first detected in photometry mode at 1.2 mm with the 7-channel bolometer on IRAM (Bockelée-Morvan et al. 1994) and at 2 mm, 1.3 mm, and $800\ \mu\text{m}$ with UKT14 on JCMT (Sylvester et al. 1996). Our observed continuum flux densities (Table 2a) agree well with the photometry results and suggest that the disk may be resolved with a size of $2''.3 \times 1''.6$ (Figure 5). Raman et al. (2006) observed HD 169142 with the SMA in continuum at 1.3 mm and in the CO $J = 2 \rightarrow 1$ line. They barely resolve the continuum emission (FWHM $\sim 0''.9$) but find that the CO emission traces a Keplerian disk around the star. Their best fit disk model gives a radius ~ 235 AU ($1''.6$), a disk mass of $\sim 0.02\ M_{\odot}$, and an inclination of 13° . This result agrees well with the SED modeling by Dent et al. (2006), who find a disk radius of 300 AU, a disk mass of $0.04\ M_{\odot}$ and an inclination angle of $\sim 30^{\circ}$. Our observed disk size, $r \sim 140$ AU, is consistent with these previous measurements. The star was also observed by the PACS imager on *Herschel* in continuum at 160 and $70\ \mu\text{m}$ (Meeus et al. 2010). Our graybody fit includes all (sub-)millimeter and far infrared data up to $100\ \mu\text{m}$, except the $200\ \mu\text{m}$ ISO value (Walker & Heinrichsen 2000), which appears anomalously low, and the 7 mm VLA data point, which is too high to be due only to dust. It must therefore include a significant contribution from free-free emission. When we include the accurate $160\ \mu\text{m}$ flux density from PACS, we get $\beta = 1.30$, a dust temperature of 41 K,

and a disk mass of $0.03 M_{\odot}$ (Table 4 and Figure 2). The latter is in good agreement with the results of Raman et al.. The dust emissivity that we obtained, $\beta = 1.30$, is more than twice as large as what Dent et al. (2006) found, because they did a fit to a more limited set of data and assumed that all the flux density at 7 mm was due to dust emission. As we can see from Figure 2, the fit underestimates the observed flux densities shortward of a $100 \mu\text{m}$, requiring a warm dust component as well. Since we have reliable far-infrared data on HD 169142 we also fitted the millimeter and far-infrared SED with a two-component graybody model, where we allowed the dust properties, dust temperature and size of the emitting region to vary for each component. However, we set the dust emissivity for the warm component equal to two, although the fit is not very sensitive to the emissivity of the warm gas. The two-component fit results in a slightly higher dust temperature for the cold dust, 52 K vs. 41 K. The dust emissivity for the cold dust component is now 1.38 compared to 1.30 for the single temperature fit, i.e., a marginal change. The temperature of the warm dust is 155 K. The two-component graybody fit now matches the 70, 60, and $25 \mu\text{m}$ flux densities very well, see Figure 2.

MWC 349 is a remarkable binary system at a distance of 1.2 kpc with a luminosity of $\sim 3 \times 10^4 L_{\odot}$ (Cohen et al. 1985). MWC 349 A was classified as a Be star by Merrill & Burwell (1933). Its optical and infrared spectrum is complicated. The star has very strong hydrogen and He I lines (Thompson et al. 1977; Cohen et al. 1985). Many lines are double peaked, suggesting they are formed in a Keplerian disk viewed edge-on (Hamann & Simon 1986, 1988). The secondary is at a separation of $\sim 2''.4$ and has a spectral type B0 III (Cohen et al. 1985). MWC 349 A is the brightest known radio star at centimeter wavelengths and the only known hydrogen recombination line maser source. Maser action is seen in hydrogen recombination lines from ~ 100 GHz ($\text{H}39\alpha$) to 1800 GHz ($\text{H}10\alpha$), with the all masering lines being double peaked and with the two peaks coming from the receding and approaching parts of the disk, due to Keplerian rotation (Strelunski, Smith & Ponomarev 1996). Direct imaging of the $\text{H}30\alpha$ recombination line with the SMA at 231.9 GHz confirm that the maser spots originate in an approximately edge-on disk with a rotation curve that is somewhat steeper than that expected for a simple Keplerian rotation (Weintroub et al. 2008).

The radio emission of MWC 349A is approximately proportional to $\nu^{0.6}$, consistent with what is expected from an ionized stellar wind (Olson 1975). High resolution VLA imaging shows that the radio emission is bipolar, with a dark lane separating the two lobes (White & Becker 1985; Cohen et al. 1985). Tafoya, Gómez, & Rodríguez (2004) argue that the dark lane with no free-free emission must be due to neutral gas. Tafoya, Gómez, & Rodríguez show that the flux density increases with frequency as $\nu^{0.67 \pm 0.03}$, and the angular size decreases with frequency as $\nu^{-0.74 \pm 0.03}$, confirming the presence of a biconical thermal wind that expands at constant velocity. The slow ($\sim 50 \text{ km s}^{-1}$) bipolar wind is believed to originate

from photoevaporation of the neutral disk (Hamann & Simon 1986; Lugo, Lizano & Garay 2004). Analysis of VLA data over a 20 year time period (Tafoya, Gómez, & Rodríguez 2004; Rodríguez, Gómez & Tafoya 2007) suggest that the radio emission is fading by $\sim 1.5\%$ per decade. The free-free emission still dominates at millimeter-wavelengths and perhaps even at $100\ \mu\text{m}$ (Harvey, Thronson & Gatley 1979).

Deep $\text{H}\alpha$ imaging of MWC 349 shows a faint shell to the north of the star with a radius of $75''$ (Marston & McCollum 2008). This shell is seen to the east and north-east of the star in a MIPS $70\ \mu\text{m}$ archive image, suggesting that MWC 349 A is illuminating a faint low surface brightness H II region.

Our SCUBA observations at $850\ \mu\text{m}$ and $450\ \mu\text{m}$ show a point-like source with flux densities that are consistent with free-free emission (Table 2a, Figure 6). However, if we assume that the wind is launched at $\sim 15\ \text{AU}$ from the star (Tafoya, Gómez, & Rodríguez 2004), the wind should become optically thin at $\sim 450\ \mu\text{m}$, and the free-free emission will then be proportional to $\nu^{-0.1}$. We may therefore start to pick up some dust emission shortward of $450\ \mu\text{m}$. We currently have no observations that enable us to measure the mass of dust and neutral gas in the disk.

5.2. Embedded HAEBE Stars

All embedded HAEBE stars are essentially "classical" HAEBEs, i.e., they illuminate reflection nebulae and are still located within the clouds in which they were formed. On average they are younger than the isolated HAEBEs and many drive bipolar outflows and can be deeply embedded. Their spectral classifications, and hence the ages, are also more uncertain, because some of them are very faint or invisible in the UV and visible parts of the spectrum. Some of them also have much higher accretion rates and veiling than isolated HAEBEs. Many of the embedded stars that we have observed are early to mid-B stars illuminating large reflection nebulae. With one or two exceptions they are non-detections, i.e., they no longer have observable disks in the sub-millimeter. These non-detections will be discussed in the next section (Section 6).

Lkh α 198 and **V 376 Cas** are late B and A or F stars at a distance of $\sim 600\ \text{pc}$ (Table 1). Both stars have been well studied at optical, near-infrared, far-infrared and sub-millimeter wavelengths. Lkh α 198 has a deeply embedded infrared companion, Lkh α 198 B, $\sim 6''$ to the north (Lagage et al. 1993; Koresko et al. 1997) with a luminosity of $\sim 100\ L_{\odot}$, i.e., roughly similar to that of Lkh α 198. Lkh α 198 drives a bipolar molecular outflow (Cantó et al. 1984; Nakano et al. 1990) and excites several Herbig–Haro objects. A deeply

embedded, cold protostellar object, LkH α 198-mm, $\sim 19''$ to the northwest, dominates the sub-millimeter emission in this region (Sandell and Weintraub 1994a; Henning et al. 1998) and may power the large bipolar molecular outflow (Cantó et al. 1984; Nakano et al. 1990) that originally was believed to originate from LkH α 198. LkH α 198 and LkH α 198 B lie inside an elliptical limb-brightened nebulosity. Both stars appear to excite Herbig-Haro objects (Corcoran et al. 1995; Koresko et al. 1997). Koresko et al. (1997), using adaptive optics compensated speckle observations in the H band, found a bar-like structure extending to $3''$ on each side of LkH α 198. They found LkH α 198 B to be extended at J and H as well, suggesting that both stars may be surrounded by circumstellar disks. Perrin et al. (2004) used laser guide star adaptive optics and near-infrared dual-channel imaging polarimetry to uncover a strongly polarized biconical nebula around LkH α 198 with a radius of $5''$, as well as a polarized, extremely blue, jet-like feature emanating from LkH α 198 B. Although these results strongly suggest that LkH α 198 has a disk, they still largely trace the surrounding infalling envelope. V 376 Cas has a bar feature, it illuminates a sickle-shaped nebulosity, is very highly polarized and excites several Herbig-Haro knots (Pirola, Scaltriti & Coyne 1992; Corcoran et al. 1995). All of this suggests that it is also surrounded by a circumstellar disk. Such a disk has been confirmed by speckle interferometry at H and K' (Smith et al. 2004), which show that V 376 Cas is surrounded by a compact, nearly edge-on flared disk with a radius of 100 mas.

CO $J = 2 \rightarrow 1$ mapping of the central part of the CO outflow with $20''$ spatial resolution (Sandell and Weintraub 1994a) suggested that there is more than one outflow in the vicinity of LkH α 198 and V 376 Cas. LkH α 198 and/or LkH α 198 B could be driving one outflow, V 376 Cas another, and LkH α 198-mm could be the source for the large scale CO outflow. High spatial resolution CO $J = 1 \rightarrow 0$ imaging ($\sim 6''$) with the Berkeley Illinois Maryland Array (BIMA) supplemented by single dish mapping to fill in missing short spacings (Matthews et al. 2007) confirm that there are several outflows. V 376 Cas drives one outflow, LkH α 198-mm drives another, while there appear to be two outflows associated with LkH α 198. LkH α 198 definitely powers one outflow. The second outflow is closer to LkH α 198 B, but since it does not show any high velocity wings, they associate the driver of the outflow with a yet unseen source between LkH α 198 and LkH α 198 B.

Our $850 \mu\text{m}$ map (Figure 7) shows extended dust emission over $\sim 3'$. In the northeast, the emission becomes negative due to more extended and possibly stronger emission to the west, i.e., an artifact due to chopping. The $850 \mu\text{m}$ dust emission is dominated by the protostellar source LkH α 198-mm. There is a tail of emission to the southeast from LkH α 198-mm and a fainter ridge extending north towards V 376 Cas. The southwestern extension can be explained by an extended source, $\sim 11''.4 \times 5''.6$, centered on LkH α 198 and its infrared companion with a position angle similar to that of the binary system (Table 2a). The peak of

emission is close to LkH α 198 B, which agrees with the 1.3 mm map by Henning et al. (1998), which has slightly better angular resolution and shows a secondary peak on LkH α 198. Both the 1.3 mm map and the 850 μ m map suggest that LkH α 198 and LkH α 198B are surrounded by dust disks. We estimate that at most one third of the emission from the LkH α 198 binary is due to LkH α 198. If we assume a dust temperature of 50 K and a $\beta = 1.5$, we find that LkH α 198 has a disk mass of $\leq 0.15 M_{\odot}$.

Interferometer observations (Di Francesco et al. 1997; Matthews et al. 2007) at 2.7 mm did not have enough sensitivity to detect LkH α 198 or V 376 Cas, although Di Francesco et al. did detect LkH α 198-mm. They found it to be unresolved or marginally resolved, while our SCUBA observations show it to be quite extended (FWHM $\sim 20''$) with an integrated flux density of 1.78 Jy. We do see an enhancement in continuum level near V 376 Cas, but the position we deduce is off by $3''$ from the optical position and it could simply be due to emission from the surrounding dust cloud. However, observations at 450 or 350 μ m at JCMT or CSO would have enough spatial resolution to resolve the HAEBE binary from the protostellar source and to determine how much of the emission originates from LkH α 198-IR and how much originates from LkH α 198.

V 892 Tau is a heavily obscured ($A_V \sim 10$ mag) late B star with a strong infrared excess (Elias 1978; Strom & Strom 1994). It was first discovered by Elias (1978) in a near-infrared survey of the Taurus dark cloud complex. Inspection of H $_2$ column density maps by Goldsmith et al. (2008) show it to be located in an opaque area of L 1495. Multi-epoch trigonometric parallax observations with the Very Long Baseline Array (VLBA) (Torres et al. 2009) indicate that L 1495 is on the near side of the Taurus complex at a distance of ~ 130 pc. Hernández et al. (2004) derived a spectral type of B8 Ve for V 892 Tau, while Strom & Strom (1994) classified it as B9. Spectral types as late as A6 have been reported in the literature (Berrilli et al. 1992). near-infrared speckle observations and mid-infrared interferometry show that it is a close binary with a separation of 50 mas (Smith et al. 2005; Monnier et al. 2008). Monnier et al. (2008) analyzed the SED for the binary and deduced a bolometric luminosity of $350 L_{\odot}$ (corrected to 130 pc), with both stars having the same spectral type. The inferred luminosity is too low for two B8 V stars, and the stars are more likely spectral type B9 V. Mid-infrared segment-tilting interferometry (Monnier et al. 2008) shows a circumbinary disk inclined at 60° with an inner hole diameter of 33 AU.

V 892 Tau was first detected in dust continuum at 1.3 mm by Beckwith et al. (1990). Mannings (1994) carried out extensive (sub-)millimeter photometry (1.3 and 1.1 mm, 850, 800, 750, 450, and 350 μ m) of V 892 Tau with the single pixel detector UKT14 on JCMT, and found it to have a very flat spectral index, $\alpha = 2.18 \pm 0.10$. It was mapped at 1.3 mm by Henning et al. (1998), who found it compact and unresolved. Di Francesco et al. (1997)

detected it in the dust continuum with the VLA at 7 mm and at 2.7 mm with the BIMA array, but did not resolve the continuum emission. Recent CARMA observations by Hamidouche (2010) at 2.7 and 1.3 mm resolve the disk with a size of $0''.4$ at 2.7 mm.

V 892 Tau is a very bright X-ray source (Strom & Strom 1994). It is only seen in hard X-rays, suggesting that it has low or no accretion (Hamidouche et al. 2008). However, it is a thermal radio source (Skinner, Brown, & Stewart 1993; Di Francesco et al. 1997), suggesting that there is still some accretion going on, although it is not known to drive a molecular outflow. Strom & Strom (1994) deduced an age of ~ 3 Myr by comparing its location on the H-R diagram with two different evolutionary track models. Hernández et al. (2004) assumed it to be a B8 V star and found it to lie on the main sequence. Strom & Strom (1994) found it somewhat puzzling that the star would appear older than nearby T Tauri stars, when it is still deeply embedded in the molecular cloud core and illuminates a reflection nebula. Monnier et al. (2008) find that it has an SED resembling a transition disk object and a clear inner gap in the disk, which is one of the main signatures of an evolved disk. However, since it is a binary, the gap in the disk is most likely caused by the binary.

Our SCUBA images show that V 892 Tau is unresolved at both 850 and 450 μm (Figure 8), consistent with the small size found by Hamidouche (2010). We also retrieved and analyzed archive *Spitzer* MIPS images at 24 and 70 μm . At 24 μm the star is heavily saturated and we could not deduce a flux density. The 70 μm image is of excellent quality and shows extended warm nebulosity east and north-west of the star (Figure 9). We did psf photometry of this image and deduced a color corrected flux density at 70 μm of 27.0 ± 0.4 Jy. However, examination of the residuals from psf-fitting indicate that the star is mildly saturated. The deduced flux is therefore strictly a lower limit, although probably not by much. Di Francesco et al. (1998) mapped V 892 Tau with the Kuiper Airborne Observatory (KAO) at 50 and 100 μm . They found much lower flux densities than IRAS. At 50 μm they found a peak flux density of 59.1 ± 5.5 Jy and a source size of $25''$, resulting in an integrated flux of 86 ± 45 Jy. Although the star dominates at 50 μm , the KAO observations probably include some contribution from the extended warm nebulosity, which we see in the MIPS 70 μm image.

Isothermal graybody fits fit the millimeter and sub-millimeter data very well, but underestimate the flux at 100 μm and shorter wavelengths. Since the KAO beam at a 100 μm is $\sim 30''$, the observed 100 μm flux density is an upper limit. The temperature of the dust emission is therefore somewhat uncertain; 40 K is probably a reasonable assumption. For an assumed dust temperature of 40 K we find a dust emissivity, $\beta = 0.52$, and a disk mass of $0.009 M_{\odot}$. If the dust temperature is 60 K we get $\beta = 0.40$, and a dust mass of $0.004 M_{\odot}$. In both cases the dust is somewhat optically thick at 850 μm , but less so for warmer dust.

As we can see from Figure 18 we can fit the millimeter and sub-millimeter data extremely well, but the $70\ \mu\text{m}$ flux density is underestimated. The V 892 Tau disk therefore appears very similar to the isolated HAEBE stars, which all require a warm dust component. The dust emissivity, which is reasonably well constrained, is rather low, suggesting that grain growth has already occurred in the disk. V 892 Tau has all the characteristics of an evolved disk.

LkH α 101 is a heavily obscured ($A_V \sim 10$ mag), infrared bright Herbig Be star with a spectral type \sim B0 Ve and luminosity of $4 \times 10^4\ L_\odot$, that is embedded in the dark cloud L 1482 at a distance of ~ 700 pc (Herbig, Andrews & Dahm 2004). It illuminates the reflection nebula NGC 1579 and ionizes the H II region S 222 (Herbig 1960, 1971; Herbig, Andrews & Dahm 2004). It is the brightest member of a deeply embedded cluster of heavily reddened near-infrared sources (Barsony, Schombert and Kis-Halas 1991; Aspin and Barsony 1994) and faint cm-radio sources (Becker & White 1988; Stine and O’Neal 1998), most of which are probably young PMS stars. Interferometric imaging in the near- and mid-infrared (Tuthill, Monnier & Danforth 2002; Tuthill et al. 2002) shows that LkH α 101 surrounded by a dust disk with a hot inner wall facing the central star. The disk is seen nearly face on and shows a central hole or cavity. At $11.15\ \mu\text{m}$ the size of the disk is $\sim 0''.06$ (10 AU). They also find that the star is a binary system with a low luminosity companion $\sim 0''.18$ to the northwest; this result has been independently confirmed by speckle interferometry (Alvarez et al. 2004). LkH α 101 is a strong radio source with a spectrum consistent with a spherically symmetric constant velocity wind (Becker & White 1988; Gibb & Hoare 2007, and references therein). Although the star has been well studied in the centimeter regime, there is a lot of scatter in the free-free flux densities and size, even if we only look at VLA A-configuration data (Figure 12). This may be due to contamination from the surrounding H II region and because different array configurations resolve out more or less of the extended emission. It is also possible that the free-free emission is variable. If we use all high-spatial resolution observations (i.e., VLA A-array and MERLIN) available in the literature we get a spectral index $\alpha = 0.71 \pm 0.07$, which is steeper than but consistent with what Gibb & Hoare (2007) found, i.e., $\alpha = 0.61$.

In the sub-millimeter (Figure 11), LkH α 101 is located at the southwestern boundary of an extended elliptical cloud with a size of $3' \times 1'$. Although the map covers five of the deeply embedded VLA sources seen by Stine and O’Neal (1998), only LkH α 101 has a sub-millimeter counterpart. At $850\ \mu\text{m}$ the star appears somewhat extended with a size of $\sim 6''.5 \times 2''.6$ or ~ 2800 AU. This size is probably an over-estimate, since the mapping was done in scan-map mode with relatively poor sky transmission. The dust disk, however, is not very massive, since most of the emission at $850\ \mu\text{m}$ is due to free-free emission. In the low signal-to-noise $450\ \mu\text{m}$ map the emission is completely dominated by the surrounding dust cloud and we cannot derive a flux density for the star. After subtracting the free-free

emission we are left with ~ 180 mJy at $850\ \mu\text{m}$. If we assume $\beta = 1$ and a dust temperature of 50 K we find that LkH α 101 could have a disk mass of $\sim 0.005\ M_{\odot}$, which is similar to the disks of isolated Ae stars.

AB Aur is a bright, optically visible A1 Ve star located on the front side of the dark cloud L 1517 in the Taurus-Auriga dark cloud complex at a distance of 144 pc (van den Ancker et al. 1998; Hernández et al. 2004). It is $\sim 3'$ away from the classical T Tauri star SU Aur (spectral class G2 IIIe), which is also surrounded by an accretion disk (Weintraub, Sandell, & Duncan 1989; Andrews & Williams 2005). AB Aur was included in the Meeus et al. (2001) sample of isolated HAEBEs. However, AB Aur is not an isolated HAEBE star, since it is still located within the dark cloud in which it was formed. Its age, however, 4 ± 1 Myr (DeWarf et al. 2003) is similar to some of the younger isolated HAEBEs. Near-infrared coronagraphic imaging with adaptive optics on Subaru (Fukagawa et al. 2004) show extended emission as far as $\sim 4''$ from the star and resolve the emission into a spiral-like structure with at least two spiral arms.

AB Aur has been extensively studied in the (sub-)millimeter, both with single dish telescopes and interferometers (Mannings 1994; Mannings & Sargent 1997; Piétu, Guilloteau & Dutrey 2005; Semenov et al. 2005; Corder et al. 2005; Lin et al. 2006). The star is detected in free-free emission (Güdel et al. 1989; Skinner, Brown, & Stewart 1993; Rodríguez, Zapata, & Ho 2007) but is very faint, emitting only 0.2 ± 0.02 mJy at 3.6 cm. High spatial resolution ($0''.6$ - $2''$) interferometric imaging at millimeter wavelengths (Piétu, Guilloteau & Dutrey 2005; Corder et al. 2005; Lin et al. 2006) in various CO transitions and their isotopomers show that disk is seen nearly face-on with an inclination angle between 20° and 40° and appears to be non-Keplerian. Piétu, Guilloteau & Dutrey (2005) and Corder et al. (2005) resolve the continuum emission and find it asymmetric, possibly tracing the spiral structure seen in near-infrared. Lin et al. (2006), who observed AB Aur in $^{12}\text{CO}\ J=3 \rightarrow 2$ with the SMA, confirm by tracing the inner spiral arm seen in the near-infrared in several velocity channels that the disk deviates from Keplerian rotation. Their $870\ \mu\text{m}$ continuum observations show a central depression towards the star, suggesting the presence of a large inner dust-free hole around the star. Lin et al. suggest that both the central depression and the spiral structure with non-Keplerian motions could be caused by a giant planet forming in the disk. This view is also supported by Oppenheimer et al. (2008), who did adaptive optics coronagraphy and polarimetry of the AB Aur inner disk. They find an azimuthal clearing in the dust at a radius of ~ 102 AU along with a clearing of dust at radii inside this annulus, suggesting the formation of at least one planetary body at ~ 100 AU. Rodríguez, Zapata, & Ho (2007) also detected faint radio emission from a source located about 40 AU from AB Aur, suggesting that the star could have a low mass stellar companion.

We find AB Aur unresolved both at 850 μm and 450 μm (Figure 13), even though Lin et al. (2006) resolved it at 870 μm with a size of $3''.1 \times 1''.9$. The star also appears compact in a MIPS 70 μm image, but the star is somewhat saturated and we could not retrieve a flux density. Our flux density measurements with SCUBA (Table 2a) agree within errors with our less accurate UKT 14 photometry (Table 2b). Figure 14 shows a least-squares graybody fit to all reliable (sub-)millimeter and far-infrared data of AB Aur, resulting in a dust temperature of 66 K and a dust emissivity index, $\beta = 1.05$. If one assumes a normal gas-to-dust ratio, the mass of the disk is $\sim 0.006 M_{\odot}$. This disk mass is consistent with the results of Lin et al. (2006) and Corder et al. (2005), but lower by a factor of three compared to the mass obtained by Piétu, Guilloteau & Dutrey (2005).

VY Mon is a late B to early A star at the southern edge of the bright reflection nebula IC 446 at a distance of 800 to 900 pc (Casey & Harper 1990). The star is heavily reddened and variable with a bolometric luminosity of $\sim 870 L_{\odot}$ for a distance of 800 pc. Thé, de Winter and Pérez (1994) assigned it a spectral class B8:e, while Mora et al. (2001) classified it as A5 Vep. The observed luminosity appears too high for an A5 star, and we have therefore adopt the spectral classification by Thé, de Winter and Pérez, i.e., B8. The star is a faint radio source (Felli et al. 1982). VY Mon drives a high-velocity outflow, which we mapped in CO $J = 2 \rightarrow 1$ on JCMT³. Figure 15 shows high velocity emission from about -28 to $+18 \text{ km s}^{-1}$. The outflow is very compact and appears to be seen pole on, since the blue and red-shifted outflow lobes are completely overlapping (Figure 16). Wang & Looney (2007) analyzed near-infrared and *Spitzer* IRAC observations of IC 446 and find that VY Mon is part of a compact group of 26 YSOs within a radius of 0.5 pc.

VY Mon was mapped at 1.3 mm by Henning et al. (1998), who found strong, compact 1.3 mm emission centered on the star and faint extended emission from the dark cloud south of VY Mon. We have no SCUBA observations of VY Mon, and our single beam photometry with UKT14 only goes down to 800 μm (Table 2b). At 1.3 mm our observed flux density is higher than what Henning et al. (1998) measured from their higher spatial resolution IRAM observations, suggesting that we pick up some extended emission from the surrounding cloud in our larger beam. A graybody fit to the (sub-)millimeter data underestimates the far-infrared flux densities observed by Casey & Harper (1990) and gives $\beta = 1.9$ and a disk mass of $1.9 M_{\odot}$. This mass is almost certainly too high to be from the disk alone and suggests that our single dish observations may include a substantial fraction from the surrounding infalling envelope. The high value of β is also consistent with unevolved (small) dust grains, which is additional evidence that this flux is capturing emission from

³The original data for these CO observations are missing in the JCMT archive and in our personal archive, but we have preserved in our records and present in this paper the maps derived previously from those data.

the infalling envelope.

AFGL 961 is a deeply embedded ($A_V \geq 18$ mag), young, high-luminosity, double star system with a separation of $\sim 6''$ (Castelaz et al. 1985). Both stars appear to be early B stars and are surrounded by extended nebulosity in the near-infrared (Castelaz et al. 1985; Aspin 1998). AFGL 961 is southwest of the the H II region NGC 2244 (the Rosette nebula) and part of the Mon OB2 association, which lies at a distance of 1.4 - 1.6 kpc (Turner 1976; Hensberge, Pavloski & Verschueren 2000). Here we adopt 1.5 kpc for the distance to AFGL 961. The double star system is located at the center of a large bipolar molecular outflow (Lada and Gautier 1982; Dent et al. 2009). The main outflow has an extent of $5'$ at a P.A. of 45° , but Dent et al. found at least one other, more compact outflow orthogonal to the main outflow. Early millimeter continuum observations (Henning, Pfau & Altenhoff 1990) easily detected AFGL 961, but had insufficient spatial resolution to identify which star is responsible for the dust emission. The same was true with a more recent (sub-)millimeter imaging survey by Klein et al. (2005), who showed that AFGL 961 is embedded in a dense sub-millimeter core with a size of 0.3 pc and a mass of $\sim 550 M_\odot$.

The eastern component, AFGL 961 A (also known as AFGL 961 E) is more deeply embedded and a faint free-free emission source (Bally & Predmore 1983), with stronger thermal excess in the near-infrared than AFGL 961 B (also known as AFGL 961 W), although both stars have Br α in emission (Aspin 1998). AFGL 961 B shows the $2.3 \mu\text{m}$ CO bandheads in emission, while the eastern source shows a featureless spectrum except for the Br α emission. Analysis of 2MASS and deeper near-infrared imaging (Li & Smith 2005; Román-Zúñiga et al. 2008) shows that the majority of stars in the Rosette molecular cloud complex are contained in clusters. In the near-infrared AFGL 961 with its two early B stars, appears to be a very small cluster that is barely detectable in the deep near-infrared imaging by Román-Zúñiga et al. (2008), who identify it as PL06. Recent high-spatial resolution mid-infrared and sub-millimeter imaging with the SMA (Williams et al. 2009) show that PL06 is a deeply embedded, very young cluster. They find three continuum sources at 1.4 mm. The strongest one, SMA 1 coincides with AFGL 961 A, while two of them have no near- or mid-infrared counterparts. SMA 2 appears to be starless, but accreting, i.e., a pre-stellar, collapsing dense core, while SMA 3 drives an outflow, and is possibly driving the large NE-SW outflow. SMA 3 is therefore a Class 0 protostar. They also identify a third mid-infrared source, AFGL 961 C, $\sim 30''$ west of A, with strong mid-infrared excess, but they did not detect it in continuum at 1.4 mm. AFGL 961 A was also detected with the VLA at 7 mm, with a flux density of 8.1 ± 0.1 mJy (Zapata et al. 2009).

At $850 \mu\text{m}$ we find a strong elliptical source centered slightly northwest of AFGL 961 A and superposed on relatively strong, extended emission from the surrounding cloud (Fig-

ure 17). At $450\ \mu\text{m}$ the elliptical source is resolved into two compact sources. The eastern one is approximately centered on AFGL 961 A, possibly with some contribution from SMA 2. The second $450\ \mu\text{m}$ source, AFGL 961 SMM overlaps with SMA 3, but is definitely centered east of SMA 3, suggesting that there are even more sub-millimeter sources in the AFGL 961 cloud core. To learn more about this complicated young cluster, we therefore also retrieved and reduced *Spitzer* archive MIPS 24 and $70\ \mu\text{m}$ images of AFGL 961. The $70\ \mu\text{m}$ image is plotted in gray scale in Figure 17 and overlaid with the $850\ \mu\text{m}$ SCUBA image in contours. In Figure 17 we also separately plot both the 70 and the $24\ \mu\text{m}$ images over the same area mapped by SCUBA. AFGL 961 A and B are heavily saturated both at 24 and $70\ \mu\text{m}$, but SMA 3 coincides with a clear $70\ \mu\text{m}$ peak. There is, however, a clear extension to the southeast towards A & B confirming that the western $450\ \mu\text{m}$ source has a $70\ \mu\text{m}$ counterpart. What we see at 450 and $70\ \mu\text{m}$ are probably two partially blended sources, one of which coincides with SMA 3. At $24\ \mu\text{m}$ AFGL 961 C is also seen as a double source, but with the southeastern component stronger than C. The second source (which we call 961 D) is also seen by Williams et al. (2009) at $20\ \mu\text{m}$ as a faint extension to the southwest. At $70\ \mu\text{m}$ there is no clear peak at C and D although both sources lie within the relatively bright $70\ \mu\text{m}$ core. A much stronger ridge of emission is seen protruding to the south-southeast of A & B. This ridge of emission is also seen in the SCUBA images, and suggests that there may be yet more deeply embedded sources hidden in the AFGL 961 cloud core.

Analysis of the embedded cluster population is outside the scope of this paper, but AFGL 961 A has all the characteristics of a very young Herbig Be star, which most likely is surrounded by an accretion disk and an infalling envelope. Although Williams et al. (2009) did not find an outflow from the star, the spectral index of the free-free emission between 5 and 15 GHz is consistent with the free-free emission originating in an ionized wind or jet (Snell & Bally 1986). A graybody fit to all (sub-)millimeter data gives a dust temperature of $\sim 37\ \text{K}$, a dust emissivity, $\beta \sim 1.51$, resulting in a total mass of the disk/envelope of $12.5\ M_{\odot}$. This fit overestimates slightly the flux density of SMA 1 at $1.4\ \text{mm}$, but is rather close to the sum of SMA 1 and 2, suggesting that we pick up emission from both sources in our much larger SCUBA beam. On the other hand the fit severely underestimates the $7\ \text{mm}$ flux density, which only comes from A (SMA 1), suggesting that part of the emission may be free-free emission, rather than thermal dust emission.

To get a better idea of the true luminosity and mass of AFGL 961 A we have additionally explored the archive of two-dimensional axisymmetric radiative transfer models of protostars calculated for a large range of protostellar masses, accretion rates, disk masses, and disk orientations created by Robitaille et al. (2006). This archive also provides an on-line regression tool for selecting all the best fit SEDs. We use all near-, mid-infrared and millimeter photometry that resolve the star as well as a *Spitzer* IRS Short-High (SH, i.e., 9.9

- 19.6 μm) spectrum from the *Spitzer* archive. Our results are similar to what Williams et al. (2009) found using the same tool. The best fit models predict a stellar mass of 10 - 12 M_{\odot} , obscured by 12 - 18 mag of visual extinction. These models result in a disk mass of 0.02 - 0.4 M_{\odot} , an envelope mass of 20 - 30 M_{\odot} , an envelope accretion rate of $10^{-6} M_{\odot} \text{ yr}^{-1}$, a stellar age of $\sim 10^4$ yr and a bolometric luminosity of $\sim 3,000 L_{\odot}$. Williams et al. (2009) find a slightly higher luminosity, $L_{bol} \sim 4000 L_{\odot}$, but otherwise our results are very similar. De Wit et al. (2009) modeled the observed SED of AFGL 961 A with a spherical model with a radial density profile described by a simple power law using partially the same data as we do. Their best fit model predicts a power law index of 0.5 and gives a total mass of 25 M_{\odot} and a luminosity of $\sim 6000 L_{\odot}$. However, some of the data, like MIPS 70 μm and our SCUBA data included in their SED, includes contributions from the nearby sources SMA 2 and AFGL961 B and therefore the derived luminosity is over-estimated.

AFGL 961 A appears to be a very young star driving an ionized outflow (and possibly a molecular outflow) that is surrounded by a large accretion disk. The modeling results by us and Williams et al. predict a protostellar mass of 10 - 12 M_{\odot} and a luminosity of 3000 - 4000 L_{\odot} , which correspond to a B2 star. Since the star is still heavily accreting, it may end up as perhaps a B1 star by the time it reaches the main sequence.

R Mon is a deeply embedded HAEBE star at the apex of the NGC 2261 nebula, also known as Hubble’s Variable Nebula. In the catalogue by Thé, de Winter and Pérez (1994) the spectral type is given as B0e. This is clearly incorrect, since the bolometric luminosity of the star is only $\sim 740 L_{\odot}$ at a distance of 800 pc (Cohen et al. 1985). Mora et al. (2001) classified it as B8 IIIev, which is consistent with the stellar luminosity of $\sim 450 L_{\odot}$, determined by Natta et al. (1993). It is a binary system with a low-mass companion located $\sim 0''.7$ to the northwest (Close et al. 1997). The star drives a prominent molecular outflow and excites the HH object HH 39, located in a small anonymous dark cloud $\sim 7'$ north of R Mon (Cantó et al. 1981; Jones & Herbig 1982; Brugel et al. 1984). R Mon was the first HAEBE star to be detected with a millimeter-interferometer (Sargent & Beckwith 1987). They did not have enough sensitivity to detect the star with the OVRO three-antenna array in continuum at 3 mm, but detected $^{13}\text{CO } J = 1 \rightarrow 0$ in the envelope surrounding the star. The star is a faint VLA source, 0.29 ± 0.03 mJy at 6 cm (Skinner, Brown, & Stewart 1993), with a spectral index in the radio regime of $\alpha = 0.9 \pm 0.4$, consistent with wind excited free-free emission. The first (sub-)millimeter (1300, 1100, 800, 450, and 350 μm) detection of R Mon was reported by Mannings (1994), who also determined that R Mon had a disk/envelope with a substantial mass of 0.24 M_{\odot} . Recently Fuente et al. (2003) detected the continuum emission from R Mon at 2.7 mm using the PdB interferometer. They found a total flux of 6.4 mJy and claimed that the emission was extended on the $3''$ - $4''$ level. They also observed R Mon with the VLA at 1.3 and 0.7 cm, but do not report integrated

flux densities. In a follow-up paper (Fuentes et al. 2006), they observed R Mon with the PdB interferometer in the continuum at 2.7 and 1.3 mm and in the rotational lines of ^{12}CO $J = 1 \rightarrow 0$ and $J = 2 \rightarrow 1$. Although they find a Keplerian signature in their CO images and derive a mass for the central star of $8 M_{\odot}$, based on the bolometric luminosity R Mon is a late B (see above) and cannot be as massive as $8 M_{\odot}$. The derived CO rotation curve is most likely heavily contaminated by the strong outflow from the star.

We have observed R Mon at various wavelengths between 350 and 1300 μm in the dust continuum with the single pixel bolometer UKT14. The star was detected at all wavelengths (Table 2b). Peak-up observations of the star suggest that the emission is compact, which agrees with the results by Fuentes et al. (2006), who barely resolved it at 1.3 mm with a size of $0''.3$. Fitting an isothermal graybody model provides a dust opacity index $\beta = 1.3$ and a disk mass $\sim 0.1 M_{\odot}$ (Table 4). The disk mass we derive is much larger than found by Fuentes et al. (2006), because we find a much higher dust emissivity, 1.3 vs 0.3 - 0.5 deduced by Fuentes et al. Our observations cover a much larger frequency range than Fuentes et al., and, since the free-free emission is negligible in the sub-millimeter regime, our deduced dust emissivity is rather well constrained (see Figure 19). It is possible, however, that the envelope may contribute to the observed dust emissivity, especially since most of our data come from single pixel observations.

HR 5999 (HD 144568) illuminates a bright reflection nebula in the central part of the Lupus 3 dark cloud complex at a distance of 208 pc (Preibisch et al. 2007). The star varies strongly and irregularly on time scales of weeks (Pérez et al. 1992). HR 5999 was classified as A6 III with an error of about one subclass (Blondel & Tjin A Djie 2006) and forms a $\sim 45''$ wide proper-motion binary system with the A1.5 star HR 6000 (Preibisch et al. 2007). van Boekel et al. (2005) found a similar spectral type as Blondel & Tjin A Djie, A5-7 III/IVe, and deduced a stellar mass of $3.2 \pm 0.5 M_{\odot}$ and an age of 0.5 Myr. The star has a strong far-infrared excess (Hillenbrand et al. 1992) and shows broad silicate emission in the mid-infrared (Siebenmorgen et al. 2000), but it is a rather faint millimeter source and it was not detected at 1.3 mm (Henning et al. 1994). Preibisch et al. (2007) observed the star in the mid-infrared with MIDI at the ESO Very Large Telescope Interferometer (VLTI) and was able to resolve the circumstellar disk around the star. They found that the disk is highly inclined, at 58° , and truncated at 2.6 AU, likely due to a close binary. We barely detect the disk as an unresolved point source at 850 μm (Table 2a). A graybody fit to the 1.3 mm upper limit by Henning et al. (1994), our 850 μm flux density, the 100 μm IRAS upper limit, and the IRAS 60 μm flux density, yields a dust temperature of 41 K, a $\beta = 1.75$, and a dust mass of $\sim 0.009 M_{\odot}$, which is comparable to the mass estimated by Siebenmorgen et al. (2000).

MWC 297 is a highly reddened ($A_V \sim 8$ mag) early type star of spectral class B1.5 Ve, with a luminosity of $3 \times 10^3 L_\odot$ and a distance of 250 pc (Drew et al. 1997). It has very strong and variable Balmer line emission (Finkenzeller & Mundt 1984) and is a relatively strong radio source (Skinner, Brown, & Stewart 1993; Drew et al. 1997). Di Francesco et al. (1998) found the far-infrared emission from MWC 297 to be extended with a size of about one arcminute at 100 μm . However, at 1.3 mm the map of MWC 297 (Henning et al. 1998) shows that the millimeter emission from the star appears to be compact, and that there is strong emission from the surrounding dust cloud to the northeast of the cloud. The 1.3 mm map also shows compact emission from a very red 2MASS source (J18273709-034938), with a K magnitude of 8, located about $40''$ west of MWC 297. Manoj et al. (2008), using the SMA, found the 1.3 mm continuum emission to be unresolved with a size of ≤ 80 AU. They did not detect molecular gas emission in the $J=2 \rightarrow 1$ rotational transitions of ^{12}CO , ^{13}CO , and C^{18}O . They deduced a very low dust emissivity index, $\beta = 0.1 - 0.3$, and suggested that the low β index could be due to grain growth if the dust is optically thin. Alonso-Albi et al. (2009) observed the star with the PdB interferometer at 1.3 and 2.6 mm and with the VLA at 1.3 cm and 7 mm. They also found the millimeter emission to be compact and modeled the SED with a disk with a radius of ~ 28 AU seen approximately face-on, consistent with near-infrared interferometric observations (Acke et al. 2008), who found that the disk is seen with an inclination of $\leq 40^\circ$.

Our sub-millimeter maps (Figure 20) agree with the 1.3 mm map. MWC 297 dominates the emission at 850 μm , while the star is quite faint at 450 μm . At 450 μm the emission from the surrounding cloud is much stronger than from MWC 297, suggesting that the sub-millimeter SED is exceptionally flat. Follow-up observations by Sandell et al. (in prep) with BIMA and the VLA, show that the observed shallow SED at millimeter wavelengths is due to free-free emission. They observed MWC 297 with the VLA in the AnB configuration at 6 and 2.0 cm and also re-analyzed VLA data obtained by Skinner, Brown, & Stewart (1993). The Skinner, Brown, & Stewart CnD data show that MWC 297 powers a large bipolar ionized jet. A fit to the VLA data shows that the radio emission has a spectral index, $\alpha \sim 0.97$, while the size decreases as $\nu^{-0.8}$, as is typically seen in collimated thermal jets. If we include data at wavelengths out to 3 mm, we get a spectral index, $\alpha \sim 1.03$, i.e., essentially the same as we got from the more uncertain fit from VLA data alone (Figure 21). The thermal emission from the jet can therefore explain all the emission at 3 mm and there is no evidence for any excess due to cold dust emission. There is a hint of a dust excess at 850 μm and almost certainly some excess at 450 μm , suggesting that the wind becomes optically thin somewhere around 300 - 600 GHz. MWC 297 looks therefore very similar to MWC 349, in that the emission in the millimeter and sub-millimeter regime is dominated by free-free emission. The bipolar morphology seen in the VLA maps suggests that the disk is seen

nearly edge-on, as is the case for MWC 349. Both stars appear to be surrounded by disks, which are largely ionized and only contain a small fraction of neutral gas and dust.

The BD+40°4124 region forms a small pre-main-sequence stellar cluster with three bright emission line stars. Herbig (1960) identified the first two, BD+40°4124 and V 1686 Cyg, as HAEBE stars. The third star, V 1318 Cyg, is a deeply embedded binary system with a separation of $\sim 5''$ and a total luminosity of $\sim 1600 L_{\odot}$ (Aspin, Sandell & Weintraub 1994). The southern member of this binary, V 1318 Cyg S, is more deeply embedded with a visual extinction of 10 mag or more. Aspin, Sandell & Weintraub (1994) found that the position of V 1318 Cyg S coincides with the position of a compact sub-millimeter source that has a luminosity similar to that of a HAEBE star. None of the stars in the BD+40°4124 cluster show any free-free emission at centimeter wavelengths (Skinner, Brown, & Stewart 1993; Palla et al. 1995), except perhaps BD+40°4124, near which Skinner, Brown, & Stewart detected faint emission at 3.6 cm and 6 cm.

Palla et al. (1995) discovered a compact molecular outflow and an H_2O maser, which appear to be excited by V 1318 Cyg S. Looney et al. (2006), however, who observed the region in the 3.1 mm continuum with BIMA, found that the dust emission is offset by $1''.1$ to the north-east from V 1318 Cyg S, and argue that the dust emission originates from a deeply embedded intermediate mass protostar V 1318 Cyg S-mm, rather than from either component of V 1318 Cyg S identified by Aspin, Sandell & Weintraub (1994). These results are supported by the less accurate results by Di Francesco et al. (1997), who detected the star in continuum at 2.7 mm with the PdB interferometer, and found a similar offset, $0''.9$, from the southern component. More importantly, VLBA observations of the H_2O masers toward BD+40°4124 (Marvel 2005) indicate that it is associated with the sub-millimeter source rather than with the optically visible star. It is therefore the invisible millimeter source that drives the outflow, not V 1318 Cyg S.

Figure 22 shows the 850 and 450 μm SCUBA images of the BD+40°4124 region. It is clear from these images that neither BD+40°4124 and V 1686 Cyg are associated with any significant sub-millimeter continuum emission. Because of the extended emission from the molecular cloud in which these stars were born, we cannot place a very stringent limit on the dust emission; at 850 μm our upper limit is ~ 35 mJy beam $^{-1}$. Examination of MIPS 24 and 70 μm images show that all HAEBE stars in this region are saturated at 24 μm (Table 3). At 70 μm there is some extended emission near BD+40°4124, most likely heated dust from the surrounding reflection nebulosity. There is strong, compact, 70 μm emission from the vicinity of V 1318 Cyg S (Table 3), almost certainly coming from the deeply embedded protostar, V 1318 Cyg S-mm. This is where we find a strong, extended ($8'' \times 3''$) sub-millimeter source (Table 2a). Although it is possible that some of the emission could

be due to V 1318 Cyg S, we assume that all the emission comes from the deeply embedded millimeter source. A graybody fit to the SCUBA and MIPS data give a dust emissivity of 0.85 and a total mass of $1.9 M_{\odot}$ (Table 4), suggesting that we see the disk and envelope of a young high-mass protostar.

PV Cep is an irregularly variable star at the head of the cometary nebula GM 29 that illuminates this fan-shaped nebula; it is located at a distance of 500 pc (Cohen et al. 1981). Its spectral classification is uncertain, because the optical spectrum is strongly veiled (Hernández et al. 2004). Cohen et al. (1981) suggest a spectral type between B5 and F2, perhaps A5. The latter would be consistent with the observed bolometric luminosity of $\sim 80 - 175 L_{\odot}$ (Evans II, Levreault & Harvey 1986; Ábrahám et al. 2000). It drives a giant parsec-scale Herbig-Haro outflow (Reipurth, Bally, & Devine 1997) and molecular outflow (Levreault 1984; Arce and Goodman 2002a,b). The outflow appears to be precessing (Arce and Goodman 2002b), suggesting that PV Cep could be a binary system, although no companion has yet been detected. Torrelles et al. (1986) discovered an H_2O maser $5''$ to the south of PV Cep, which could mark the location of another young star, because H_2O masers excited by low-luminosity stars are usually close to the star. More recent observations show H_2O maser activity close to PV Cep (Marvel 2005). PV Cep coincides with a faint VLA source at 3.5 cm (Anglada et al. 1992).

PV Cep was mapped at 1.3 mm by (Fuente et al. 1998a), who found a compact source centered on the star. It was recently imaged on CARMA by Hamidouche (2010), who resolved it at 2.7 and 1.3 mm with a size of $\sim 0''.5$ (250 AU). Our maps at $850 \mu m$ and $450 \mu m$ (Figure 23) go deeper than the single dish map at 1.3 mm by Fuente et al. (1998a). We resolve PV Cep in the sub-millimeter with a size of $1200 \text{ AU} \times 700 \text{ AU}$ at PA 74° (Table 2a), which is roughly perpendicular to the outflow. We also see faint, extended emission with a diameter of $\sim 1'$ from the dense surrounding cloud core at both 850 and $450 \mu m$. PV Cep was found to be unresolved at 50 and $100 \mu m$ (Natta et al. 1993), which is in good agreement with the compact size that we find in the sub-millimeter. Our observed source size, however, is much larger than what Hamidouche (2010) found with CARMA and the 1.3 mm flux density found by Fuente et al. (1998a) is about twice as large as what is seen by CARMA, suggesting that the array filters out some of the extended emission. A graybody fit to the (sub-)millimeter single dish data, ISO (Ábrahám et al. 2000), and KAO far-infrared data (Figure 24) gives a dust temperature of 29 K, a dust emissivity index, $\beta = 1.59$, resulting in a mass of $\sim 1.0 M_{\odot}$. This mass estimate is much larger than what one would expect to find even for a young circumstellar disk. It therefore seems that the single dish data maybe dominated by the compact infalling envelope, although Hamidouche (2010) finds $0.8 M_{\odot}$, suggesting that even array observations are dominated by the envelope.

V 645 Cyg powers a low velocity molecular outflow in the north-south direction (Schulz et al. 1989; Verdes-Montenegro et al. 1991). The star coincides with a faint, somewhat extended VLA source (Girart et al. 2002) roughly aligned with the outflow. Girart et al. (2002) also found a faint extended, $\sim 6' \times 2'$, H II region close to the star, which could be excited by V 645 Cyg. Since V 645 Cyg is known to power a 1665 MHz OH maser (Morris and Kazès 1982), and a Class II CH₃OH maser (Slysh et al. 1999), it must be a high-mass star, since these masers are only excited by high mass stars. Clarke et al. (2006) classified it as a transition object between a massive YSO and a young Oe type star in a weak H II region.

Di Francesco et al. (1997) marginally detected V 645 Cyg at 2.7 mm with the IRAM array. We find V 645 Cyg to coincide with a bright sub-millimeter source embedded in narrow east-west cloud ridge which turns mostly northward east of the star. The emission is clearly extended (Table 2a), but at a distance of 4.2 kpc it is clear that the sub-millimeter emission is dominated by the dense envelope, rather than a circumstellar disk. An isothermal fit to the data in Table 2a gives a mass of 85 M_{\odot} for the elliptical sub-millimeter source, which is far more than what one would expect even for a very young circumstellar disk.

MWC 1080 A must be an early B star, because it has strong Balmer and Fe II lines showing P Cygni type emission profiles (Finkenzeller & Mundt 1984). It drives a prominent bipolar outflow seen pole on (Cantó et al. 1984). Distance estimates vary. Here we have adopted 2.2 kpc (Table 1) from Cantó et al. (1984). MWC 1080 is a hierarchical multiple system. The primary, MWC 1080 A, is an eclipsing binary. The period of 2.9 days (Shevchenko et al. 1994). MWC 1080 B is also a PMS star and more heavily reddened than the primary (Leinert, Richichi & Haas 1997; Polonski et al. 2002). A third companion is found $\sim 5''.2$ east of the primary (Polonski et al. 2002; Pirzkal et al. 1997). MWC 1080 is a strong far-infrared source with a source size of $\sim 50'' - 60''$ (Evans II, Levreault & Harvey 1986; Di Francesco et al. 1998; Ábrahám et al. 2000). VLA observations (Girart et al. 2002) show three free-free emission sources in the vicinity of MWC 1080 with VLA 4 coinciding with MWC 1080 A. It has a flux density of 0.2 mJy at 6 cm and was also detected by Skinner, Brown, & Stewart (1993) at 3.6 cm with a flux density of 0.18 mJy. Fuente et al. (1998a) and Henning et al. (1998) both observed MWC 1080 with the IRAM 30 m telescope and found strong extended continuum emission towards MWC 1080 A and B.

Our short integration 850 μ m map (Figure 26) is dominated by strong extended emission from the reflection nebula surrounding MWC 1080 and perhaps nearby embedded sources. MWC 1080 A, i.e., VLA 4, coincides with a faint emission peak in an extended east-west ridge. The other two VLA sources lack sub-millimeter counterparts. We consider MWC 1080 A a marginal detection with a flux density of $\sim 250 \pm 50$ mJy. This appears plausible since deep IRAM interferometer observations at 2.7 mm and 1.4 mm (Fuente et al. 2003) show

extended emission towards MWC 1080 A. At 1.4 mm Fuente et al. find that MWC 1080 A coincides with a faint unresolved source. The observed flux density is much less than what Fuente et al. (1998a) found from their single dish observations, suggesting that interferometer has resolved out most of the emission. If we assume that the observed 850 μm flux density comes from a circumstellar disk surrounding MWC 1080 A we can make some simple assumptions to estimate the mass of the disk. For a dust temperature of 50 K and a typical dust emissivity, $\beta = 1.5$, we get a disk mass of 0.009 M_{\odot} .

6. Non-detections

Most of our non-detections are early to mid-B stars. These stars illuminate large reflection nebulae and are strong 60 and 100 μm sources in the IRAS point source catalogue. Only a few, however, appear to be surrounded by dusty disks that have enough cold dust to be detected with a single dish telescope in the sub-millimeter. Our sample also includes two stars which are not HAEBE stars but instead appear to be supergiants. Neither of these two, HD 316285 and MWC 300, are associated with any dust emission. These are discussed at the end of this section.

MWC 137 is a B0ep star that excites the H II region S 266 (Fich 1993). Both the radio and the optical appearance are very similar: a ring-like nebulosity with a radius of $\sim 30''$ and two spiral-like arcs connecting to the central star (Figure 27). Although MWC 137 has long been known to be a radio source, see e.g., Altenhoff et al. (1976), early single dish observations picked up emission from the extended H II region, not the central star. Radio emission from MWC 137 was first detected by Skinner, Brown, & Stewart (1993) at 3.6 cm. They found the emission to be compact and unresolved.

The star appeared to have been detected at 1.3 mm in photometric observations at the CSO by (Hillenbrand et al. 1992). It was mapped with the IRAM 30 m telescope at 1.3 mm by Fuente et al. (1998a) and Henning et al. (1998). Both maps show an extended narrow dust ridge extending over the nebulosity with a stronger emission peak $\sim 30''$ northeast of the star and a fainter one to the southwest, both peaks approximately coinciding with the boundary of the H II region. There is only faint emission towards the star itself. Our 850 μm map looks very similar, although we see a second arc bounding the nebula to the south. We see no enhancement in dust emission toward MWC 137; if anything the emission is close to a minimum at the position of the star. Di Francesco et al. (1997) obtained a marginal detection of the star at 2.7 mm with the IRAM interferometer, while the deep observations by Fuente et al. (2003) yield clear detections at both 2.7 mm and 1.4 mm. At 1.4 mm Fuente et al. derive a source size of $1''.8 \times 0''.8$ and find a total flux density of 10

mJy. Fuente et al. (2003) also detected the star with the VLA at 1.3 cm and 7 mm, where they find it to be compact and unresolved. The VLA data suggest that MWC137 has a thermal wind with a spectral index $\alpha = 0.8 - 1.0$, i.e. similar to what we find for MWC297 and LkH α 101. It therefore appears that the free-free emission completely dominates at millimeter wavelengths. MWC137 appears similar to MWC349, MWC297, and LkH α 101, but the free-free emission is much fainter, suggesting that it is more evolved and has already photo-ionized most of its disk.

LkH α 215 illuminates the reflection nebula NGC 2245. It is a late B star. Valenti, Fallon & Johns-Kru (2003) classify it as a B8 star based on low-resolution IUE spectra, while Hernández et al. (2004) give it a spectral type B6 with an uncertainty of 2.5 subclasses. It is part of the young Mon R1 association, which has a distance of 800 pc (Herbst et al. 1982). Although Mannings (1994) reported a detection of LkH α 215 with sub-millimeter photometry on JCMT, Fuente et al. (1998a), who mapped LkH α 215 and the surrounding reflection nebula in ^{13}CO $J = 1 \rightarrow 0$, CS $J = 3 \rightarrow 2$ and 1.3 mm continuum with the IRAM 30 m telescope, did not detect it. They found no CS emission in the vicinity of LkH α 215 and even though they detected 1.3 mm dust emission, it did not peak on the star.

Figure 28 shows our 850 μm image overlaid on a POSS image of the region. One can see a faint dust ridge near LkH α 215. This emission, which is stronger east of the star, is probably not associated with LkH α 215, although we cannot exclude the possibility that LkH α 215 is still surrounded by a small accretion disk. However, we find a much stronger unresolved source, LkH α 215-SMM, northwest of the reflection nebula ($\alpha_{2000.0} = 06^h 32^m 35^s.265$, $\delta_{2000.0} = +10^\circ 10' 18''.3$), which has no optical or near-infrared counterpart. The flux density of this source is 152 ± 22 mJy at 850 μm , 220 ± 80 mJy at 750 μm , and 875 ± 250 mJy at 450 μm .

HD 259431 is a B6 star that illuminates the reflection nebula NGC 2247. This star appears similar to LkH α 215. They are both part of the Mon R1 association and probably of similar age, 0.05 - 0.1 Myr (Testi, Palla & Natta 1998).

Mannings (1994) reported a marginal 450 μm detection, but as is evident from the 850 μm image (Figure 29) there is extended dust emission towards NGC 2247, but no emission associated with the position of the star. There are two faint 850 μm continuum sources outside the nebula; NGC 2247-SMM1: $\alpha_{2000.0} = 06^h 33^m 07^s.99$, $\delta_{2000.0} = +10^\circ 18' 19''$, and NGC 2247-SMM2: $\alpha_{2000.0} = 06^h 27^m 07^s.76$, $\delta_{2000.0} = +10^\circ 20' 22''$, with integrated flux densities of 0.38 mJy and 0.16 mJy, respectively. Neither source has an optical or near-infrared counterpart.

LkH α 25, spectral type B7 (Hernández et al. 2004), does not illuminate a reflection

nebulousity (Herbig 1960), nor was it detected by IRAS. *Spitzer* IRAC archive images show that the star is inside a large, roughly spherical nebula with a diameter of $6'$ - $8'$. Although the star is not centered in the nebula, it is $\sim 2'$ from the southern part of the nebula (which is also the brightest part of the nebula at $8\ \mu\text{m}$), suggesting that it may be the illuminating source of the nebula. LkH α 25 has been observed by two groups at 1.3 mm (Henning et al. 1998; Fuente et al. 1998a), but neither of them detected the star in millimeter continuum emission. We do not detect it either. Our sub-millimeter map (not shown) shows that the star lies in a region free of dust emission, although there is a small dust emission region less than one arcmin to the southeast of the star and a large dust cloud ($\sim 10' \times 3'$) about two arcminutes west of the star extending mostly to the north. This cloud complex is almost certainly associated with NGC 2264.

CD-42° 1172 is a well-studied, bright B0ep star illuminating a clumpy, arc-shaped nebula with a size of $\sim 40''$, showing both reflection and emission characteristics (Hutsemékers & Van Drom 1990). Although several studies have questioned whether CD-42° 1172 is a PMS star (see e.g., Borges Fernandes et al. 2007), there should not be any doubt that this is a young star. It is embedded in an opaque dark cloud and is the brightest member of a small cluster of PMS stars (Habart et al. 2003; Boersma et al. 2009). Distance estimates vary. Here we have adopted 1.15 kpc (Borges Fernandes et al. 2007), which is based on the interstellar absorption lines of Na I and Ca II K lines. The star is associated with strong far-infrared emission (Weintraub 1990; Natta et al. 1993) and sub-millimeter emission (Mannings 1994), but it is questionable whether the emission comes from a circumstellar disk. Boersma et al. (2009) present an IRAC color image of the CD-42° 1172 region. The star is saturated in all IRAC images and even a secondary peak north of the star is an artifact due to the heavily saturated CD-42° 1172. The IRAC image shows that the star is surrounded by a one arcminute nebulousity glowing in PAH emission and it also shows a smaller nebulous region about $45''$ to the northwest.

Henning et al. (1998) mapped CD-42° 1172 in 1.3 mm continuum with the IRAM 30 m telescope. They found the star to be associated with an extended dust cloud, but there is no enhancement in the dust emission at the position of the star. Our 850 and 450 μm images (Figure 30) look very similar to the 1.3 mm map and show no enhancement of the dust emission towards the star, only emission from the cloud ridge in which it is embedded. We see two sub-millimeter sources to the northwest of CoD-42° 1172, neither of which have any near- or mid-infrared counterparts (Habart et al. 2003). SMM 1 is a point-like source offset $-6''8, +7''3$ from the star in RA and Dec, i.e., $\alpha_{2000.0} = 16^h 59^m 06^s 286$, $\delta_{2000.0} = -42^\circ 42' 00'' 7$, with a flux density of 670 mJy at 850 μm . SMM 2 is a strong (2.4 Jy), extended source about $50''$ northwest of the star: $\alpha_{2000.0} = 16^h 59^m 03^s 911$, $\delta_{2000.0} = -42^\circ 41' 32'' 6$. The latter is clearly seen in the 1.3 mm map by Henning et al. (1998) and

appears to coincide with the northwestern nebulosity seen in the IRAC image shown by Boersma et al. (2009).

We therefore also downloaded and analyzed MIPS images of CD–42° 1172, which has been observed as part of the MIPS GAL legacy project. The 24 and 70 μm MIPS images are shown in Figure 30, on which we overlaid the 850 μm SCUBA image with contours. In the 24 μm image the nebulosity surrounding CD–42° 1172 is completely saturated. One plausible explanation to why the nebulosity would be saturated is that it is an H II region ionized by the star or by a thermal wind from the star. The star, however, was not detected in the VLA survey by Skinner, Brown, & Stewart (1993), nor was it seen by Thompson, Ugruhart & White (2004), who used the Australia Compact Array. Thompson, Ugruhart & White detected two sources at 13 cm. One is probably extragalactic; the other one, SFO 85a, is close to, but not coincident with the extended SMM 2 northwest of CD–42° 1172. The emission is also extended in the MIPS 70 μm image, suggesting that this region may contain several embedded stars.

TY CrA and HD 176386 illuminate the reflection nebulae NGC 6727 and NGC 6726 in the Corona Australis molecular cloud. TY CrA is a triple system with a close eclipsing binary (Casey et al. 1995). The primary is a B8-B9V star with a luminosity of 67 L_{\odot} , and an age of ~ 3 Myr (Casey et al. 1998). HD 176386 is a binary star with the primary being an A0V star and the secondary a low-mass K7 star (Meyer et al. 2009).

Figure 31 shows an 850 μm sub-image of a large SCUBA scan map, which has also been published by Nutter, Ward-Thompson & André (2005). It is clear from this 850 μm map that neither star has any sub-millimeter excess. Hillenbrand et al. (1992) reported a 1.3 mm detection of TY CrA, but as we can see from Figure 31, the emission observed by Hillenbrand et al. is from the dust cloud in which the star is embedded. Neither TY CrA nor HD 176386 show any near-infrared excess (Bibo et al. 1992), suggesting that they have completely dispersed their accretion disks. The nearby Herbig Ae/Be stars, R CrA and T CrA, about 5' to the southwest, appear to be much younger, and even though neither of them have been detected in the sub-millimeter (see Figure 2 in Groppi et al. (2007)), they do show clear excess emission in the near- and mid-infrared, suggesting that they are still surrounded with accretion disks (Bibo et al. 1992).

HD 200775 is a B3 star illuminating the reflection nebula NGC 7023. We do not see any dust emission towards HD 200775 in NGC 7023 to a limit of ~ 25 mJy beam $^{-1}$ (Table 2c). NGC 7023 was observed both in scan map and jiggle map modes. There is strong dust emission from the PDR region just north and northwest of the star and fainter emission to the east and southwest at the boundary between the reflection nebula and the surrounding dust cloud (Figure 32). Fuente et al. (1998b) show that the cavity around HD 200775 has

very likely been excavated by an energetic, bipolar outflow in an earlier evolutionary stage of the star, but that the star no longer shows any evidence of a bipolar outflow. They detected faint continuum emission at 3.4 mm with the IRAM interferometer, but the observed flux density, 3 mJy, is about what one would expect from a thermal wind. Recently, however, Okamoto et al. (2009) detected HD 200775 with the SMA at 350 GHz with a flux density of 35 mJy, i.e., consistent with our $3\text{-}\sigma$ upper limit, see Figure 32. They also found unresolved excess emission in the mid-infrared using the 8.2 m Subaru telescope, confirming that the star is still surrounded by a disk.

HD 316285 is listed as an extreme emission line object in Thé, de Winter and Pérez (1994); however, HD 316285 is a P Cygni type supergiant, possibly a luminous blue variable, and definitely not a young Herbig Be star (Hillier et al. 1998). It is extremely luminous and lies at a distance of ~ 1.85 kpc (Table 1). It has very little or no hot dust, but shows strong far-infrared emission from cold dust (McGregor, Hyland & Hillier 1988).

van der Veen et al. (1994) did sub-millimeter photometry with the single pixel bolometer UKT14 on JCMT and reported flux densities at 1.1 mm, 800 and 450 μm although the flux density at 800 μm was suspiciously low. In Figure 33 we present large 850 and 450 μm images in the direction of HD 316285. Although there is strong sub-millimeter emission in the field, HD 316285, is in an area with relatively weak dust emission. There is a marginal peak in the dust emission at 850 μm , but not at 450 μm (Figure 33). We count it as a non-detection. The upper limit we derive from these observations is rather high, 70 mJy at 850 μm for an unresolved source (Table 2c).

MWC 300 was listed as a HAEBE star by Herbig (1960) and included in the catalogue by Thé, de Winter and Pérez (1994). However, it has also been classified as a B[e] star or supergiant (Allen & Swings 1976; Appenzeller 1977). Miroshnichenko et al. (2004), who analyzed more than ten years of optical and near-infrared spectroscopy and mid-infrared imaging, were able to determine the distance (1.8 ± 0.2 kpc) and hence the luminosity ($L = 1.3 \times 10^5 L_{\odot}$), which together with all the other observed characteristics and with detailed modeling identify this star as a B[e] supergiant and most likely a binary.

Henning et al. (1994) reported an approximately three-sigma detection of the star in continuum emission at 1.3 mm. We find no emission at all towards MWC 300 with a rather stringent upper limit, 7 mJy beam^{-1} (Table 2c), suggesting that the results by Henning et al. were spurious.

7. Discussion

In this paper we present results from an extensive sub-millimeter survey of HAEBE stars, many of which have been detected both at 850 and 450 μm . First we note that our study includes a total of 39 objects that were potential HAEBE stars. However, HD 316285 and MWC 300, which were classified as potential HAEBE stars when we surveyed them, are now classified as supergiants. We therefore have observed a total of 37 objects now thought to be HAEBE stars. Of these we have detected 27 stars (73%) in emission at 850 μm or 800 μm , either in SCUBA mapping or UKT14 photometry, or both⁴. We have also detected 17 of these stars at 450 μm . Although many of these stars have already been observed at millimeter and/or sub-millimeter wavelengths (Hillenbrand et al. 1992; Mannings 1994; Henning et al. 1998; Fuente et al. 1998a; Natta et al. 2004; ?), our study provides the largest sub-millimeter sample of HAEBE stars analyzed in a consistent way. We have also included *Spitzer* MIPS photometry for those sources for which such data were publicly available. In our analysis we fit a simple isothermal graybody model to the observed SEDs from far-infrared to millimeter wavelengths. This allows us to determine the temperature of the cold dust, the dust emissivity, and the disk mass.

We find that disks are ubiquitous in Herbig Ae and F stars, but are very rare in early B stars. This does not mean that early B stars do not form with disks, but instead suggests that any such disks evolve rapidly and get destroyed quickly by photoevaporation. There are currently about five or six early B-stars known to have disks. The three stars we detected in this survey — MWC 297, MWC 349, and LkH α 101 — look rather different from the accretion disks surrounding Herbig Ae and T Tauri stars. The gas in these disks is largely ionized, and the emission at millimeter and sub-millimeter wavelengths is dominated by a thermal wind powered by photoevaporation. Only LkH α 101 appears to have a dust excess at millimeter wavelengths, suggesting that it is perhaps younger than the other two and has not yet had time to photoevaporate the disk. All three stars may have some neutral gas in the midplanes of their disks, although there are no detections of molecular gas toward any of these three stars at radio wavelengths. MWC 137 and HD 200775, which we did not detect in our SCUBA survey, are even fainter and possibly more evolved. Our survey also includes two deeply embedded objects (AFGL 961 A and V 1318 Cyg-mm), which have luminosities comparable to early B-stars. The disks/envelopes around these stars look very similar to Class 0 or Class I protostars, although they appear more massive than disks around young low mass stars. Our results therefore suggest that at least some B stars form with accretion

⁴We note, however, that this is not an unbiased survey, most targets were chosen, because they had a high likelihood to be surrounded by accretion disks.

disks in an analogous way to how low mass stars form with disks.

Disks around HAEBE stars appear both larger and more massive than disks around T Tauri stars. We are not aware of any accretion disk around a T Tauri star that has been resolved with a single dish telescope in sub-millimeter continuum emission. Yet at least three HAEBE disks, those around MWC 480, HD 163296 and PV Cep, have been resolved with SCUBA. The sizes that we find agree well with sizes derived from millimeter-aperture synthesis observations. Overall, however, there is no clear correlation between disk size and spectral type in our sample, or even any correlation between disk mass and spectral type.

What we do find, however, is a clear correlation between dust emissivity and disk mass in the sense that a lower dust emissivity corresponds to a lower disk mass. This is shown in Figure 34, where we have taken disk masses and emissivities from the isothermal graybody fits given in Table 4. The only data we omitted from this plot were the two protostellar sources (AFGL 961 A and V 1318 Cyg-mm) and the very distant star V 645 Cyg, because here the masses are dominated by the envelopes, rather than the accretion disks. As we can see from Figure 34 the correlation is rather good ($r = 0.8$). What this suggests is that when β decreases, the mass of the cold dust that we can detect decreases. Note that our modeling assumes that the dust opacity is constant at $250\ \mu\text{m}$, i.e., the “standard” Hildebrand opacity, while newer studies show that large grains, corresponding to low β -values, have lower opacity at $250\ \mu\text{m}$, see e.g. Draine (2006). Our disk mass estimates may therefore be underestimated for low β -values. Comparison with other studies, including detailed modeling of some of the disks in our sample, indicate that the agreement in disk mass is surprisingly good, and usually within a factor of two. Since a low β -value suggests grain growth (Natta et al. 2004; Rodmann et al. 2006), the disk mass might not actually be dropping; rather, the dust mass could be getting buried into large grains, pebbles, and planetesimals. Once buried, we cannot detect it anymore. Thus, low β , which is correlated with low “detectable” disk mass, might be a good indicator of planetesimal growth rather than of decreasing disk mass of solids. All stars that show low β -values are isolated HAEBE stars, i.e., they are relatively old, 3 - 15 Myr, which seems to be the time required for significant grain growth.

A few of these stars have SEDs that suggest they are transition stars, i.e., they show weak near-infrared excesses but strong mid-to-far-infrared excesses, suggesting that they have developed gaps largely free of dust (Najita, Strom & Muzerolle 2007). Another characteristic feature of transition sources, which has become apparent in this study, is that the millimeter and far-infrared regions of the SEDs for these HAEBEs show that the outer portions of the disks around these stars have both cold and warm dust components. All transition stars have cold outer disks, which dominate the emission in the millimeter and sub-millimeter regime, while most of the emission at $60\ \mu\text{m}$ or shorter wavelengths comes from warmer dust ($T_d \geq$

100 K) in the disk, i.e., presumably emission from the hot surface layers of the disk or the inner rim or “wall” (Calvet et al. 2002; Isella, Carpenter & Sargent 2009). The same trend is seen for most of the isolated HAEBE stars, i.e., there is a clear excess at 60 μm requiring a warmer dust component in addition to the cold outer disk, which dominates the emission at wavelengths longer than 100 μm . This is not seen in younger HAEBE disks, like R Mon, PV Cep or AB Aur, or for ex. young FU Ori disks (Sandell, Jessop and Jenness 2001), which are all well fit with a single temperature isothermal fit down to 60 μm . A warm dust component, producing a clear excess at 60 μm is therefore a clear sign of a disk approaching the transition disk stage.

The strong correlation between disk mass and dust emissivity and lack of correlation between spectral type and disk mass suggests that the evolutionary age of the disk affects the measurable disk mass much more strongly than does the mass of the central star. HAEBE stars do have somewhat larger and more massive disks than T Tauri stars. For example, in the large SCUBA survey of Taurus-Auriga by Andrews & Williams (2005), the most massive T Tauri disk is 0.2 M_{\odot} , while there are at least three HAEBE stars in our sample (Table 4) that have an equally large or more massive disk.

8. Summary

We have studied a large sample of HAEBE stars in the sub-millimeter using SCUBA on JCMT. We find that disks around Ae and F stars ubiquitous, while disks around early B stars are rare. We have, however, identified several examples of disks in early B stars. For very young embedded stars with the luminosity of an early B star, they look similar to other young disks, albeit more massive. In early B-stars, which already illuminate H II regions, such disks are largely ionized and have very little cold dust. The emission in the sub-millimeter in all of these cases is dominated by a thermal wind, presumably driven by photoionization of the disk.

We find several examples of HAEBE stars (LkH α 215, HD 259431, CD–42° 1172, MWC 297, and TY CrA) for which our imaging survey clearly shows that the emission previously identified as dust emission from circumstellar disks around these stars instead originates from ionized gas (as in the case of MWC 297), or from nearby younger objects, or from the surrounding molecular clouds in which these stars reside. These stars are, in fact, free of detectable dust emission at long wavelengths; we conclude that previous SED models of these stars that derive properties of their circumstellar disks are incorrect.

Our survey includes several examples of isolated HAEBEs, which have ages of 3 - 15

Myrs and still have gas-rich disks. A few of these are transitional stars, which have already formed large inner gaps (perhaps due to planet formation) and show evidence for grain growth. Most of the isolated HAEBEs show signs of disk evolution. They have cold outer disks, which dominate the emission in the far-infrared and sub-millimeter, but show strong excesses at 60 μm due to warm gas in their disks, i.e., they cannot be fitted with a single temperature isothermal dust model.

This work made extensive use of the SIMBAD Astronomical Database at the Centre de Données astronomiques de Strasbourg, France, and NASA’s Astrophysics Data System Abstract Service. This research used the facilities of the Canadian Astronomy Data Centre operated by the National Research Council of Canada with the support of the Canadian Space Agency. This work is based in part on observations made with the *Spitzer* Space Telescope, which is operated by the Jet Propulsion Laboratory, California Institute of Technology under a contract with NASA. We thank Meredith Hughes for giving us flux densities she observed with the SMA and we also acknowledge useful discussions and help from William Vacca and Bhaswati Mookerjee. Comments and suggestions by the referee were also appreciated.

REFERENCES

- Ábrahám, P., Leinert, Ch., Burkert, A., Henning, Th., & Lemke, D. 2000, A&A, 354, 965
- Acke, B., et al. 2008, A&A, 485, 209
- Acke, B., van den Ancker, M. E., & Dullemond, C. P, 2005, A&A, 436, 209
- Alonso-Albi, T., Fuente, A., Bachiller, R., Neri, R., Planesas. P., Berné, O, & Joblin, C. 2009, A&A, 497, 117
- Altenhof, W. J., Braes, L. L. E., Olon, F. M., & Wendker, H. J. 1976, 46, 11
- Alvarez, C., Hoare, M., Glindemann, A., & Richichi, A. 2004, A&A, 427, 505
- Andrews, S. M., & Williams, J. P. 2005, ApJ, 631, 1134
- Anglada, G., Rodríguez, L. F., Cantó, J., Estalella, R., & Torrelles, J.M. 1992, ApJ, 395, 494
- Allen, D. A., Swings, J.-P. 1976, A&A, 47, 293

- Appenzeller, I. 1977, *A&A*, 61, 21
- Arce, H. G., & Goodman, A. A. 2002a, *ApJ*, 575, 911
- Arce, H. G., & Goodman, A. A. 2002b, *ApJ*, 575, 928
- Aspin, C. 1998, *A&A*, 335, 1040
- Aspin, C., Sandell, G., & Weintraub, D. A. 1994, *A&A*, 282, L25
- Aspin, C., & Barsony, M. 1994, *A&A*, 288, 849
- Augereau, J. C., Lagrange, A. M., Mouillet, D., & Ménard, F. 2001, *A&A*, 365, 78
- Augereau, J. C., Lagrange, A. M., Mouillet, D., & Ménard, F. 1999, *A&A*, 350, L51
- Bally, J., & Predmore, R. 1983, *ApJ*, 265, 778
- Barsony, M., Schombert, J. M., Kis-Halas, K. 1991, *ApJ*, 362, 674
- Becker, R. H., & White, R. L. 1988, *ApJ*, 324, 893
- Beckwith, S. V. W., Sargent, A. I., Chini, R. S., & Güsten, R. 1990, *AJ*, 99, 924
- Berrilli, F., Corciulo, G., Ingrosso, G., Lorenzetti, D., Nisini, B., & Strafella, F. 1992, *ApJ*, 398, 254
- Beskrovnaya, N. G., Pogodin, M. A., Miroshnichenko, A. S., Thé, P. S., Savanov, I. S., Shakhovskoy, N. N., Rostopchina, A. N., Kozlova, O. V., & Kuratov, K. S. 1999, *A&A*, 163
- Bibo, E. A., Thé, P. S., & Dawanas, D. N. 1992, *A&A*, 260, 293
- Blondel, P. F. C., & Tjin A Djie, H. R. E. 2006, *A&A*, 456, 1045
- Bockelée-Morvan, D., André, P., Colom, P., Colas, F., Crovisier, J., Despois, D., & Jorda, L. 1994, in *Circumstellar Dust Disks and Planet Formation*, Proceedings of the 10th IAP Astrophysics Meeting, Institut d’Astrophysique, Paris, July 4-8, 1994, Gif-sur-Yvette: Editions Frontieres, —c1994, Eds R Ferlet, & A. Vidal-Madjar., p.341
- Boersma, C., Peeters, E., Martín-Hernández, N. L., van der Wolk, G., Verhoeff, A. P., Tielens, A. G. G. M., Waters, L. B. F. M., & Pel, J. W. 2009, *A&A*, 502, 175
- Borges Fernandes, M., Kraus, M., Lorenz Martins, S., & de Araújo, F. X. 2007, *MNRAS*, 377, 1343

- Brown, R. L., Broderick, J. J., & Knapp, G. R. 1976, MNRAS, 175, 87P
- Brown, J., Blake, G. A., Dullemond, C. P., Mérim, B., Augerau, J. C., Boogert, A. C. A., Evans II, N. J., Geers, V. C., Lahuis, F., Kessler-Silacci, J. E., Pontoppidan, K.M., & van Dishoeck, E. F. 2007, ApJ, 664, L107
- Brown, J., Blake, G. A., Qi, C., Dullemond, C. P., Wilner, D. J., & Williams, J.P. 2009, ApJ, 704, 496
- Brugel, E. W., Mundt, R., & Bührke, T. 1984, ApJ, 287, L73
- Calvet, N., D’Alessio, P., Hartmann, L., Wilner, D., Walsh, A., & Sitko, M. 2002, ApJ, 568, 1008
- Cantó, J., Rodríguez, L. F., Barral, J.F., & Carral, P. 1981, ApJ, 244, 102
- Cantó, J., Rodríguez, L. F., Calvet, N., & Levreault, R. M. 1984, ApJ, 282, 631
- Carmona, A., van der Ancker, M. E., & Henning, Th. 2007, A&A, 464, 687
- Casey, B. W., Mathieu, R. D., Vaz, L. P. R., Andersen, J., & Suntzeff, N. B. 1998, AJ, 115, 1617
- Casey, B. W., Mathieu, R. D., Suntzeff, N. B., & Walter, F. M. 1995, AJ, 109, 2156
- Casey, S. C., & Harper, D.A. 1990, ApJ, 362, 663
- Castelaz, M. W., Grasdalen, G. L., Hackwell, J. A., Capps, R. W., & Thompson, D. 1985, AJ, 90, 1113
- Chapillon, E., Guilloteu, S., Dutrey, A., & Piétu, V. 2008, A&A, 488, 565
- Clarke, A. J., Lumsden, S. L., Oudmaijer, R. D., Busfield, A. L., Hoare, M. G., Moore, T. J. T., Sheret, T. L., Urquhart, J. S. 2006, ApJ, 457, 183
- Close, L. M., Roddier, F., Hora, J. L., Graves, J. E., Northcott, M., Roddier, C., Hoffman, W. F., Dayal, A., & Fazio, G. G. 1997, ApJ, 489, 210
- Cohen, M., Bieging, J. H., Dreher, W., & Welch, W. J. 1985, ApJ, 292, 249
- Cohen, M., Harvey, P. M., & Schwartz, R. D. 1985, ApJ, 296, 633
- Cohen, M., Kuhl, L. V., Harlan, E. A., & Spinrad, H. 1981, ApJ, 245, 920
- Cohen, M., & Kuhl, L. V. 1979, ApJS, 41, 743

- Cohen, M. 1977, *ApJ*, 215, 533
- Corcoran, D., Ray, T. P., & Bastien, P. 1995, *A&A*, 293, 550-558
- Corder, S., Eisner, J., & Sargent, A. 2005, *ApJ*, 622, L133-L136
- Coulson, I. M., & Walther, D. M. 1995, *MNRAS*, 274, 977
- Dent, W. R. F., Greaves, J. S., Coulson, I. M. 2005, *MNRAS*, 359, 653
- Dent, W. R. F., Torelles, J. M., Osorio, M., Calvet, N., & Anglada, G. 2006, *MNRAS*, 365, 1283
- Dent, W. R. F., Hovey, G. J., Dewdney, P. E., Burgess, T. A., Willis, A. G., Lightfoot, J. F., Jenness, T., Leech, J., Matthews, H. E., Heyer, M., & Poulton, C. 2009, *MNRAS*, 395, 1805
- DeWarf, L. E., Sepinski, J. F., Guinan, E. F., Ribas, I., & Nadalin, I. 2003, *ApJ*, 590, 357
- de Winter, D., & Thé, P. S. 1990, *Ap&SS*, 166, 99
- De Wit, Hoare, M. G., Fujiyoshi, T., Oudmaijer, R. D., Honda, M., Kataza, H., Miyata, T., Okamoto, Y. K., Onaka, T., Sako, S., & Yamashita, T. 2009, *A&A*, 494
- de Zeeuw, P. T., Hoogerwerf, R., & de Bruijne, J. H. J. 1999, *AJ*, 117, 354
- Di Francesco, J., Evans II, N. J., Harvey, P. M., Mundy, L. G., Guilloteau, S., & Chandler, C. 1997, *ApJ*, 482, 433
- Di Francesco, J., Evans II, N. J., Harvey, P. M., Mundy, L. G., & Butner, H. M. 1998, *ApJ*, 509, 324
- Doering, R. L., Meixner, M., Holfeltz, S. T., Krist, J. E., Ardila, D. R., Kamp, I., Clampin, M. C, Lubow, S. H. 2007, *AJ*, 133, 2122
- Draine, B. T. 2006, *ApJ*, 636, 1114
- Drew, J. E., Busfield, G., Hoare, M. G., Murdoch, K. A., Nixon, C.A., & Oudmaijer, R. D. 1997, *MNRAS*, 286, 538
- Dunkin, S. K., Barlow, M. J., & Ryan, S. G. 1997, *MNRAS*, 286
- Dunkin, S. K., & Crawford, I. A. 1998, *MNRAS*, 298, 275

- Elia, D., Strafella, F., Campeggio, L., Maiolo, B., & Pezzuto, S. 2005, *New Astronomy*, 10, 545
- Elias, J. H. 1978 *ApJ*, 224, 857
- Eisner, J. A., Lane, B. F., Akeson, R. L., Hillenbrand, L. A., & Sargent, A. I. 2003, *ApJ*, 588, 360
- Emerson, D. T. 1995, in *Multi-feed systems for radio telescopes*, ASP Conf. Ser. Vol. 75, Eds. D. T. Emerson, & J. M. Payne (Astronomical Society of the Pacific: San Francisco), p. 327
- Evans II, N. J. , Levreault, R. M., & Harvey, P. M. 1986, *ApJ*, 301, 894
- Evans II, N. J. , et al. 2003, *PASP*, 115, 965
- Felli, M., Gahm, G. F., Harten, R. H., Liseau, R., & Panagia, N., 1982, *A&A*, 107, 354
- Fich, M. 1993, *ApJS*, 86, 475
- Finkenzeller, U., & Mundt, R. 1984, *A&AS*, 55, 109
- Fisher, R. S., Telesco, C. M., Piña, R. K., Knacke, R. F., & Wyatt, M. C. 2000, *ApJ*, 532, L141
- Fuente, A., Martín-Pintado, J., Bachiller, R., Neri, R., & Palla, F. 1998, *A&A*, 334, 253
- Fuente, A., Martín-Pintado, J., Bachiller, R., Neri, R., & Moriarty-Schieven, G. D. 1998, *A&A*, 339, 575
- Fuente, A., Neri, R., Martín-Pintado, J., Bachiller, R., Rodríguez-Franco, A., & Palla, F. 2001, *A&A*, 366, 873
- Fuente, A., Rodríguez-Franco, A., Testi, L., Natta, A., Bachiller, R., & Neri, R. 2003, *ApJ*, 598, L39
- Fuente, A., Alonso-Albi, T., Bachiller, R., Natta, A., Testi, L., Neri, R., & Planesas, P. 2006, *ApJ*, 649, L119
- Fukagawa, M. et al. 2004, *ApJ*, 605, L53
- Gibb, A. G., & Hoare, M. G. 2007, *MNRAS*, 380, 246
- Girart, J. M., Curiel, S., Rodríguez, L. F., & Cantó, J. 2002, *Rev. Mex A. A.*, 38, 169

- Goldsmith, P. F., Heyer, M., Narayanan, G., Snell, R., Li, D., & Brunt, C. 2008, *ApJ*, 680, 428
- Grady, C. A., Woodgate, B., Bruhweiler, F. C., Boggess, A., Plait, P., Lindler, D. J., Clampin, M., & Kalas, P. 1999, *ApJ*, 523, L151
- Grady, C. A., Devine, D., Woodgate, B., Kimble, R., Bruhweiler, F. C., Boggess, A., Lindsy, J. L., Plait, P., Clampin, M., & Kalas, P. 2000, *ApJ*, 544, 895
- Grady, C. A., Schneider, G., Sitko, M. L., Williger, G. M., Hamaguchi, K., Brittain, S. D., Ablordeppey, K., Apai, D., Beerman, L., Carpenter, W. J., K., Collins, K. A., Fuugawa, M., Hammel, H. B., Henning, Th., Hines, D., Kimes, R., Lynch, D. K., Meñard, F., Pearson, R., Russell, R. W., Silverstone, M., Smith, P. S., Troutman, M., Wilner, D., Woodgate, B., & Clampin, M. 2009, *ApJ*, 699, 1822
- Greaves, J. S., Mannings, V., & Holland, W. S. 2000, *Icarus*, 143, 155
- Grinin, V. P., Kiselev, N. N., Minikulov, N. Kh., Chernova, C. P., & Voshchinnikov, N. V. 199, *Ap&SS*, 186, 283
- Groppi, C., Hunter, T. R., Blundell, R., & Sandell, G. 2007, *ApJ*, 670, 489
- Guimarães, M. M., Alencar, S. H. P., Corradi, W. J. B., & Vieira, S. L. A. 2006, *A&A*, 457, 581
- Güdel, M., Benz, A. O., Catala, C., & Praderie, F. 1989, *A&A*, 217, L9
- Habart, E., Testi, L., Natta, A., & Vanzi, L. 2003, *A&A*, 400, 575
- Hamann, F., & Simon, M. 1988, *ApJ*, 327, 876
- Hamann, F., & Simon, M. 1986, *ApJ*, 311, 909
- Hamidouche, M. 2010, *ApJ*, 722, 204
- Hamidouche, M., Wang, S., & Looney, L.W. 2008, *AJ*, 135, 1474
- Hamidouche, M., Looney, L.W., Mundy, L.G. 2006, *ApJ*, 651, 321
- Harvey, P. M., Thronson, H. A., Jr., & Hoffman, W. F. 1979, *ApJ*, 231, 115
- Harvey, P. M., Campbell, M. F., & Hoffman, W. F. 1977, *ApJ*, 215, 151
- Henning, Th., Pfau, W., & Altenhoff, W. J. 1990, *A&A*, 227, 542

- Henning, Th., Launhardt, R., Steinacker, J., & Thamm, E. 1994, *A&A*, 291, 546
- Henning, Th., Burkert, A., Launhardt, R., Leinert, Ch., & Stecklum, B. 1998, *A&A*, 336, 565
- Hensberge, H., Pavlovski, K., & Verschueren, W. 2000, *A&A*, 358, 553
- Herbig, G. H., Andrews, S. M., & Dahm, S. E. 2004, *AJ*, 128, 1233
- Herbig, G. H. 1960, *ApJS*, 4, 337
- Herbig, G. H. 1971, *ApJ*, 169, 537
- Herbig, G. H., & Bell, K. R., 1988, Third Catalog of Emission-Line Stars of the Orion Population, Lick Observatory Bulletin No. 1111, Univ. of California (HBC)
- Herbst, W., Miller, D. P., Warner, J. W., & Herzog, A. 1982, *AJ*, 87, 98
- Hernández, J., Calvet, N., Briceño, C., Hartmann, L., & Berlind, P. 2004, *AJ*, 127, 1682
- Hildebrand, R.H. 1983, *QJRAS*, 24,267
- Hillenbrand, L. A., Strom, S. E., Vrba, F. J., & Keene, J. 1992, *ApJ*, 397, 613
- Hillenbrand, L. A., Meyer, M. A., Strom, S. E., & Skrutskie, M. F. 1995, *AJ*, 109, 280
- Hillier, D. J., Crowther, P. A., Najarro, F., & Fullerton, A. W. 1998, *A&A*, 340, 483
- Holland, W.S., Robson, E.I., Gear, W.K., Cunningham, C., Lightfoot, J.F., Jenness, T., Ivison, R.J., Stevens, J.A., Ade, P.A.R., Griffin, M.J., Duncan, W.D., Murphy, A., & Naylor, D.A. 1999, *MNRAS*, 303, 659
- Hughes, A.M., Wilner, D.J., Qi, C., & Hogerheijde, M. R. 2008a, *ApJ*, 678, 1119
- Hughes, A.M., Wilner, D.J., Kamp, I., & Hogerheijde, M. R. 2008b, *ApJ*, 681, 626
- Hutsemékers, D., & Van Drom, E. 1990, *A&A*, 238, 134
- Isella, A., Carpenter, J. M., & Sargent, A. I. 2009, *ApJ*, 701, 260
- Isella, A., Testi, L., Natta, A., Neri, R., Wilner, D., & Qi, C. 2007, *A&A*, 469, 213
- Jenness, T., & Lightfoot, J.F. 1999, Starlink User Note 216.6, Rutherford Appleton Laboratory, Particle Physics & Astronomy Research Council

- Jenness, T., Stevens, J. A., Archibald, E. N., Economou, F., Jessop, N.E., & Robson, E. I. 2002, MNRAS, 336, 14
- Jensen, E. L. N., Mathieu, R. D., & Fuller, G. A. 1996, ApJ, 458, 312
- Jones, B. F., Herbig, G. H., 1982, AJ, 87, 1223
- Keller, L. D., Sloan, G. C., Forrest, W. J., Ayala, S., D’Alessio, P., Shah, S., Calvet, N., Najita, J., Li, A., Hartmann, L., Sargent, B., Watson, D. M., & Chen, C. H. 2008, ApJ, 684, 411
- Klein, R., Posselt, B., Schreyer, K., Forbrich, J., & Henning, Th. 2005, ApJS, 161, 361
- Koresko, C. D., Harvey, P. M., Christou, J. C., Fugate, R. Q., & Li, W. 1997, ApJ, 485, 213
- Kuhn, J. R., Potter, D., & Parise, B. 2001, ApJ, 553, L189
- Lada, C. J., & Gautier III, T. N. 1982, ApJ, 261, 161
- Lagage, P.O., Olofsson, G., Cabrit, S., Cesarsky, C. J., Nordh, L., & Rodriguez Espinoza, J.M. 1993, ApJ, 417, L79
- Leinert, Ch., van Boekel, R., Waters, L. B. F. M., et al. 2004, A&A, 423, 537
- Leinert, C., Richichi, A., & Haas, M. 1997, A&A, 318, 472
- Levreault, R. M. 1984, ApJ, 277, 634
- Li, J. Z., & Smith, M. 2005, ApJ, 130, 721
- Lin, S-Y., Ohashi, N., Lim, J., Ho, P.T.P., Fukagawa, M., Tamura, M. 2006, ApJ, 645, 1297
- Looney, L.W., Wang, S., Hamidouche, M., Safier, P.N., & Klein, R. 2006, ApJ, 642, 330
- Lugo, J., Lizano, S., & Garay, G., 2004, ApJ, 614, 807
- Mannings, V. 1994, MNRAS, 271, 587
- Mannings, V., & Sargent, A. I. 1997, ApJ, 490, 792
- Mannings, V., Koerner, D. W., & Sargent, A. I. 1997, Nature, 388, 555
- Mannings, V., & Sargent, A. I. 2000, ApJ, 529, 391-401
- Manoj, P., Ho, P. T. P., Ohashi, N., Zhang, Q., Hasegawa, T., Chen, H.-R., Bhatt, H. C., Ashok, N. M. 2008, ApJ, L187

- Manoj, P., Bhatt, H. C., Maheswar, G., & Muneer, S. 2006, *ApJ*, 653, 657
- Marsh, K. A., Silverstone, M. D., Becklin, E. E., Koerner, D. W., Werner, M. W., Weinberger, A. J., & Ressler, M. E. 2002, *ApJ*, 573, 425
- Marston, A. P., & McCollum, B. 2008, *A&A*, 477, 193
- Martin-Píntado, J., Neri, R., Thum, C., Planesas, P., & Bachiller, R. 1994, *A&A*, 286, 890
- Marvel, K.B. 2005, *AJ*, 130, 2732
- Matthews, B. C., Graham, J. R., Perrin, M. D., & Kalas, P. 2007, *ApJ*, 671, 483
- McGregor, P. J., Hyland, A. R., & Hillier, D. J. 1988, *ApJ*, 324, 1071
- Meeus, G., Pinte, C., Woitke, P., et al. 2010, *A&A*, 518, L124
- Meeus, G., Waters, L. B., F. M., Bouwman, J., van den Ancker, M. E., Waelkens, C., & Malfait, K. 2001, *A&A*, 365, 476
- Merín, B., et al. 2004, *A&A*, 419, 301
- Merrill, P. W., & Burwell, C. G. 1933, *ApJ*, 78, 87
- Meyer, M. R., & Wilking, B. A. 2009, *PASP*, 121, 350
- Millan-Gabet, R., Schloerb, F. P., & Traub, W. A. 2001, *ApJ*, 546, 358
- Miroshnichenko, A. S., Hofmann, K.-H., Schertl, D., Weigelt, G., et al. 2009, *A&A*, 498, 115
- Miroshnichenko, A. S., Levato, H., Bjorkman, K. S., Grosso, M., et al. 2004, *A&A*, 417, 731
- Monnier, J. D., Tannirkulam, A., Tuthill, P. G., Ireland, M., Cohen, R., Danchi, W. C., & Baron, F. 2008, *apj*, L97
- Mora, A., Merín, B., Solano, E., Montesinos, B., et al. 2001, *A&A*, 378, 116
- Morris, M., & Kazès, I. 1982, *A&A*, 111, 239
- Najita, J. R., Strom, S. E., & Muzerolle, J. 2007, *MNRAS*, 378, 369
- Natta, A., Testi, L., Neri, R., Shepherd, D. S., & Wilner, D. J. 2001, *A&A*, 416, 179
- Natta, A., Prusti, T., Neri, R., Wooden, D., Grinin, V. P., & Mannings, V. 2001, *A&A*, 371, 186

- Natta, A., Grinin, V., & Mannings, V. 2000, in *Protostars and Planets IV*, Eds. V. Mannings, A. Boss, & S. S. Russell (University of Arizona Press: Tucson), p. 559
- Natta, A., Palla, F., Butner, H. M., Evans II, N. J., & Harvey, P. M. 1993, *ApJ*, 406, 674
- Nakano, M., Kogure, T., Yoshida, S., & Tatematsu, K. 1990, *PASJ*, 42, 567
- Nutter, D. J., Ward-Thompson, D., & André, P. 2005, *MNRAS*, 357, 975
- Okamoto, Y. K., Kataza, H., Honda, M., Fujiwara, H., Momose, M., Ohashi, N., Fujiyoshi, T., Sakon, I., Sako, S., Yamashita, T., Miyata, T., & Onaka, T. 2009, *ApJ*, 706, 665
- Olnon, F. M. 1975 *A&A*, 39, 217
- Oppenheimer, B. R., et al. 2008, *ApJ*, 679, 1574
- Palla, F., Testi, L., Taylor, G. B., Prusti, T., Felli, M., Natta, A., & Stanga, R. M. 1995, 293, 521
- Pérez, M. R., van den Ancker, M. E., de Winter, D., & Bopp, B. W. 2004, *A&A*, 416, 647
- Pérez, M. R., Webb, J. R., & Thé, P. S. 1992, *A&A*, 257, 209
- Perrin, M. D., Graham, J. R., Kalas, P., Lloyd, J. P., Max, C. E., Gavel, D. T., Pennington, D. M., & Gates, E. L. 2004, *Science*, 303, 1345
- Piétu, V., Dutrey, A., & Guilloteau, S. 2007, *A&A*, 467, 163
- Piétu, V., Dutrey, A., Guilloteau, S., Chapillon, E., & Pety, J. 2005, *A&A*, 460, L43
- Piétu, V., Guilloteau, S., & Dutrey, A. 2005, *A&A*, 443, 945
- Piétu, V., Dutrey, A., & Kahane, C. 2003, *A&A*, 398, 565
- Pirola, V., Scaltriti, F., & Coyne, G. V. 1992, *Nature*, 359, 399
- Pirzkal, N., Spillar, E. J., Dyck, H. M. 1997, *ApJ*, 481, 392
- Poetzel, R., Mundt, R., & Ray, T. P. 1989, *A&A*, 224, L13.
- Polomski, E. F., Telesco, C. M., Piña, R., & Schulz, B. 2002, *AJ*, 124
- Pontoppidan, K. M., Blake, G. A., van Dishoeck, E. F., Smette, A., Ireland, M. J., & Brown, J. 2008, 684, 1323
- Preibisch, Th., Kraus, S., Driebe, Th., van Boekel, R., & Weigelt, G. 2007, *A&A*, 458, 235

- Raman, A., Lisanti, M., Wilner, D. J., Qi, C., & Hogerheijde, M. 2006, *AJ*, 131, 2290
- Reipurth, B., & Zinnecker, H. 1993, *A&A*, 278, 81
- Reipurth, B., Bally, J., & Devine, D. 1997, *ApJ*, 114, 2708
- Ray, T. P., Poetzel, R., Solf, J., & Mundt, R. 1990, *ApJ*, 357, L45
- Robitaille, T. P., Whitney, B. A., Indebetouw, R., Wood, K., & Denzmore, P. 2006, *ApJS*, 167, 256
- Rodmann, J., Henning, Th., Chandler, C. J., Mundy, L. G., & Wilner, D. J. 2006, *A&A*, 446, 211
- Rodríguez, L. F., Gómez, Y., & Tafuya, D. 2007, *ApJ*, 663, 1083
- Rodríguez, L.F., Zapata, L., Ho, P.T.P. 2007, *Revista Mexicana de Astronomia y Astrofisica*, 43, 149
- Román-Zúñiga, C. G., Elston, R., Ferreira, B., & Lada, E. A. 2008, *ApJ*, 672, 861
- Sandell, G. 1994, *MNRAS*, 271, 75
- Sandell, G., & Weintraub, D.A. 1994a, *A&A*, 292, L1
- Sandell, G., & Weintraub, D.A. 1994b, in *The Nature and Evolutionary Status of Herbig Ae/Be Stars*, ASP Conf. Ser. Vol. 62, Eds. P.S. Thé, M.R. Pérez, & E.P.J. van Heuvel (Astronomical Society of the Pacific: San Francisco), p. 261
- Sandell, G., & Weintraub, D.A. 1998, “Secondary Calibrators for Scuba,” <http://www.jach.hawaii.edu/~wsh/scuba/astronomy/calibrators.html>
- Sandell, G. 2000, *A&A*, 358, 242
- Sandell, G., & Weintraub, D.A. 2001, *ApJS*, 134, 115
- Sandell, G., Jessop, N., & Jenness, T. 2001, “The SCUBA map reduction Cookbook”, *Starlink Cookbook 11.2*, Rutherford Appleton Laboratory, Particle Physics & Astronomy Research Council
- Sault, R.J., Teuben, P.J., & Wright, M.C.H. 1995, in *ASP Conf. Ser. 77: Astronomical Data Analysis Software and Systems IV*, Eds. R.A. Shaw, H.E. Payne, & J.J.E. Hayes (Astronomical Society of the Pacific: San Francisco), p. 433

- Sargent, A., & Beckwith, S. 1987, *ApJ*, 323, 294
- Semenov, D., Pavlyuchenkov, Ya., Schreyer, K., Henning, Th., Dullemond, C., & Bacmann, A. *ApJ*, 621, 853
- Schulz, A., Black, J. H., Lada, C. J., Ulich, B. L., Martin, R. N., Snell, R. L., & Erickson, N. J. 1989, *ApJ*, 341
- Sheret, I., Dent, W. R. F., & Wyatt, M. C. 2004, *MNRAS*, 348, 1282
- Shevchenko, V. S., Grankin, N., Ibragimov, M. B., Kondratiev, V. Y., & Melnikov, S. 1994, in *The Nature and Evolutionary Status of Herbig Ae/Be Stars*, ASP Conf. Ser. Vol. 62, Eds. P. S. Thé, M. R. Pérez, & E.P.J. van Heuvel (Astronomical Society of the Pacific: San Francisco), p. 43
- Shore, S. N., Brown, D. N., Bopp, B. W., Robinson, C. R., Sanduleak, N., & Feldman, P. D. 1990, *apjs*, 73, 461
- Siebenmorgen, R., Prusti, T., Natta, A., & Müller, T. G. 2000, *A&A*, 361, 258
- Simon, M., Dutrey, A., & Guilloteau, S. 2000, *ApJ*, 545, 1034
- Skinner, S. L., Brown, A., & Stewart, R. T. 1993 *ApJS*, 87, 217
- Sloan, G. C., et al. 2005, *ApJ*, 632, 956
- Slysh, V. I., Val'tts, I. E., Kalenskii, S. V., Voronkov, M. A., Palagi, F., Tofani, G., & Catarzi, M. 1999, *A&AS*, 134, 115
- Smith, K. W., Balega, Y. Y., Hofmann, K.-H., Preibisch, T., Schertl, D., & Weigelt, G. 2004, *A&A*, 413, 217
- Smith, K. W., Balega, Y. Y., Hofmann, K.-H., Lachaume, R., Preibisch, T., Schertl, D., & Weigelt, G. 2005, *A&A*, 431, 307
- Snell, R. L., & Bally, J. 1986, *ApJ*, 303, 683
- Stine, P. C., & O'Neal, D. 1998, *AJ*, 116, 890
- Strelnitski, V. S., Smith, H. A., & Ponomarev, V. O. 1996, *ApJ*, 470, 1134
- Strom, S. E., Strom, K. M., Yost, J., Carrasco, L., & Grasdalen G. L. 1972 *ApJ*, 173, 353
- Strom, K. M., Strom, S. E. 1994, *ApJ*, 424, 237

- Sylvester, R. J., Skinner, C. J., Barlow, M. J., & Mannings, V. 1996, MNRAS, 279, 915
- Sylvester, R. J., Dunkin, S. K., & Barlow, M. J. 2001, MNRAS, 327, 133
- Tafoya, D., Gómez, Y., & Rodríguez, L. F. 2004, ApJ, 610, 827
- Testi, L., Natta, A., Shepherd, D. S., & Wilner, D. J. 2003, A&A, 323
- Testi, L., Palla, F., & Natta, A. 1998, A&AS, 133, 81
- Thé, P. S., de Winter, D., & Pérez, M. R. 1994, A&AS, 104, 315
- Thi, W. F., et al. 2001, ApJ, 561, 1074
- Thompson, M. A., Urquhart, J. S., & White, G. J. 2004, A&A, 415, 627
- Thompson, R. I., Strittmatter, P.A., Erickson, E. F., Witteborn, F. C., & Strecker, D. W. 1977, ApJ, 218, 170
- Torrelles, J. M., Ho, P. T. P., Moran, J. M., Rodríguez, L. F., & Cantó, J. 1986, ApJ, 307, 787
- Torres, R. M., Loinard, L., Mioduszewski, A. J., & Rodríguez, L. F. 2009, ApJ, 698, 242
- Turner, D. G. 1976, ApJ, 210, 65
- Tuthill, P. G., Monnier, J. D., & Danchi, W. C. 2002, Nature, 409, 1012
- Tuthill, P. G., Monnier, J. D., Danchi, W. C., Hale, D. D. S., & Townes, C. H. 2002, ApJ, 577, 826
- Valenti, J. A., Fallon, A. A., & Johns-Krull, C. M. 2003, ApJS, 147, 305
- van Boekel, R., Min, M., de Koter, A., Dominik, C., van den Ancker, M. E., & Bouwman, J. 2005, A&A, 437, 189
- van den Ancker, M. E., de Winter, D., & Tjin A Djie, H. R. E. 1998, A&A, 330, 145
- van der Veen, W. E. C. J., Waters, L. B. F. M., Trams, N. R., & Matthews, H.E. 1994, A&A, 285, 551
- Verdes-Montenegro, L., Gómez, J.F., Torrelles, J. M., Anglada, G., Estalella, R., & López, R. 1991, ApJ, 244, 84
- Vieira, S. L. A., Corradi, W. J. B., Alencar, S. H. P., Mendes, L. T. S., Torres, C. A. O., Quast, G. R., Guimarães, M. M., & da Silva, L. 2003, AJ, 126, 2971

- Voshchinnikov, N. V., Molster, F. J., & Thé, P. S. 1996, *A&A*, 312, 243
- Walker, H. J., & Butner, H. M. 1995, *Ap&SS*, 224, 389
- Walker, H. J., & Heinrichsen, I. 2000, *Icarus*, 143, 147
- Walker, H. J., & Wolstencroft, R. D. 1988, *PASP*, 100, 1509
- Wallenquist, A. 1937, *Uppsala Medd.*, 71
- Wang, S., & Looney, L. W. 2007, *ApJ*, 659, 1360
- Weinberger, A. J., Becklin, E. E., Schneider, B. A., Smith, P. J., Lowrance,, P. J., Silverstone, M. D., Zuckerman, B., & Terile, R. J. 1999, *ApJ*, 525, L53
- Weinberger, A. J., Rich, R. M., Zuckerman, B., & Matthews, K. 2000, *ApJ*, 544, 937
- Weintraub, D.A. 1990 *ApJS*, 74, 575
- Weintraub, D. A., Sandell, G., & Duncan, W. D. 1989, *ApJ*, 340, L69
- Weintroub, J., Moran, J. M., Wilner, D. J., Young, K. H., Rao, R., & Shinnaga, H. 2008, *ApJ*, 677, 1140
- Weigelt, G., Balega, Y. Y., Hofmann, K.-H., Preibisch, T. 2002, *A&A*, 392, 937
- White, R. L., & Becker, R. L. 1985, *ApJ*, 297, 677
- Williams, J. P., Mann, R. K., Beaumont, C. N., Swift, J. J., Adams, J. D., Hora, J. Kassis, M., Lada, E. A., & Román-Zúñiga, C. G. 2009, *ApJ*, 699, 1300
- Zapata, L. A., Menten, K., Reid, M., & Beuther, H. 2009, *ApJ*, 691, 332

Table 1. Stellar parameters of our target stars

Star	Alt. Name	$\alpha(2000.0)$ [h m s]	$\delta(2000.0)$ [° ' "]	Spectral Type	ref.	L_{tot} [L_{\odot}]	ref.	Distance [pc]	ref.	Project ID
LkH α 198	V633 Cas	00 11 26.06	+58 49 29.1	B9	1	150	27,28	600	9	m96bc63,m97bn21,
V 376 Cas	HBC 325	00 11 26.71	+58 50 04.1	A3-F2	1	436	13	600	9	m01bi09
V892 Tau	Elias 3–1	04 18 40.62	+28 19 15.5	B8-9	1,29	400	11	130	12	m99an21
LkH α 101	HBC 40	04 30 14.39	+35 16 24.3	B0 Ve	14	4×10^4	14	700	31	m97bu34
AB Aur	HD 31293	04 55 45.84	+30 33 04.3	A1 Ve	1	93	1,35	144	5	m97bn21,nlserv
MWC 480	HD 31648	04 58 46.27	+29 50 37.0	A5 V	4	39	5,33	131	5	m01bi09
HD 34282	V1366 Ori	05 16 00.48	−09 48 35.3	A3 Ve	4,34	22.3	34	350	34	m96bh17,m00au06
HD 35187	BD+24°826	05 24 01.17	+24 57 37.6	A2e+A7	58	23.4	13	150	58	m97bc36
HD 36112	MWC 758	05 30 27.53	+25 19 57.1	A7 III	8	31.3	13	200	5,8	m97bc36
MWC 137	V1308 Ori	06 18 45.46	+15 16 53.4	B0ep	3	1.5×10^3	36	1300	2	m99an21,m01bi09
LkH α 215	V699 Mon	06 32 41.80	+10 09 33.6	B6-8	1, 37	2.95×10^3	13	800	38	m99bu03
VY Mon	HBC 202	06 31 06.94	+10 26 05.0	B8:e	3	870	39	800	38	UKT14 data
HD 259431	MWC 147	06 33 05.19	+10 19 20.0	B6	1	1.07×10^4	13	800	38	m99bu03
AFGL 961 A	IRAS 06319+0415	06 34 37.6	+04 12 43.9	B2-B3/B5	6	3×10^3	16	1500	17	m98ai11
R Mon	MWC 151	06 39 09.95	+08 44 10.8	B8 IIIev	4	740	13	800	52,53	UKT14 data
LkH α 25	V590 Mon	06 40 44.64	+09 48 02.1	B7	1	63	13	800	13,24	m00bc32
HD 135344B	SAO 206462	15 15 48.44	−37 09 15.9	F4Ve	7	8.5	13	140	7, 47	m96bu90
HD 141569	SAO 140789	15 49 57.75	−03 55 16.4	A0 Ve	4	23	13	99	13,5	m00ua06
HD 142666	V1026 Sco	15 56 40.02	−22 01 40.0	A8 Ve	25	17	13	145	13,25	m97bc36
HD144432	SAO 184124	16 06 57.96	−27 43 09.8	A9 IIIe	8	15	13	~145	13,25	m97bc36
HR 5999	HD 144668	16 08 34.29	−39 06 18.3	A6 IIIe	8	115	13	208	13	m01bi09
HD 150193	MWC 863	16 40 17.92	−23 53 45.2	A3 IIIe	8	49	13	150	13	m01bi09
CD−42° 11721	V921 Sco	16 59 06.77	−42 42 08.4	B0ep	40,41	2.34×10^4	16	1150	42	m99au36
KK Oph	HBC 273	17 10 08.07	−27 15 18.2	A5 Ve	8	26	13	160	13,26	m01bi09
HD 316285	MWC 272	17 48 14.04	−28 00 53.2	Be	43	2.8×10^5	43	1850	43	m98au64
HD 163296	MWC 275	17 56 21.29	−21 57 21.9	A3Ve	25,50	35	49	122	5	m97bn21,m0Xa/bec05
HD 169142	MWC 925	18 24 29.78	−29 46 49.4	A7 Ve	8	22	8,49	145	25,47	m97bc36
MWC 297	NZ Ser	18 27 39.53	−03 49 52.2	B1.5 Ve	4	1.07×10^4	19	250	59	m97bi09
MWC 300	V431 Sct	18 29 25.69	−06 04 37.3	B[e]	3	1.3×10^5	20	1800	20	m99au36
HD 176386	CD−37° 13023	19 01 38.93	−36 53 26.6	A0V	48	36	48	130	47	m00au58
TY Cr A	CD−37° 13024	19 01 40.83	−36 52 33.9	B8V	45,46	67	46	130	47	m00au58
BD+40°4124	V1685 Cyg	20 20 28.37	+41 21 51.4	B3	1	6.0×10^4	13	980	5	m97bn21
V 1686 Cyg	LkH α 224	20 20 29.26	+41 21 28.6	F9	1	257	13	980	5	m97bn21
V 1318 Cyg S	LkH α 225 S	20 20 30.59	+41 21 26.0	A5-Fe	2	1600	22	980	5	m97bn21

Table 1—Continued

Star	Alt. Name	$\alpha(2000.0)$ [h m s]	$\delta(2000.0)$ [$^{\circ}$ ' '']	Spectral Type	ref.	L_{tot} [L_{\odot}]	ref.	Distance [pc]	ref.	Project ID
MWC 349	V 1478 Cyg	20 32 45.53	+40 39 36.6	Be	44	3×10^4	44	1200	44	m01bi09
PV Cep	HBC 696	20 45 53.96	+67 57 38.9	A5	1	80	54	500	56	m97bn21, & UKT14 data
HD 200775	MWC 361	21 01 36.92	+68 09 47.8	B3	1	1.9×10^3	36	430	5	m99bu03,m01bi09
V 645 Cyg	RAFGL 2789	21 39 58.24	+50 14 21.2	B1-2	57	$2 - 6 \times 10^4$	57	4200	57	m01bi09
MWC 1080 A	V 628 Cas	23 17 25.59	+60 50 43.6	B0eq	30	4.6×10^4	54	2200	55	m01bi09

(1) Hernandez et al. (2004), (2) Hillenbrand et al.(1992), (3) Thé et al. (1994), (4) Mora et al. (2001), (5) van den Ancker et al. (1998), (6) Castelar et al. (1985), (7) van Boekel et al. (1995), (8) Blondel et al. (2006), (9) Chavarría-K (1985), (10) Natta et al. (1992), (11) Monnier et al. (2008), (12) Torres et al. (2009), (13) Manoj et al. (2006), (14) Tuthill et al. (2002), (15) Bertout et al. (1999), (16) this paper (17) Williams et al. (2009), (18) Habart et al. (2003), (19) Alonso-Albi et al. (2009), (20) Miroshnichenko et al. (2004), (21) Siebenmorgen et al. (2000), (22) Marvel (2005), (23) Reipurth et al. (1997), (24) Finkenzeller & Mundt (1984), (25) van Boekel et al. (2005), (26) Leinert et al. (2004), (27) Lagage et al. (1993), (28) Natta et al. (1992), (29) Strom & Strom (1994), (30) Cohen & Kuhl (1979), (31) Herbig et al. (2004), (32) Meeus et al. (2001), (33) Dent et al. (2005), (34) Merin et al. (2004), (35) Acke et al. (2004), (36) Berilli et al. (1992), (37) Valenti et al. (2003), (38) Herbst et al. (1982), (39) Casey & Harper (1990), (40) de Winter & Thé (1990), (41) Shore et al. (1990), (42) Borges Fernandes et al. (2007), (43) Hillier et al. (1998), (44) Cohen et al. (1985), (45) Casey et al. (1995), (46) Casey et al. (1998), (47) de Zeeuw et al. (1999), (48) Meyer & Wilking (2009), (49) Acke et al. (2004), (50) Gray & Corbally (1998), (51) Cohen, Harvey & Schwartz (1985), (52) Walker (1956), (53) Close et al. (1997), (54) Evan et al. (1986) (55) Cantó et al. (1994), (56) Cohen et al. (1981), (57) Miroshnichenko et al. (2009), (58) Duncin & Crawford (1998), (59) Drew et al. (1997)

Table 2a. Positions, deconvolved sizes and integrated flux densities of target stars

HAEBE star	$\alpha(2000.0)$ [h m s]	$\delta(2000.0)$ [$^{\circ}$ ' "]	$\theta_a \times \theta_b$	P.A. [$^{\circ}$]	S(850 μ m) [mJy]	S(450 μ m) [mJy]
LkH α 198 ^a	00 11 26.23	+58 49 32.2	11".4 \times 5".6	+29 \pm 10	220 \pm 30	...
V 376 Cas ^b	00 11 26.36	+58 50 01.4	$\leq 6'' \times 6''$...	140 \pm 20	...
V 892 Tau	04 18 40.64	+28 19 16.1	point source	...	630 \pm 20	2250 \pm 100
AB Aur	04 55 45.89	+30 33 05.1	point source	...	350 \pm 20	2200 \pm 100
MWC 480	04 58 46.45	+29 50 39.0	6".4 \times 4".7	+138 \pm 4	780 \pm 20	3300 \pm 290
HD 34282	05 16 00.48	−9 48 35.3	point source	...	360 \pm 9	2700 \pm 400
HD 36112	05 30 27.56	+25 19 56.9	point source	...	197 \pm 10	1540 \pm 50
HD 35187	05 24 01.17	+24 57 37.6	point source	...	70.6 \pm 6	340 \pm 85
LkH α 101 ^c	04 30 14.38	+35 16 23.6	6".5 \times 2".6	+26 \pm 20	818 \pm 50	...
AFGL 961 A	06 34 37.54	+04 12 44.6	12".2 \times 7".0	−41 \pm 2	1950 \pm 60	14900 \pm 300
AFGL 961 SMM	06 34 36.71	+04 12 50.9	8".8 \times 5".6	−5 \pm 10	1330 \pm 50	12300 \pm 300
HD 135344 B	15 15 48.56	−37 09 15.8	point source	...	490 \pm 10	3180 \pm 230
HD 141569	15 49 57.75	−03 55 16.4	10.9 \pm 1.3	64.9 \pm 13.3
HD 142666	15 56 40.01	−22 01 39.0	$\leq 2''.2$...	313 \pm 5	1140 \pm 35
HD 144432	16 06 57.90	−27 43 09.8	129 \pm 6	...
HR 5999	16 08 34.42	−39 06 18.3	point source	...	64 \pm 20	...
HD 150193	16 40 17.85	−23 53 44.8	point source	...	101 \pm 10	...
KK Oph	17 10 08.12	−27 15 18.8	point source	...	91 \pm 15	...
HD 163296	17 56 21.42	−21 57 21.6	4".6 \times 3".2	−13 \pm 27	1900 \pm 200	8700 \pm 370
HD 169142	18 24 29.87	−29 46 48.9	$\sim 2''.3 \times 1''.6$...	565 \pm 10	3340 \pm 115
MWC 297	18 27 39.53	−03 49 50.4	$< 4''$...	570 \pm 30	1450 \pm 200
V 1318 Cyg S-mm	20 20 30.67	+41 21 29.9	8'' \times 3''	+62 \pm 1	2050 \pm 50	10200 \pm 200
MWC 349	20 32 45.53	+40 39 36.6	point source	...	2600 \pm 70	5000 \pm 1100
PV Cep	20 45 54.31	+67 57 40.7	4".9 \times 2".8	+74 \pm 10	1000 \pm 20	6550 \pm 150
V 645 Cyg	21 39 58.26	+50 14 22.3	14".2 \times 8".5	−65 \pm 3	2400 \pm 60	20800 \pm 600
MWC 1080 A	23 17 24.35	+60 50 40.4	point source	...	250 \pm 50	...

^a LkH α 198 and LkH α 198 B are blended with the nearby Class 0 source, LkH α 198-mm, resulting in uncertain size and position. LkH α 198 B appears to dominate the sub-millimeter emission.

^b Peak offset by 3'' from the optical position of V 376 Cas, possibly emission from the surrounding cloud.

^c Flux density at 750 μ m, S(750 μ m) = 940 \pm 100 mJy

Table 2b. Submillimeter photometry of compact HAEBE stars

HAEBE star	λ [μm]	HPBW [$''$]	Flux density [mJy]	Date mm/dd/yr
AB Aur	1300 ^a	32.0	136 ± 15	12/10/89
	1100	18.4	192 ± 19	08/20/88
	800	15.8	534 ± 69	08/20/88
	800	16.8	475 ± 56	08/16/90
	450	17.5	1760 ± 360	08/16/90
R Mon	1300 ^a	32.0	96 ± 15	12/09/89
	1300	19.0	36 ± 18	10/09/91
	1100	18.4	80 ± 20	08/19/88
	850	17.8	171 ± 24	08/16/90
	800	15.8	260 ± 30	08/19/88
	800	16.8	197 ± 30	08/16/90
	450	17.5	1200 ± 160	08/19/88
	350	19.0	2600 ± 500	08/19/90
VY Mon	1300	19.0	189 ± 23	10/09/91
	1100	18.5	247 ± 27	10/09/91
	800	16.5	552 ± 55	10/09/91
KK Oph	1100	18.4	36 ± 11	08/11/91
	800	16.8	109 ± 20	08/18/90
	800	16.4	119 ± 53	10/06/91
PV Cep	1300	32.0	0.375 ± 0.044	12/10/89
	1300	19.5	0.36 ± 0.023	08/18/90
	1100	18.4	0.50 ± 0.04	08/20/88
	1100	18.4	0.47 ± 0.03	10/27/88
	850	17.8	1.01 ± 0.07	08/18/90
	800	15.8	1.3 ± 0.1	08/20/88
	800	15.8	1.11 ± 0.09	10/27/88
	800	16.8	1.16 ± 0.06	08/18/90
	800	13.5	1.2 ± 0.1	08/20/88
	750	17.5	1.41 ± 0.09	08/11/91
	450	17.5	7.91 ± 0.62	08/18/90
	450	17.5	3.48 ± 1.20	08/11/91
	450	13.5	10.6 ± 0.8	08/20/88
	450	7.9	10.5 ± 0.5	08/20/88
	350	17.7	17.6 ± 1.0	08/20/88
	350	10	16.2 ± 0.7	08/20/88

^aCSO observations

Table 2c. Non-detections

Star	850 μ m upper limit [mJy/beam]	Comments
MWC 137	15	cloud emission, nearby sources
LkH α 215	22	emission from the surrounding nebula
HD 259431	20	emission from the surrounding nebula
LkH α 25	25	cloud emission
CoD–42° 11721	50	nearby sources
HD 316285	70	cloud emission
MWC 300	7	empty field
HD 176386	50	cloud emission
TY Cr A	50	cloud emission
BD+40°4124	35	cloud emission
V1686 Cyg	35	cloud emission, nearby source
HD 200775	20	emission from the surrounding nebula

Table 3. *Spitzer* MIPS flux densities of program stars

Star	24 μm [Jy]	70 μm [Jy]	AOR ID
AB Aur	S ^a	S ^a	r12662784
V 892 Tau	S ^a	$25.41 \pm 0.10^{\text{b}}$	r11119696, r11229952
AFGL 961	S ^a	S ^a	r12234249, r12234752
HR 5999	2.89 ± 0.72	3.78 ± 0.36	c2d
HD 141569	1.47 ± 0.01	4.70 ± 0.02	r11181312
HD 150193	S ^a	3.05 ± 0.29	c2d
CD−42° 11721	S ^a	S ^a	MIPSGAL
KK Oph	S ^a	S ^a	r14094848
BD+40°4124	S ^a	...	r22512128, r22512384
V1686 Cyg	S ^a	...	r22512128, r22512384
V1318 Cyg S-mm	S ^a	85.68 ± 0.66	r22512128, r22512384
MWC 349	S ^a	6.72 ± 0.30	r22510336

^aSaturated

^bMildly saturated

Table 4. Isothermal graybody fits to HAEBE “disks”

Source	T_d [K]	α	β	M_{tot} [M_\odot]	L_{dust} [L_\odot]
V 892 Tau	40	2.19 ± 0.09	0.52	0.009	0.27
AB Aur	66	2.89 ± 0.04	1.05	0.006	5.0
MWC 480	28	2.65 ± 0.06	0.81	0.02	0.23
HD 34282	29	3.03 ± 0.12	1.29	0.18	1.85
HD 35187	44	2.64 ± 0.34	0.87	0.002	0.15
HD 36112	43	3.03 ± 0.10	1.25	0.014	1.0
AFGL 961 A	37	2.73 ± 0.02	1.51	12.5	930
R Mon	62	3.08 ± 0.15	1.3	0.12	110
VY Mon ^a	38	2.31 ± 0.93	1.9	1.9	102
HD 135344 B	32	2.94 ± 0.30	1.38	0.025	0.20
HD 141569	40	2.21 ± 0.06	0.5	0.00009	0.03
HD 142666	31	2.42 ± 0.07	0.72	0.005	0.08
HD 144432	40	2.70 ± 0.39	0.59	0.002	0.10
HD 150193	44	3.03 ± 0.15	0.65	0.002	0.12
KK Oph	40	1.70 ± 2.12	0.74	0.002	0.13
HD 163296	28	2.66 ± 0.05	0.94	0.065	0.52
HD 169142	41	2.84 ± 0.06	1.30	0.03	0.50
HR 5999	41	3.03 ± 5.18	1.75	0.009	1.1
V 645 Cyg	38	2.84 ± 0.06	1.55	124	11750
V 1318 Cyg-mm	41	2.55 ± 0.06	0.85	1.9	118
PV Cep	29	3.09 ± 0.06	1.59	1.0	13.7

^aFit to UKT14 photometry data, likely to include some contribution from the surrounding cloud.

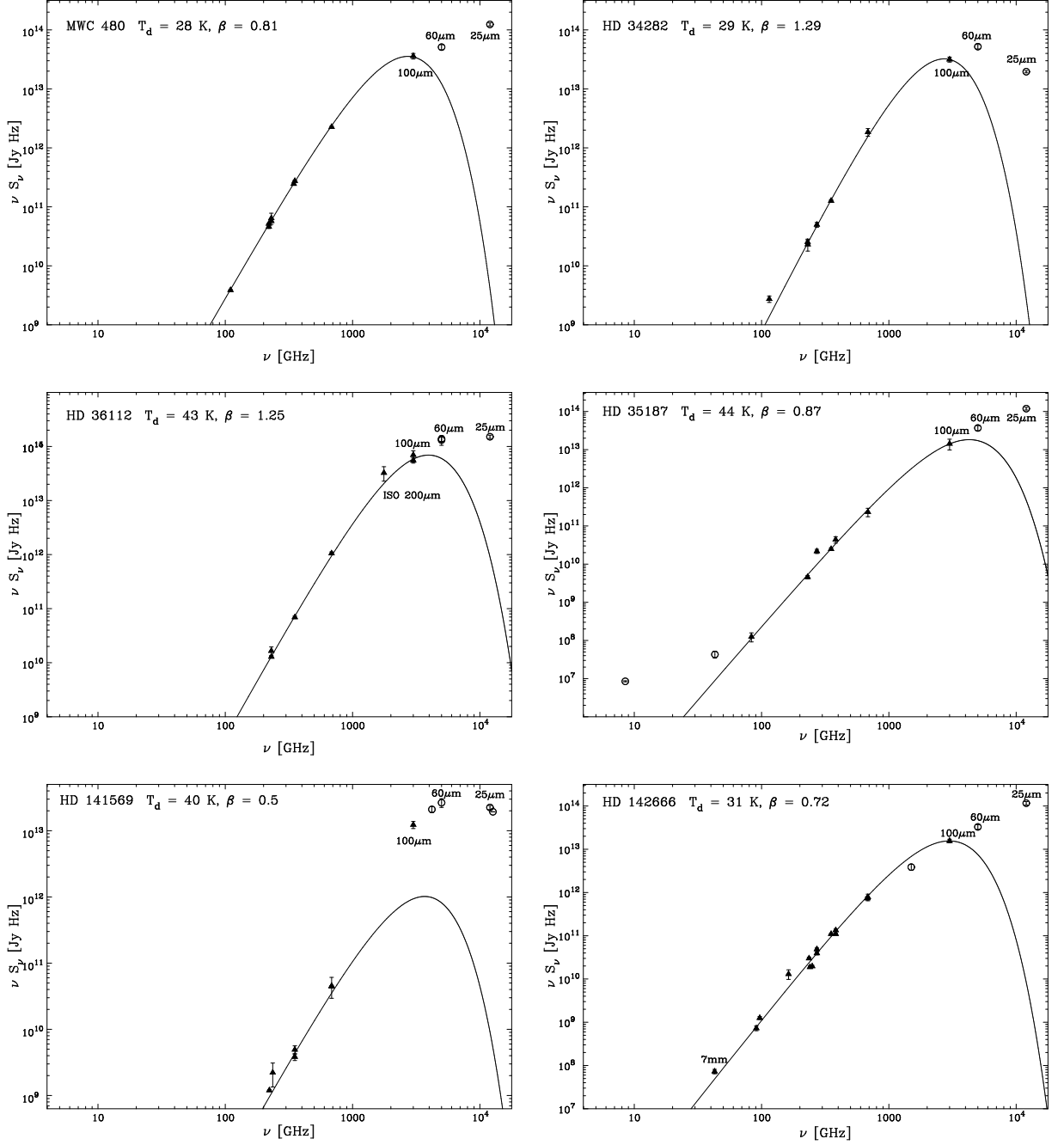


Fig. 1.— Isothermal graybody fits to SCUBA and literature data for isolated HAEBE stars. Flux densities used in the fits are marked by filled triangles, while data points marked with open circles were excluded from the fits. In the top left corner of each plot we give the name of the star and essential fit results (T_d , β).

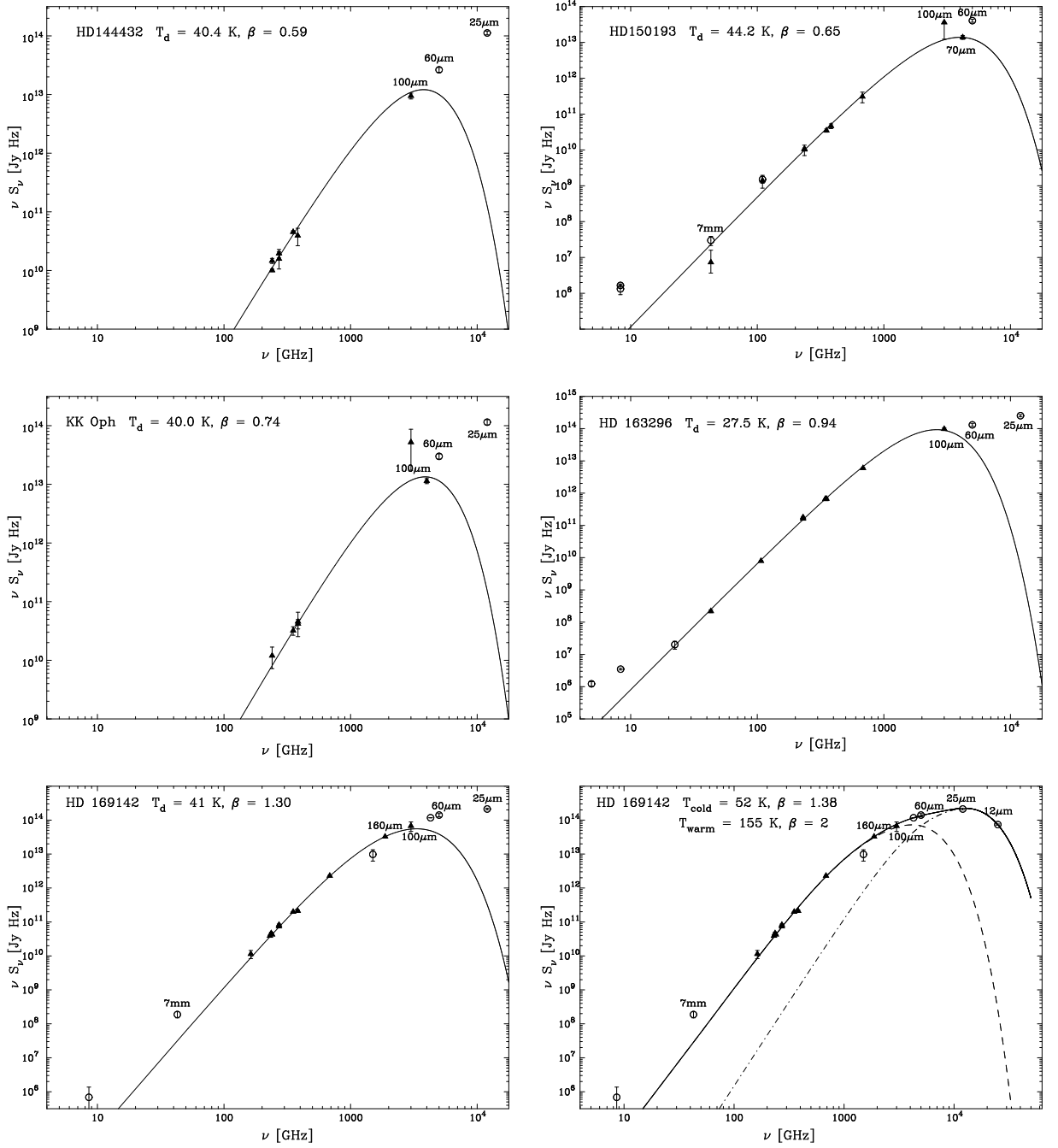


Fig. 2.— Isothermal graybody fits to isolated HAEBE stars continued. Labeling as in previous figure. In the right panel for HD 169142, we show a isothermal fit with two dust components at different temperatures. The cold dust, which dominates at the long wavelengths is shown as a dashed line, the warmer dust as a dash-dotted line, and the combined two-temperature fit as a solid line.

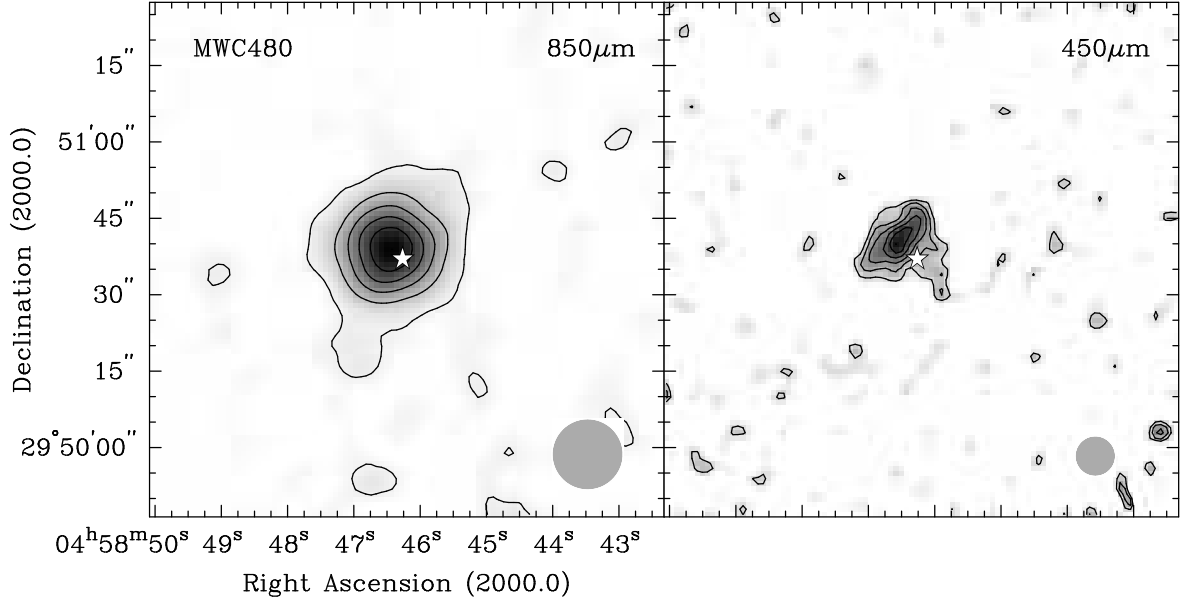


Fig. 3.— Deconvolved sub-millimeter images of MWC480 at 850 and 450 μm plotted in gray-scale and overlaid with contours. The contour levels are linear with six contours between the lowest contour level ($3\text{-}\sigma$) and the peak flux density. The $3\text{-}\sigma$ level is at 54 mJy beam^{-1} and at 840 mJy beam^{-1} for 850 and 450 μm , respectively. The disk is resolved by SCUBA both at 850 and 450 μm . The position of MWC480 is shown with a star symbol. The HPBW is plotted in the bottom left corner of each image.

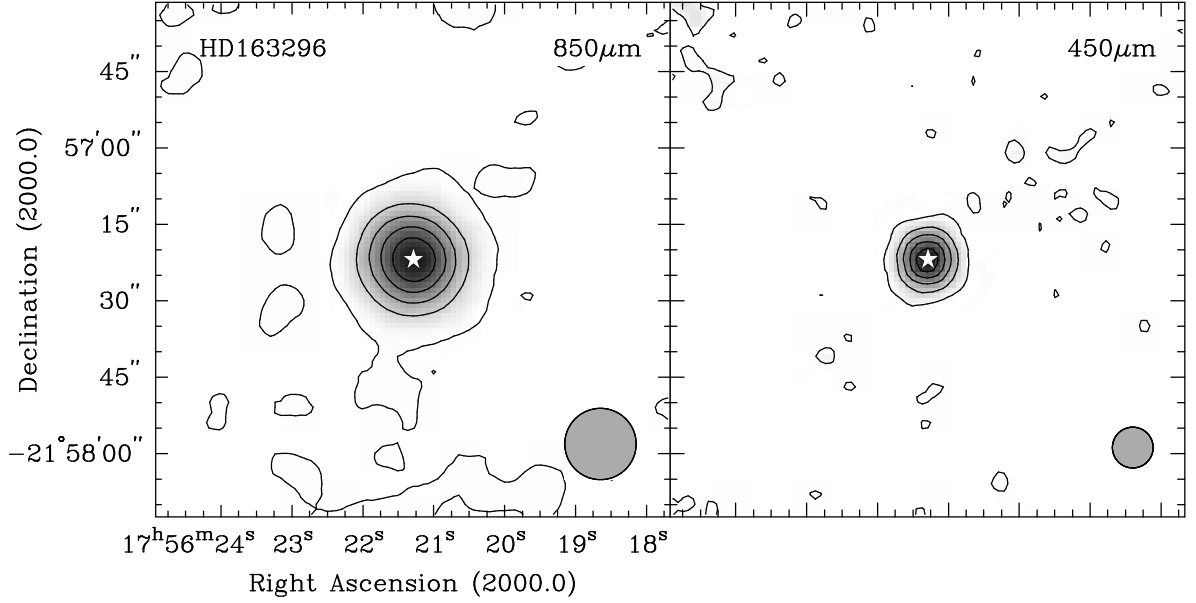


Fig. 4.— Deconvolved sub-millimeter images HD 163296 at 850 and 450 μm . The contours are plotted with linear steps. At 850 μm we plot six contours between the lowest contour level, 32 mJy beam $^{-1}$ (2σ) and the peak flux density, 1.8 Jy beam $^{-1}$. At 450 μm we plot six contours starting from 0.45 Jy beam $^{-1}$ to 7.24 Jy beam $^{-1}$. The disk is resolved by SCUBA both at 850 and 450 μm . The position of HD 163296 is marked by a star symbol. The HPBW is plotted in the bottom left corner of each image.

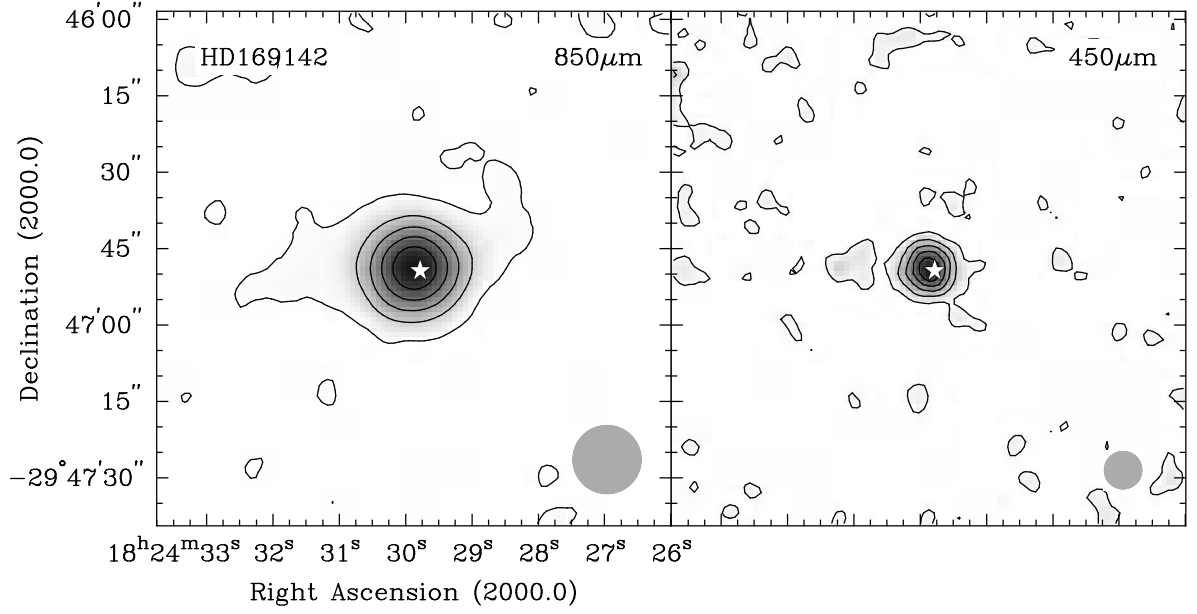


Fig. 5.— Deconvolved SCUBA images of HD 169142 in grayscale overlaid with contours. The contour levels are linear for both 850 and 450 μm with six contours starting at $2\text{-}\sigma$. At 850 μm contours go from 15 mJy beam $^{-1}$ to 537 mJy beam $^{-1}$, at 450 μm from 0.28 Jy beam $^{-1}$ to 3.17 Jy beam $^{-1}$. The disk is marginally resolved (see text).

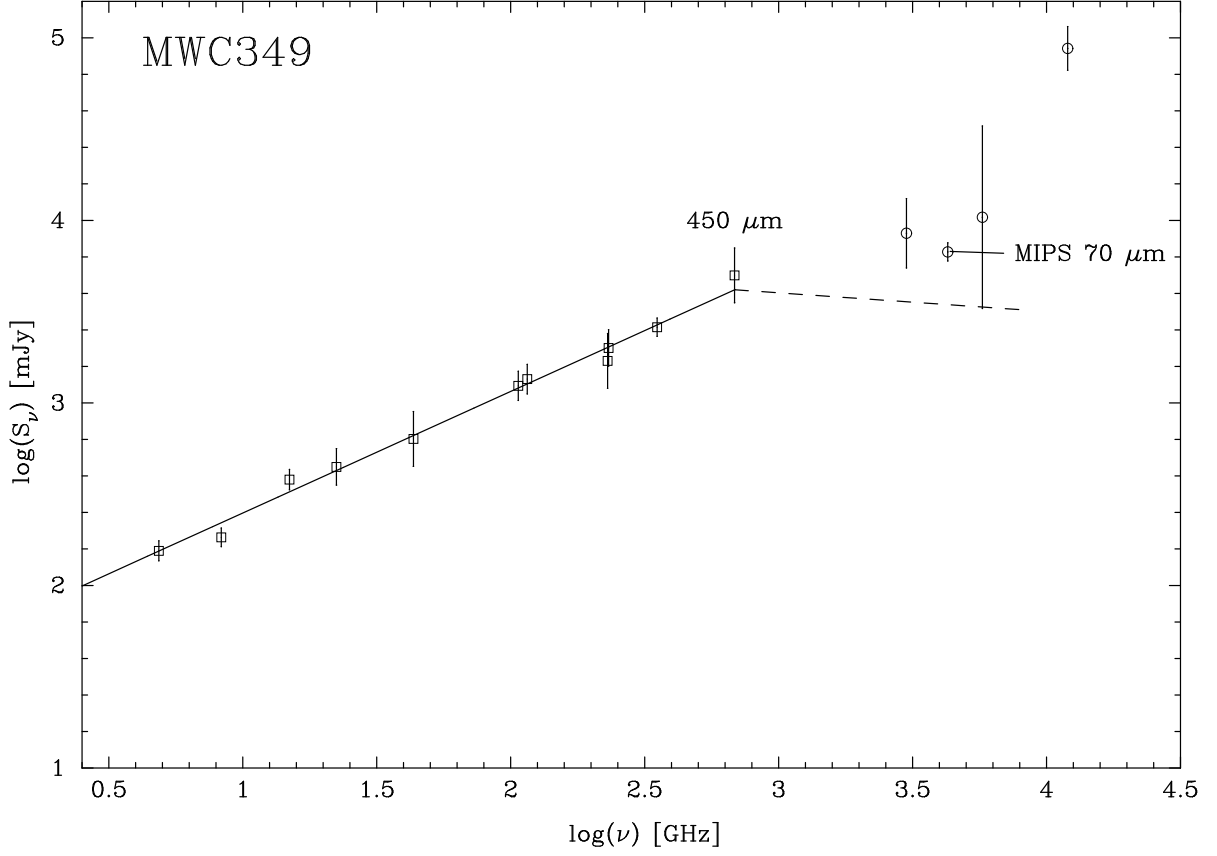


Fig. 6.— Least squares fit to radio and millimeter data for MWC 349 showing that the star has a thermal wind spectrum which dominates the emission to about $450 \mu\text{m}$ with the flux density proportional to the frequency $\nu^{0.67 \pm 0.03}$. If we assume that the wind is launched at 15 AU from the star, the wind should become optically thin at $450 \mu\text{m}$ (see text).

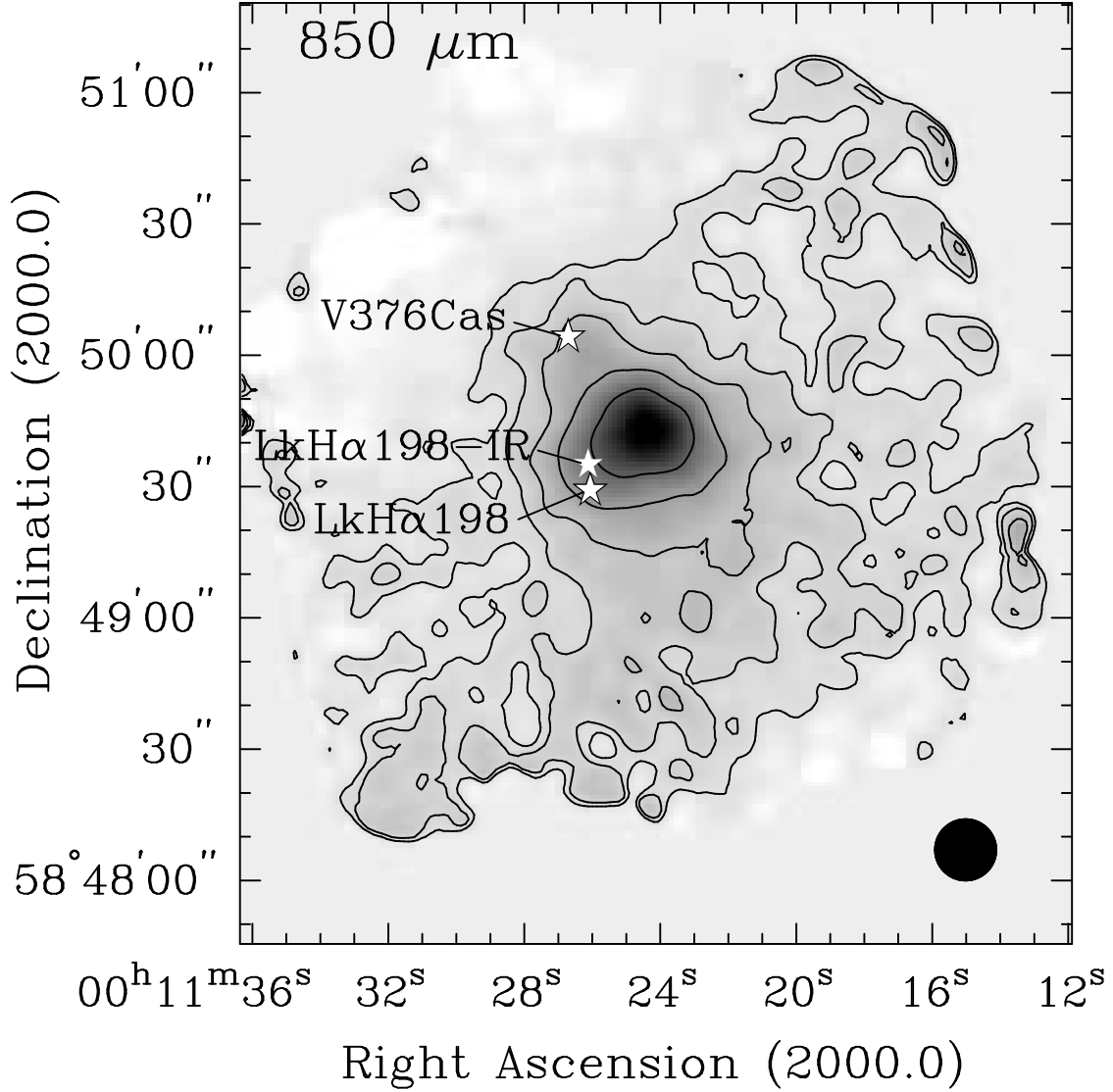


Fig. 7.— SCUBA 850 μm image in grayscale overlaid with contours of the dense cloud in which LkH α 198 and V376 Cas are embedded. The cloud core is quite extended and probably more extended to the northeast, where the image goes negative because we chopped on extended emission. The emission is dominated by a Class 0 source, LkH α 198-mm, which does not have an optical or near-infrared counterpart. This image suggests that both LkH α 198, its infrared companion and V376 Cas may be associated with dust emission, but we do not have high enough spatial resolution to separate the stars from the surrounding strong cloud emission. The contours are plotted with six logarithmic intervals from 40 mJy beam^{-1} to 750 mJy beam^{-1} . The HPBW is shown in the bottom right corner.

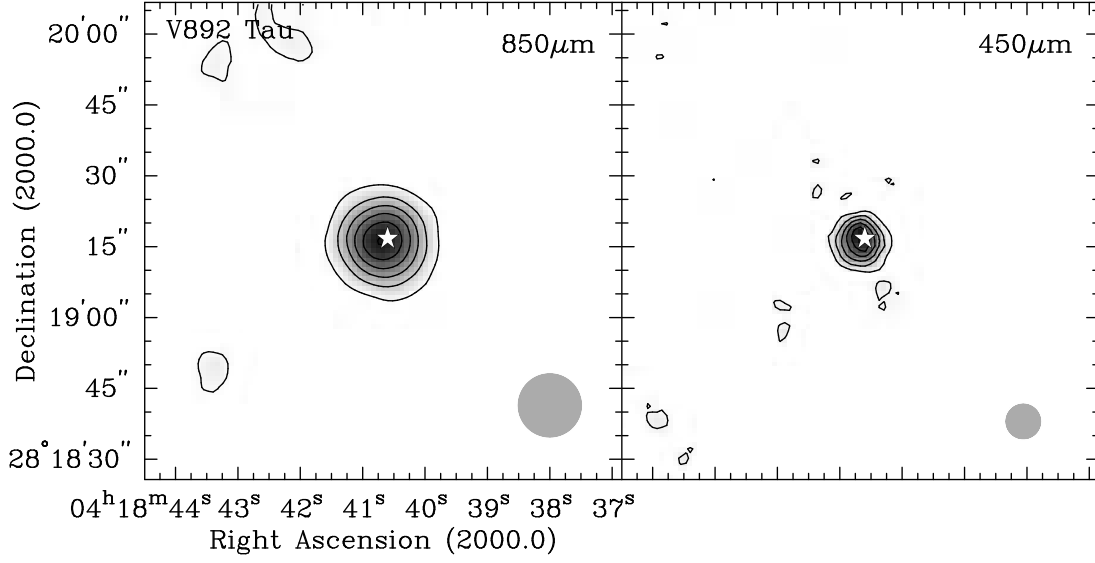


Fig. 8.— Deconvolved SCUBA images of V 892 Tau in grayscale overlaid with contours. The contour levels are evenly spaced with six contours between the lowest contour level, $\sim 2\text{-}\sigma$ and the peak flux density. At $850\text{ }\mu\text{m}$ contours go from 36 mJy beam^{-1} to 630 mJy beam^{-1} , at $450\text{ }\mu\text{m}$ from 0.2 Jy beam^{-1} to 2.25 Jy beam^{-1} . The position of V 892 Tau is marked by a star symbol. The HPBW is shown in the bottom right corner.

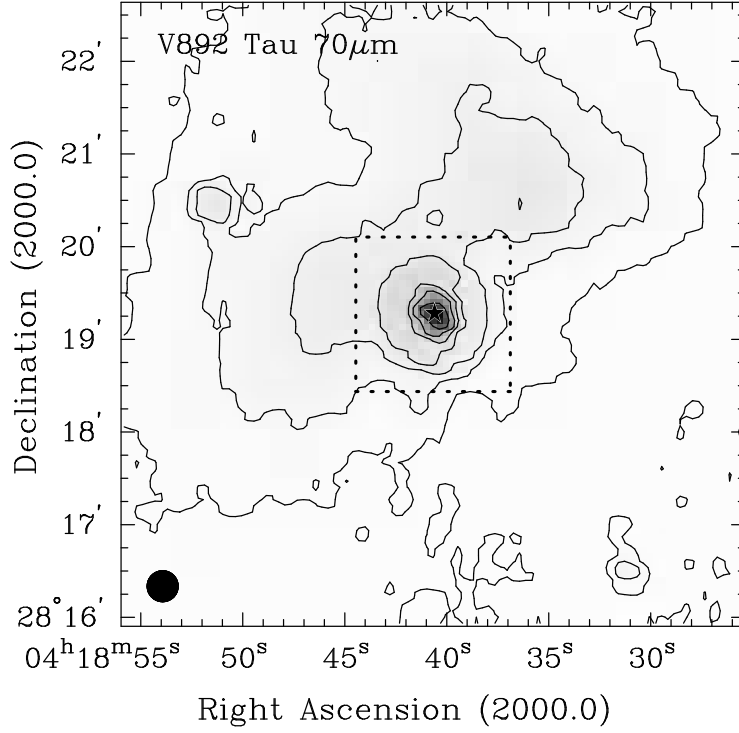


Fig. 9.— MIPS 70 μm image of V 892 Tau in grayscale overlaid with logarithmic contours and covering a much larger field than the SCUBA images. The extent of the SCUBA images is drawn as a dotted rectangle. At 70 μm there is extended nebulosity east and northwest of the star, but no sign of embedded sources in the nebulosity. Two faint 70 μm sources are visible within the displayed area. The 70 μm HPBW is shown in the bottom left corner.

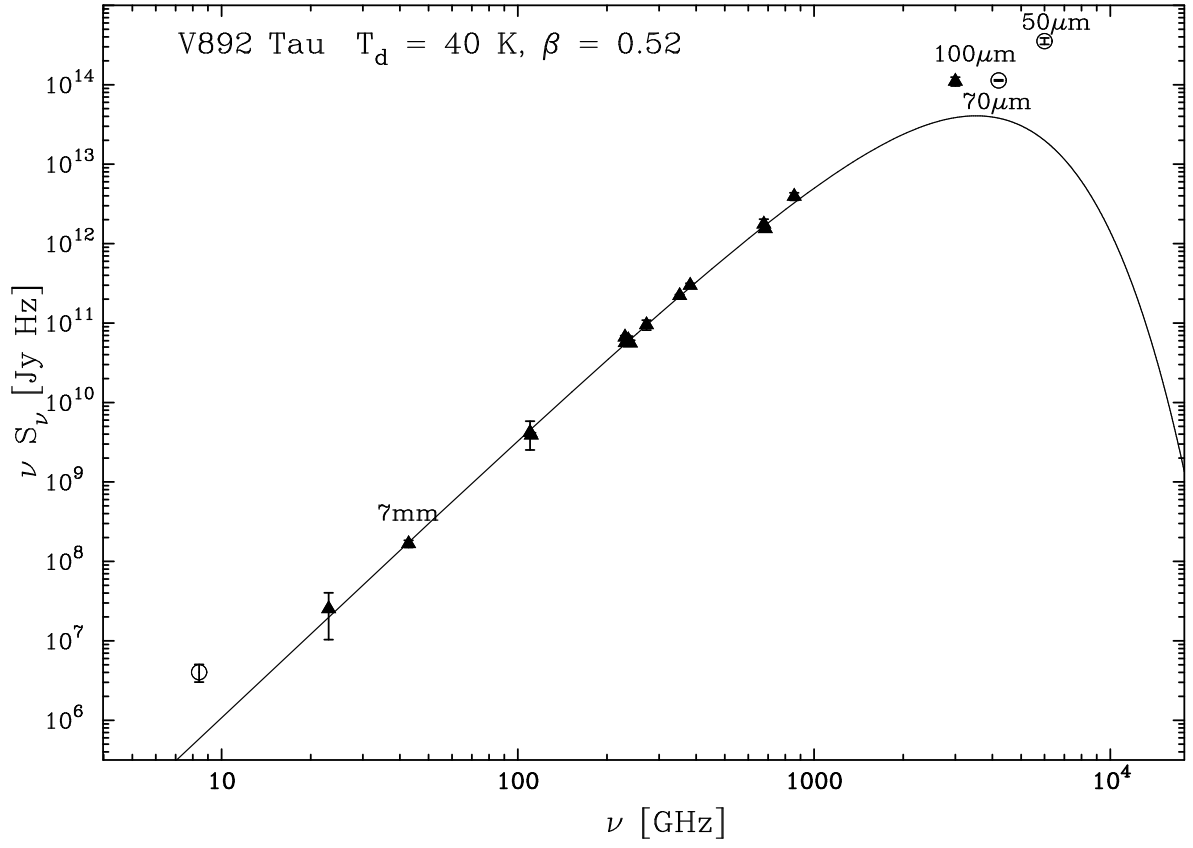


Fig. 10.— Isothermal graybody fit of V 892 Tau assuming a dust temperature of 40 K.

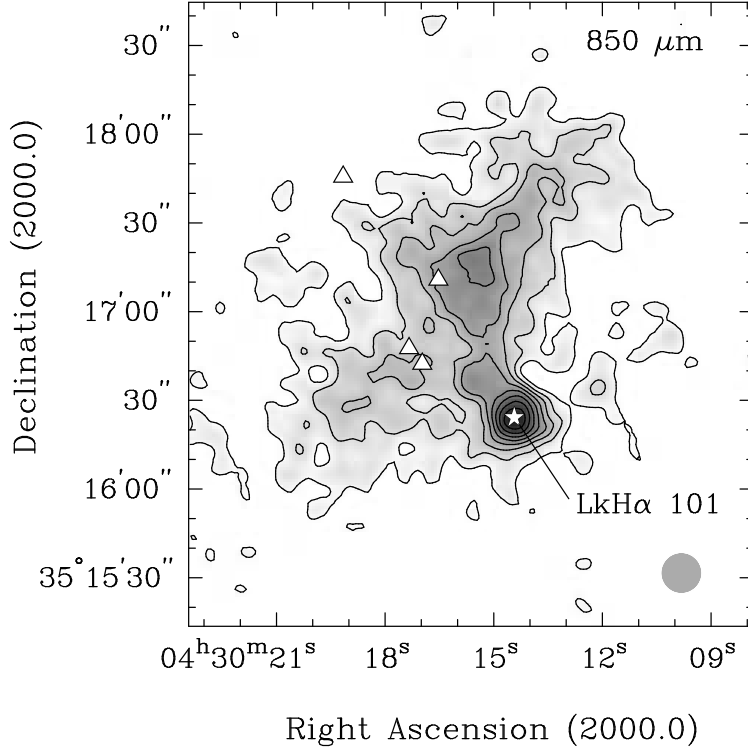


Fig. 11.— SCUBA 850 μm grayscale image of LkH α 101. The contours are linear with the lowest contour at 100 mJy beam⁻¹ and a step of 100 mJy beam⁻¹. The peak flux is 0.9 Jy beam⁻¹. The position of LkH α 101 is marked on the figure. The HPBW is shown in the bottom right corner.

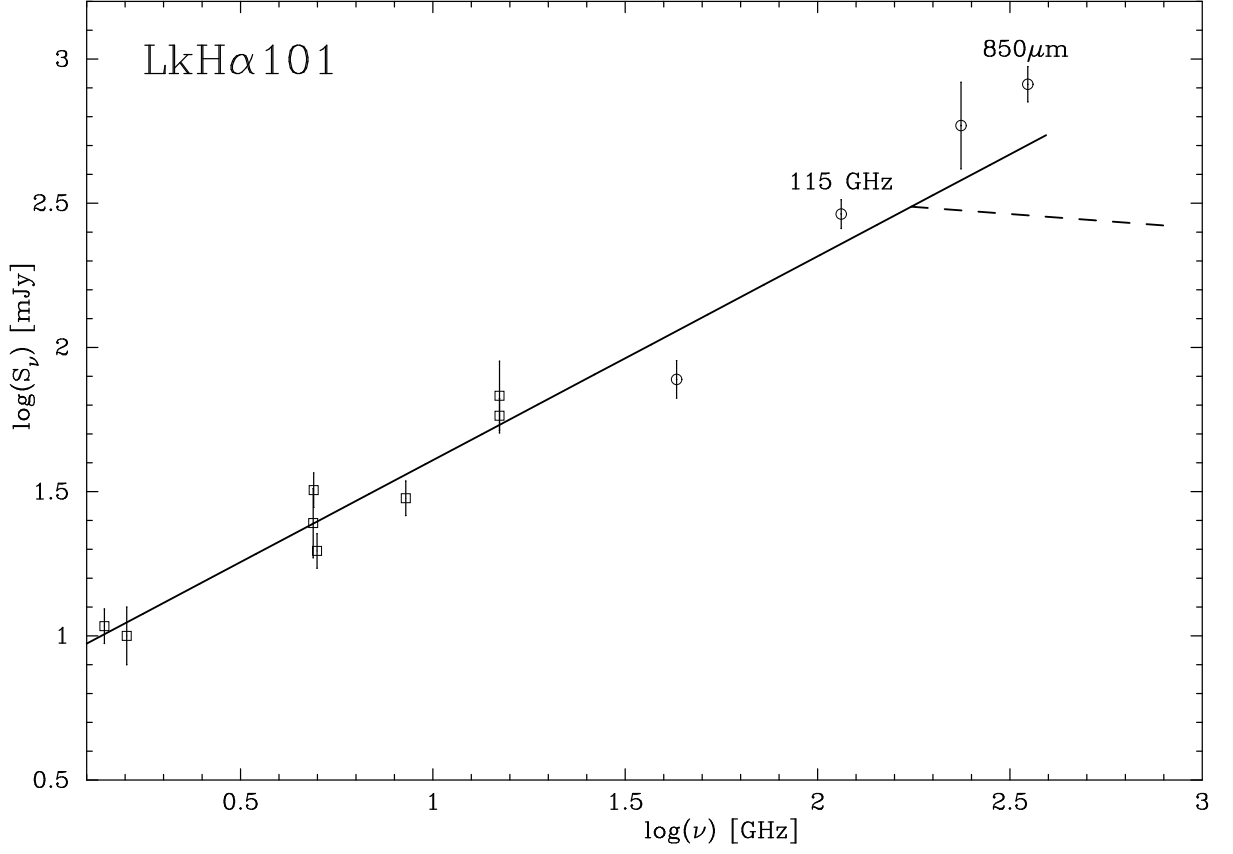


Fig. 12.— Power-law fit to VLA A-array data for LkH α 101 predicting a spectral index, $\alpha = 0.71 \pm 0.07$ for the thermal wind. If we assume that the wind is launched at 10 AU from the star, the wind will become optically thin at ~ 150 GHz.

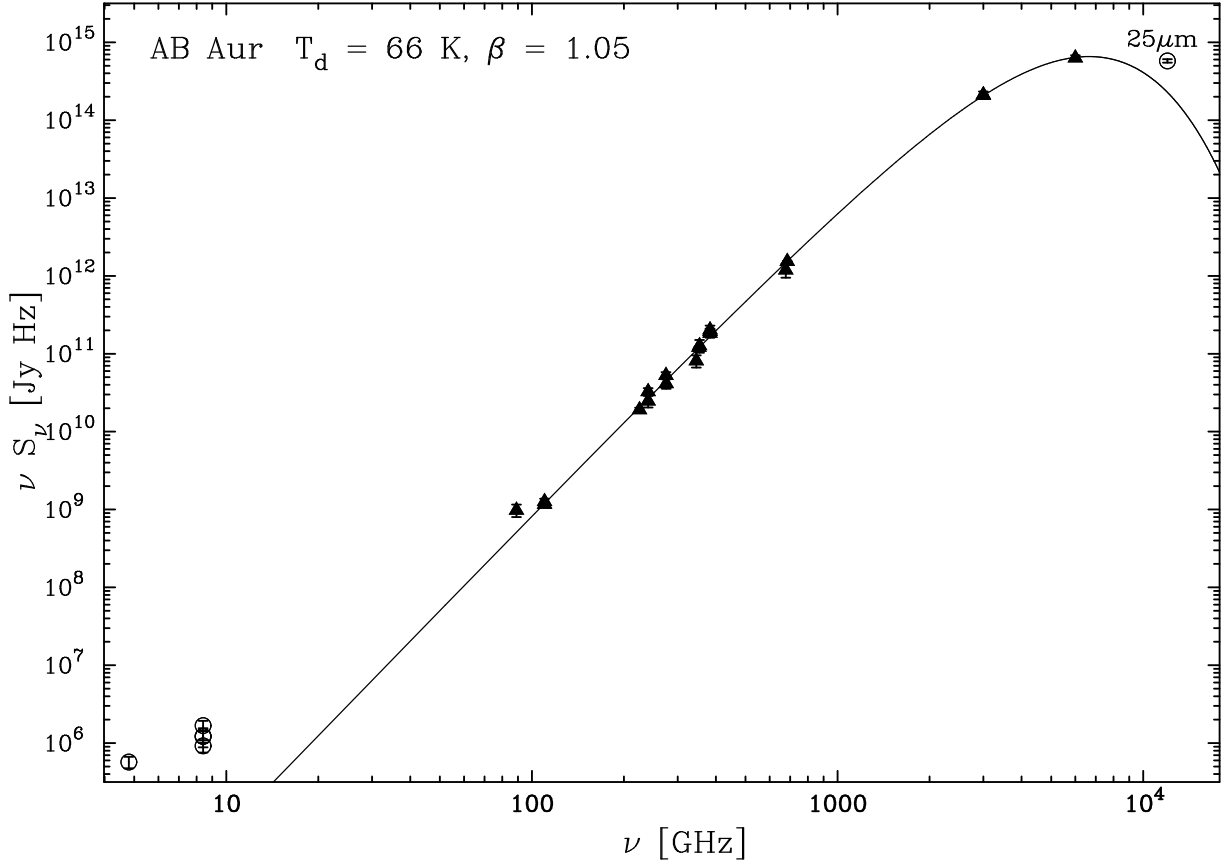


Fig. 13.— Deconvolved sub-millimeter images of AB Aur at 850 and 450 μm plotted in gray-scale and overlaid with contours. The disk is unresolved both at 850 and 450 μm . The peak flux density is 0.349 and 2.2 Jy beam $^{-1}$ for HPBW of 14'' and 8'' for the 850 and 450 μm images, respectively. The contour levels are logarithmic with six contours between the 2σ noise level and peak flux density. The 2σ noise level is 18 mJy beam $^{-1}$ at 850 μm and 110 mJy beam $^{-1}$ at 450 μm . The position of AB Aur is marked by a star symbol. The faint extension to the southwest in the 450 μm image appears to be spurious, because it does not agree in position with the faint extension seen at 850 μm .

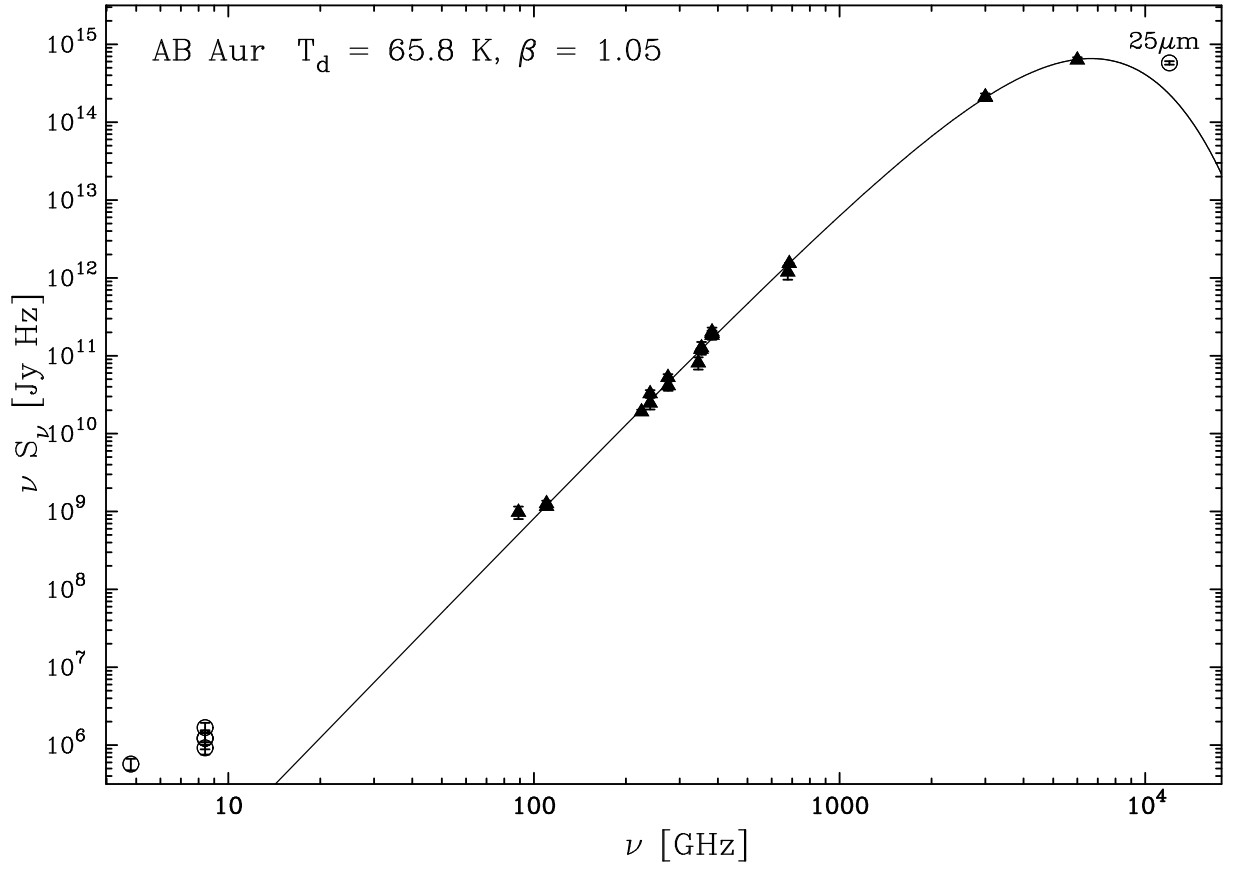


Fig. 14.— An isothermal graybody fit to the SED for AB Aur.

Fig. 15.— CO $J = 2 \rightarrow 1$ spectrum of VY Mon showing high velocity emission from about -28 to $+18$ km s $^{-1}$.

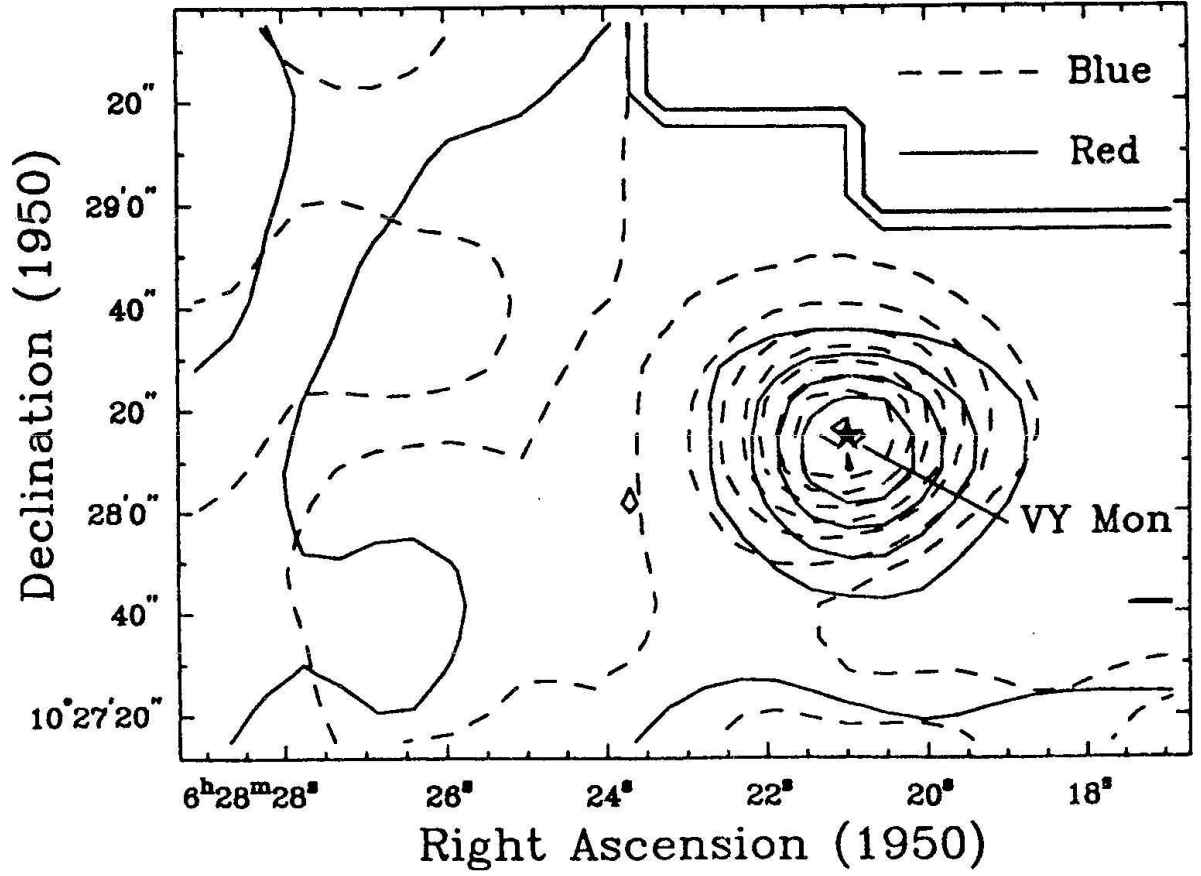


Fig. 16.— Map of CO $J = 2 \rightarrow 1$ high velocity emission around VY Mon. The solid contours show the red-shifted emission integrated over the velocity range -14 to -3 km s^{-1} with the lowest contour at 2 K km s^{-1} and steps of 6 K km s^{-1} . The dashed contours show the blue-shifted emission integrated over the velocity range $+1$ to $+12$ km s^{-1} with the lowest contour at 3 K km s^{-1} and steps of 5 K km s^{-1} . The bipolar outflow appears unresolved and centered on VY Mon, which is marked by a star symbol.

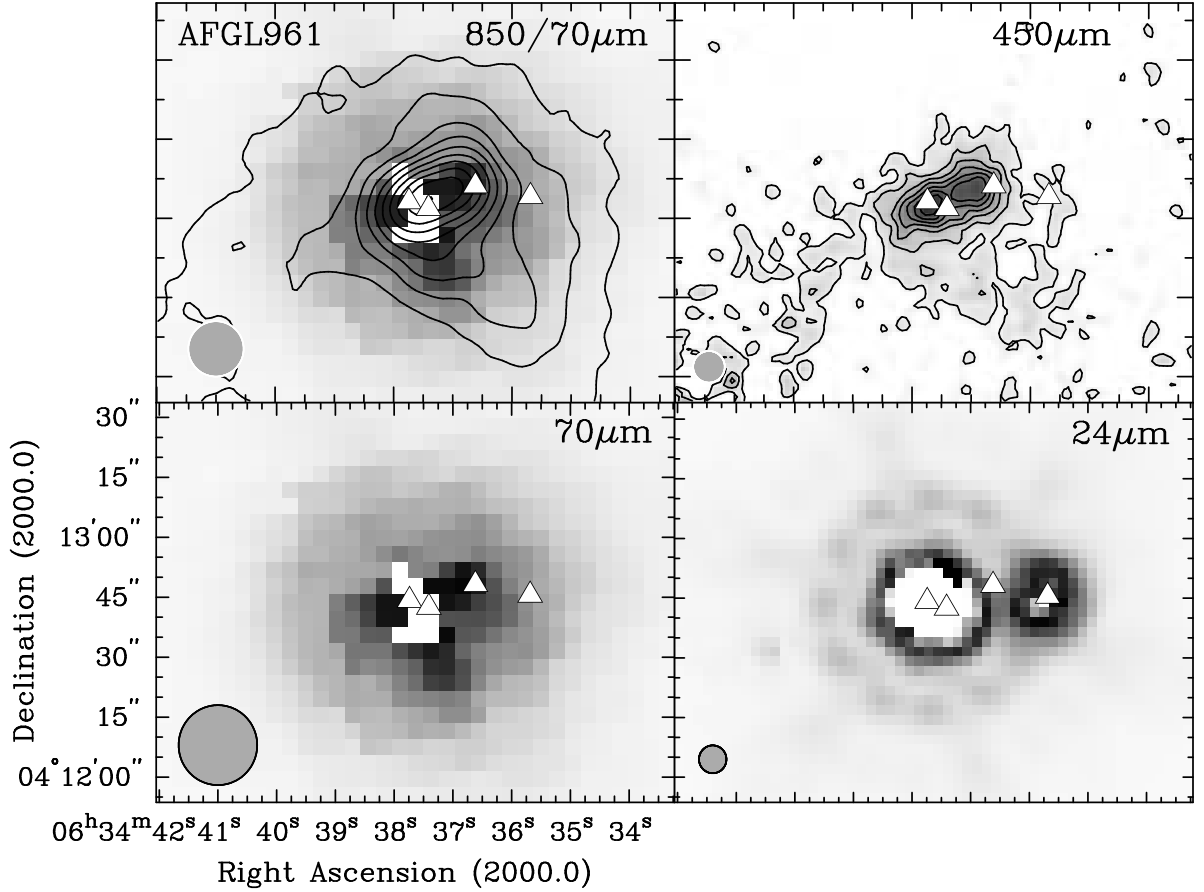


Fig. 17.— **Upper panels:** Contour plots of 850 and 450 μm SCUBA images. The 850 μm image (left) is overlaid on a MIPS 70 μm image in grayscale, also shown below. The triangles in the saturated region are AFGL 961 A (furthest to the left) and AFGL 961 B (second from left). The other two triangles are SMA 3 (second from right) and source C (furthest to the right) from Williams et al. (2009). At 850 μm we plot ten evenly spaced contours from 0.15 Jy beam^{-1} to 2.3 Jy beam^{-1} . At 450 μm we plot eight evenly spaced contours between 1.0 Jy beam^{-1} and 10 Jy beam^{-1} . **Lower panels:** MIPS 70 and 24 μm images in grayscale. Both images are severely saturated (pure white in grayscale). At 24 μm source AFGL 961 C breaks up into a double source. The source immediately to the southeast of C is saturated in the 24 μm MIPS image. The HPBW's are shown in the bottom left corner of each image.

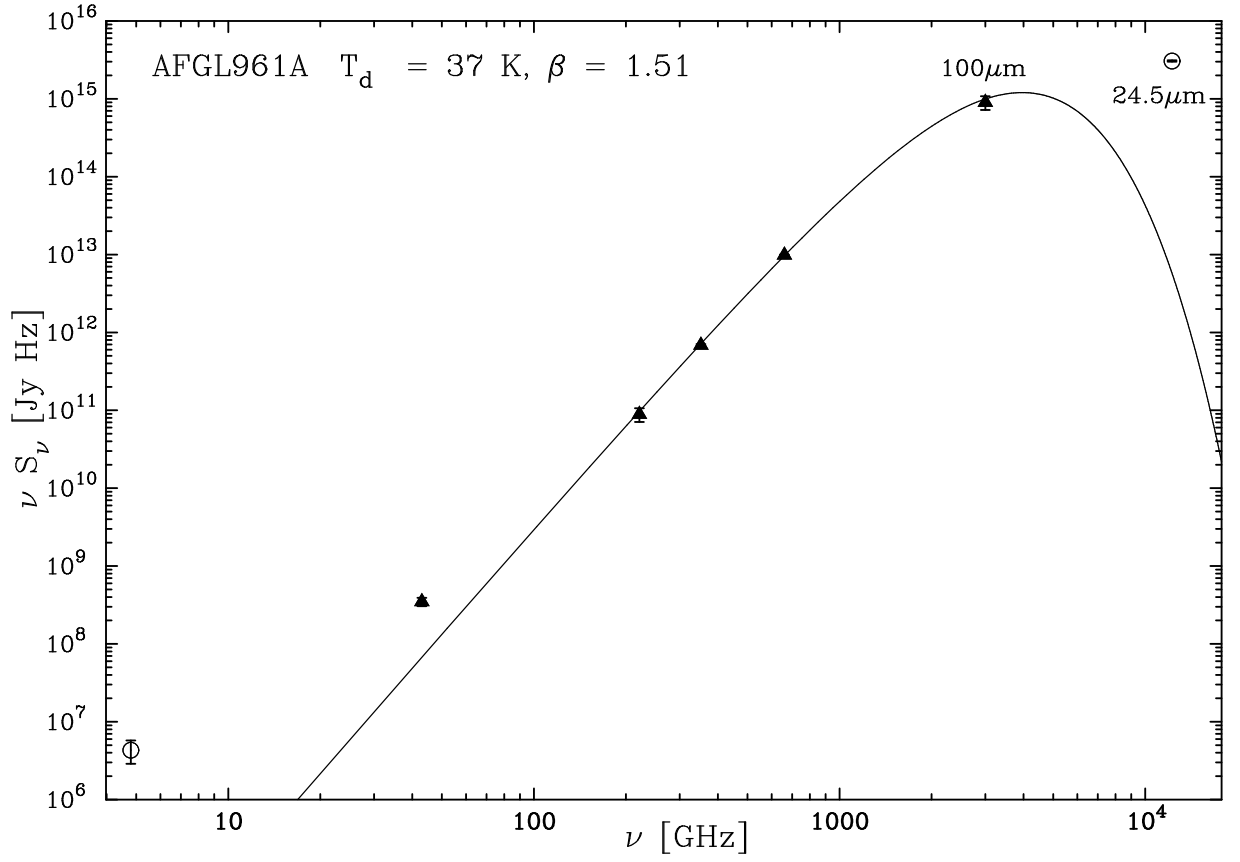


Fig. 18.— Isothermal graybody fit of AFGL 961 A.

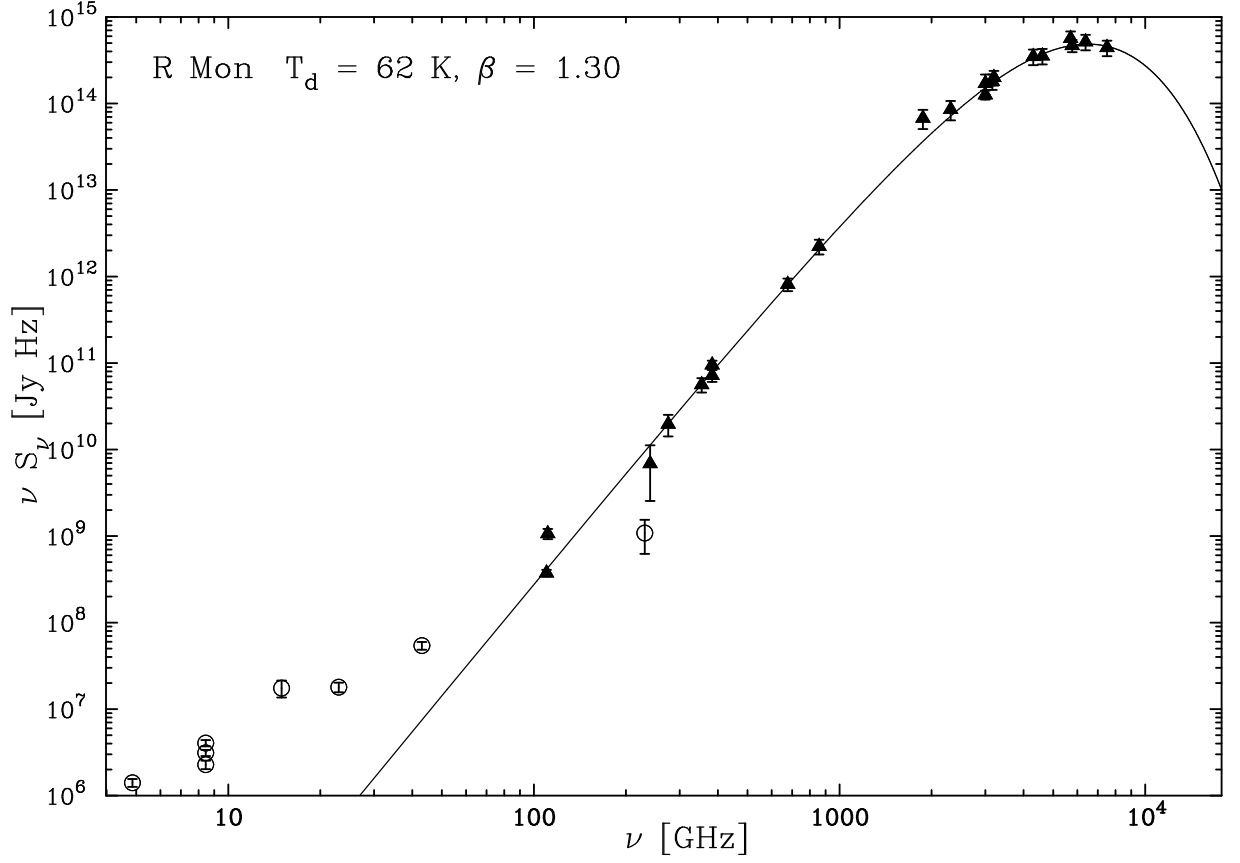


Fig. 19.— Isothermal graybody fit of R Mon to free-free corrected (sub-)millimeter data and KAO far infrared data. The 1.3 mm flux density observed by (Fuente et al. 2006) appears anomalously low and was not used in the fit.

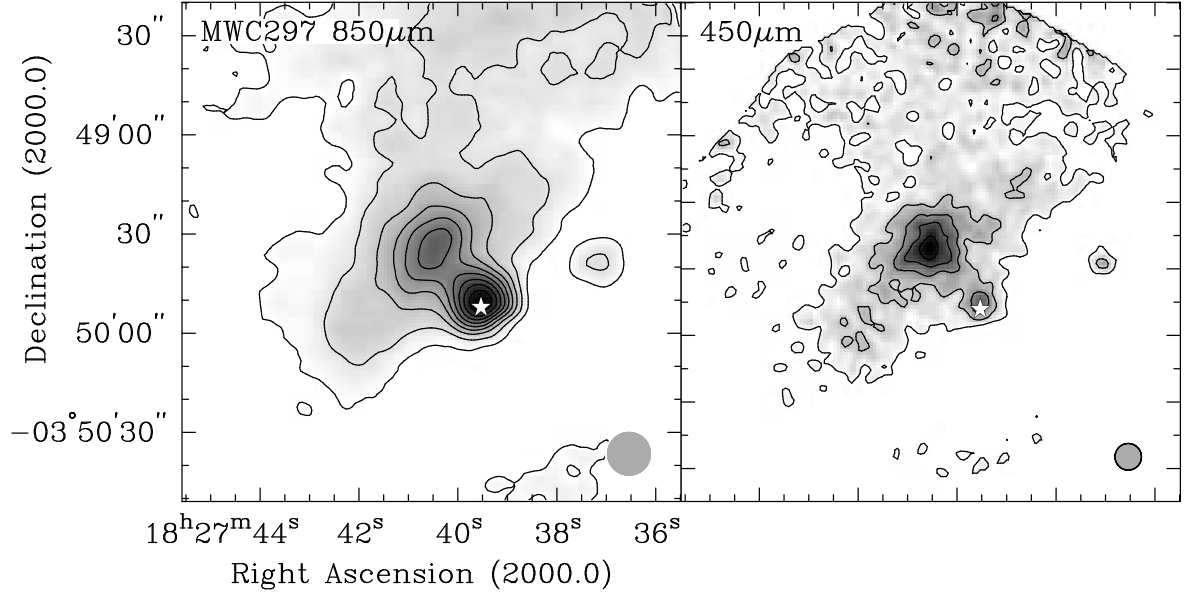


Fig. 20.— SCUBA 850 and 450 μm images in grayscale overlaid with contours of the MWC 297 region. At 850 μm we plot ten evenly spaced contours between 30 mJy beam^{-1} and 611 mJy beam^{-1} , at 450 μm six evenly spaced contours between 0.2 Jy beam^{-1} and 2.0 Jy beam^{-1} . MWC 297 is marked by a star symbol. The HPBW is shown in the bottom right corner of each image.

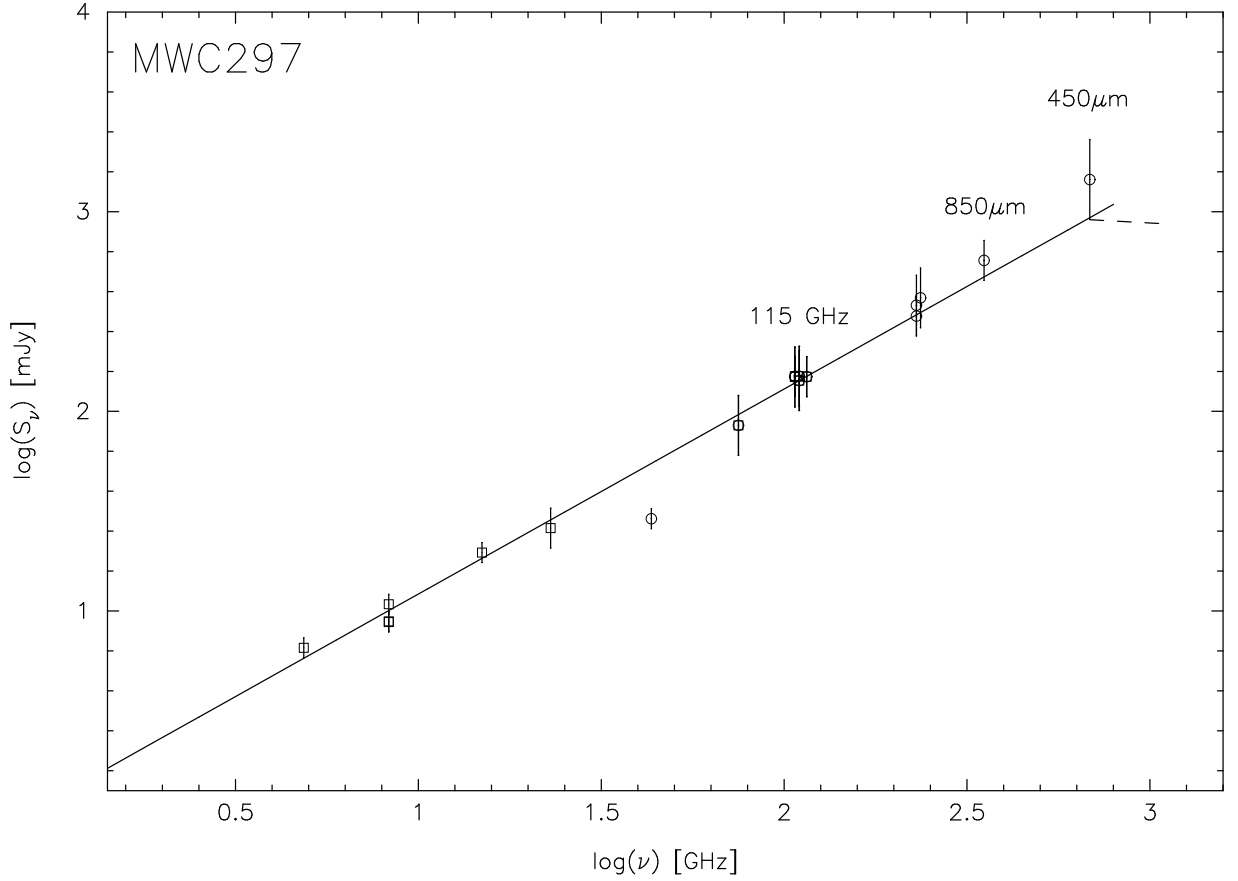


Fig. 21.— Least-squares fit to VLA and BIMA data (open squares) up to 3 mm (see text), predicting a spectral index $\alpha \sim 1$. In this fit we omitted the VLA data point at 43 GHz (Alonso-Albi et al. 2009), which appears anomalously low, suggesting that a significant fraction of the emission at this wavelength has been resolved out by the interferometer. There may be some dust excess at 850 μ m and almost certainly at 450 μ m. The dashed line shows that the free-free emission will flatten out when the whole jet becomes optically thin.

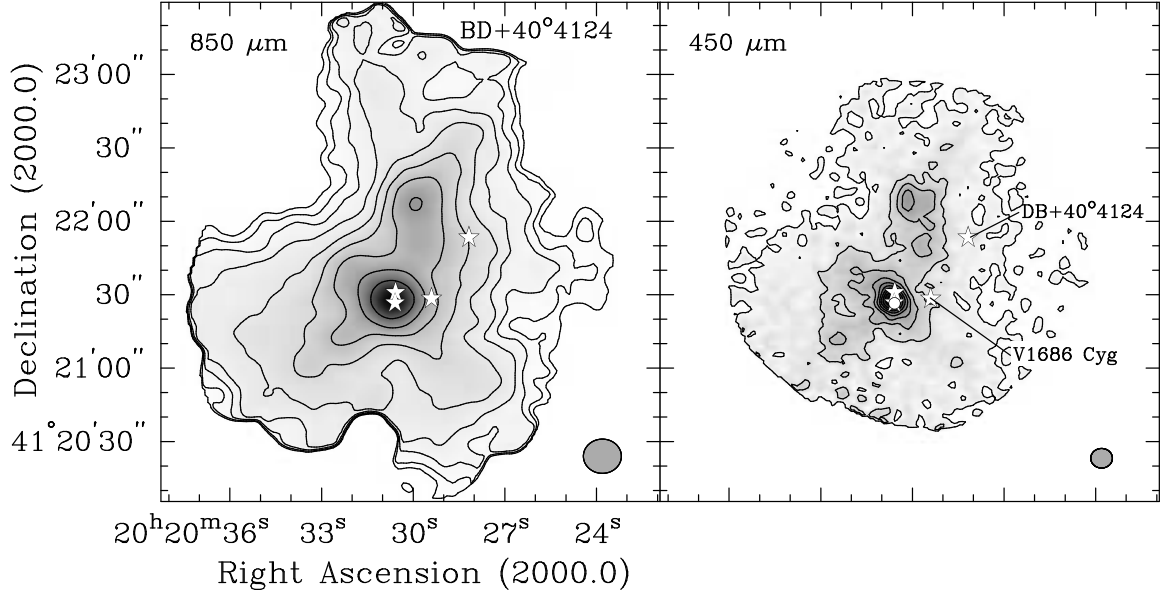


Fig. 22.— SCUBA 850 and 450 μm images of the BD 40°4124 field in grayscale overlaid with contours. The contour levels are evenly spaced with 10 contours from the 3- σ level to the peak flux density. At 850 μm the lowest contour is at 40 mJy beam $^{-1}$ and the highest at 2.45 Jy beam $^{-1}$. At 450 μm the lowest contour is at 300 mJy beam $^{-1}$ with the highest contour at 8.9 Jy beam $^{-1}$. The stars, BD 40°4124, V 1686 Cyg and V 1318 Cyg N and S are marked by star symbols and the first two are labeled on the 450 μm image. V 1318 Cyg N and S coincide with a strong sub-millimeter source, although the emission is likely completely dominated by an invisible Class 0 source situated about one arcsecond northeast of V 1318 Cyg S (see text). The HPBW is shown in the bottom right corner of each image.

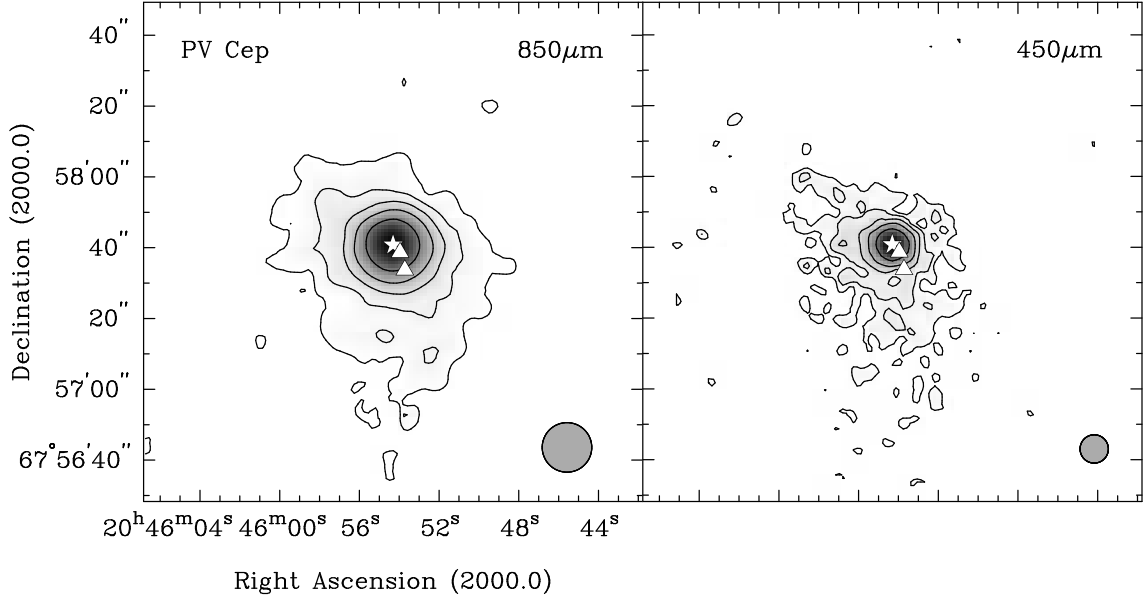


Fig. 23.— SCUBA 850 and 450 μm images of PV Cep in grayscale overlaid with contours. The contours are logarithmic with the lowest contour at the $3\text{-}\sigma$ level and the highest at the peak flux density. At 850 μm the lowest contour is at 50 mJy beam^{-1} with the peak flux density at 1 Jy beam^{-1} . At 450 μm the corresponding values for the contour levels are $300 \text{ mJy beam}^{-1}$ and 5.5 Jy beam^{-1} . PV Cep is marked by a star symbol and H_2O masers with triangles. The circumstellar disk/envelope is well resolved in these SCUBA images with a size of $\sim 3''.6$. We also see faint emission from the surrounding dust cloud in which PV Cep is embedded. The HPBWs are shown in the bottom right corner of each image.

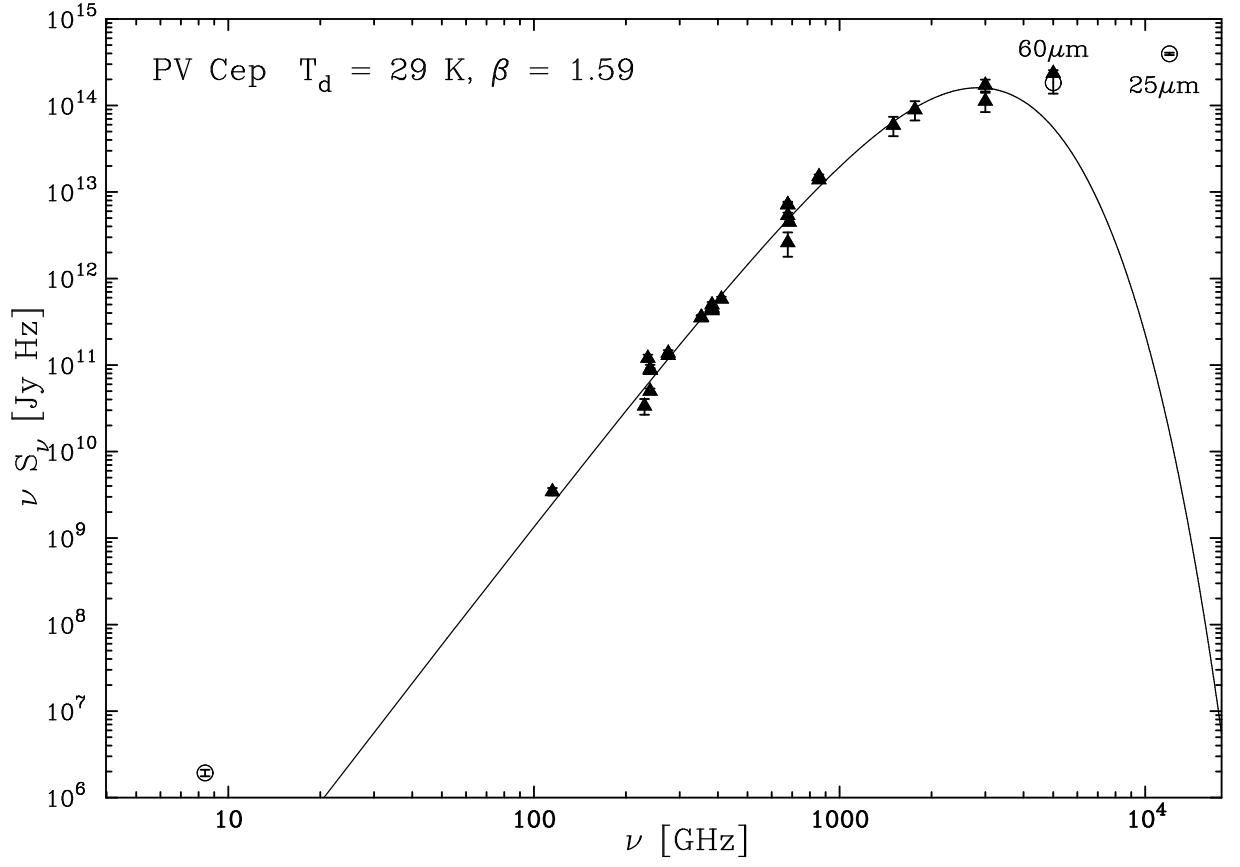


Fig. 24.— An isothermal graybody fit to the SED for PV Cep.

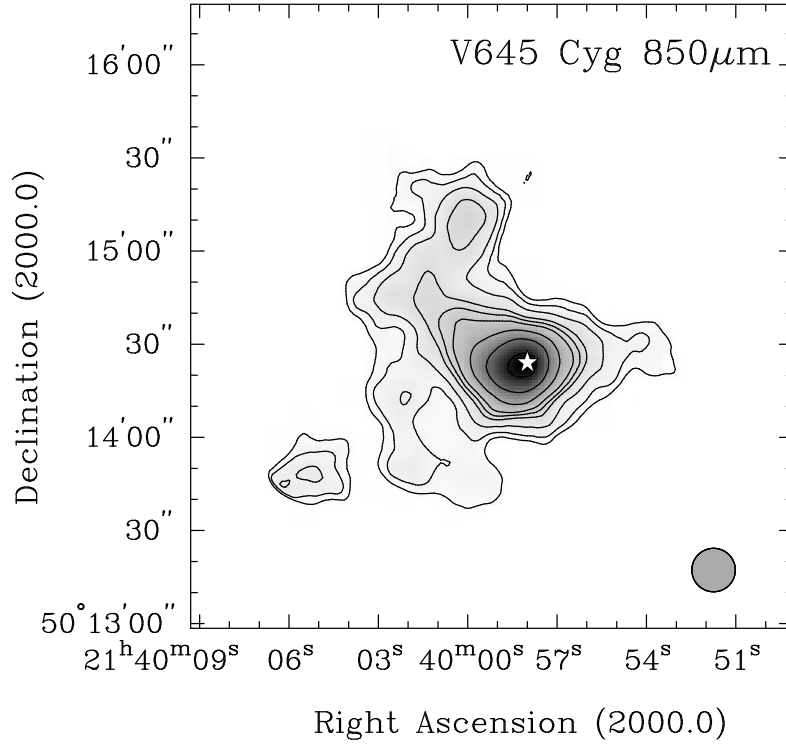


Fig. 25.— SCUBA 850 μm image of V 645 Cyg in grayscale overlaid with contours. The contours are logarithmic with eight contours between 40 mJy beam⁻¹ and 1.78 Jy beam⁻¹. The HPBW is shown in the bottom right corner.

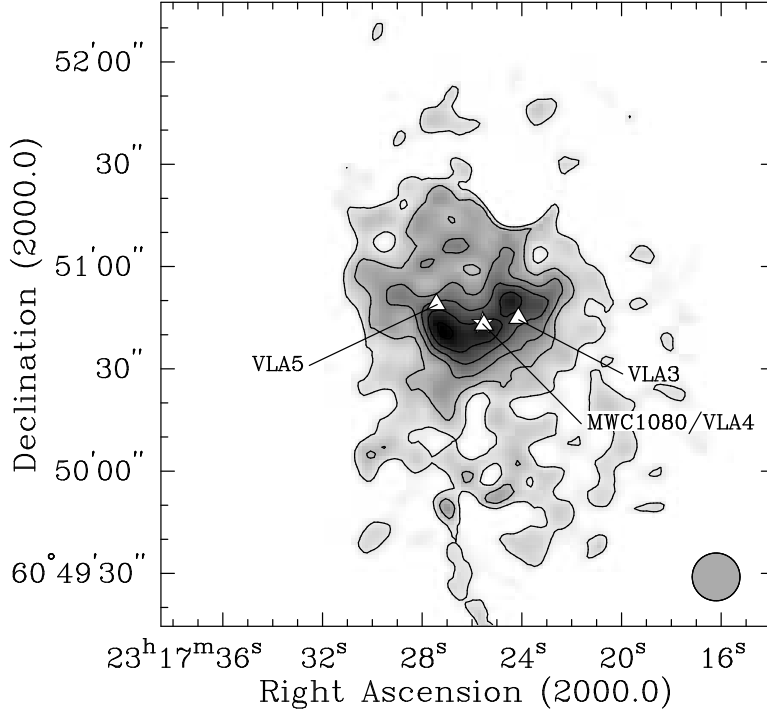


Fig. 26.— SCUBA 850 μm image of the MWC1080 field in grayscale overlaid with contours. The contours are logarithmic with six contours between $150 \text{ mJy beam}^{-1}$ and $700 \text{ mJy beam}^{-1}$. The VLA sources 3, 4 and 5 (Girart et al. 2002) are marked with triangles. VLA 4 coincides with the B0 star MWC1080 A, also marked with a star symbol. The HPBW is shown in the bottom right corner.

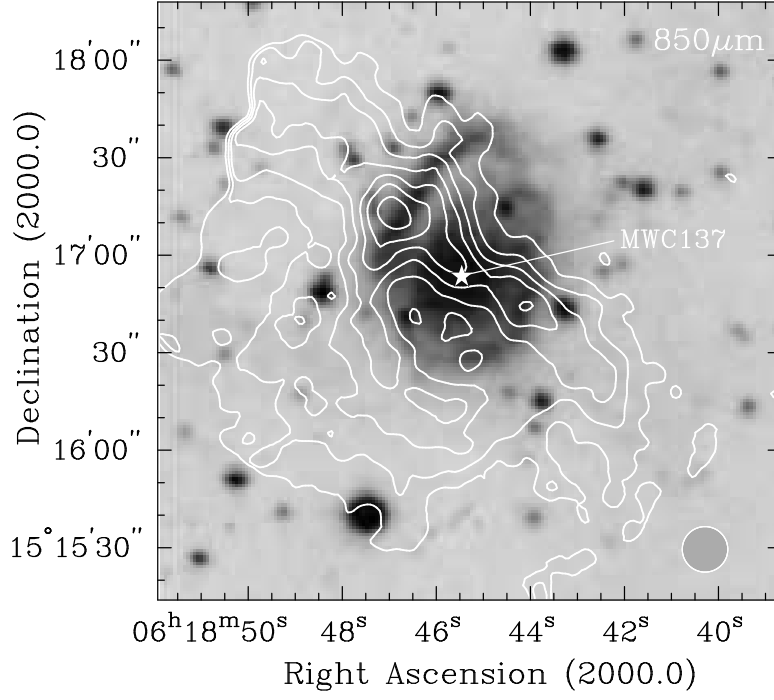


Fig. 27.— An 850 μm contour map of MWC 137 overlaid on an optical image in grayscale. The contour levels are linear starting at 50 mJy beam⁻¹ with a step of 50 mJy beam⁻¹. MWC 137 is marked by a star symbol. The HPBW is shown in the bottom right corner.

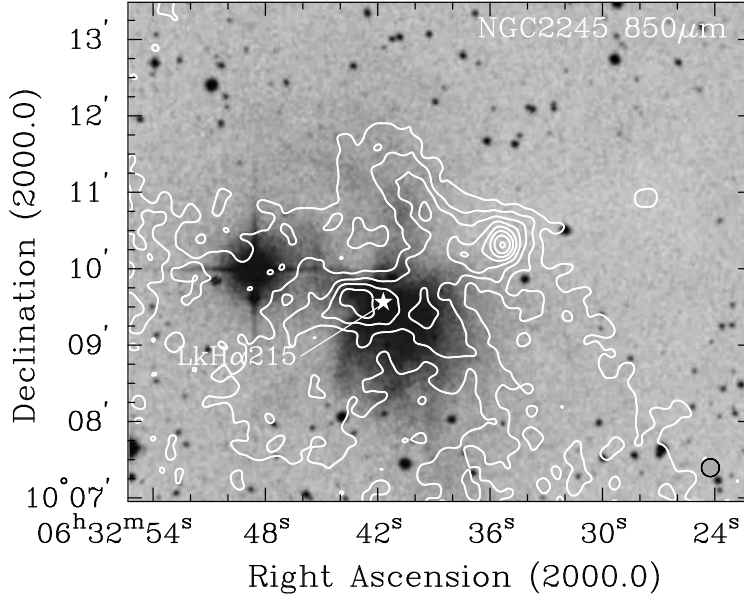


Fig. 28.— An 850 μm contour map of the reflection nebula NGC 2245 overlaid on an optical image in grayscale. The contour levels are linear starting at 60 mJy beam⁻¹ with a step of 60 mJy beam⁻¹. LkH α 215 is not detected at 850 μm . Northwest of the star and outside the reflection nebula there is a compact sub-millimeter source with an 850 μm flux density of 150 mJy, which has neither an optical nor a near-infrared counterpart. The HPBW is shown in the bottom right corner.

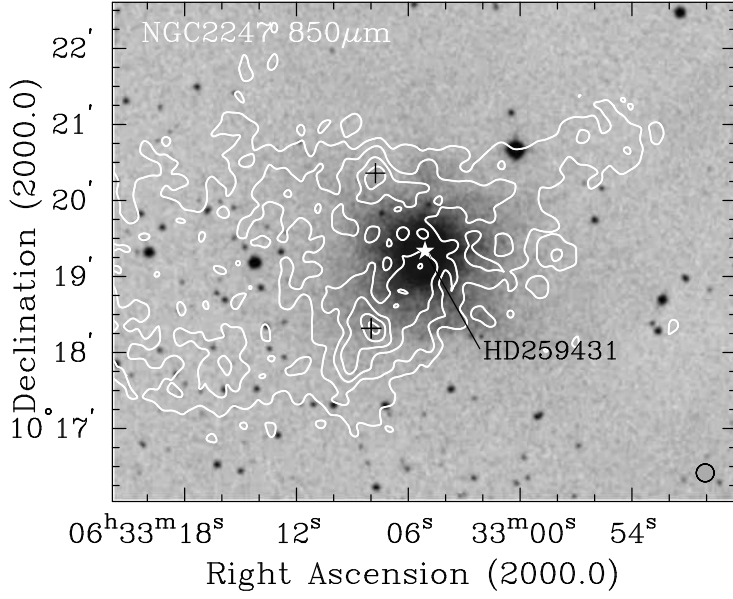


Fig. 29.— An $850 \mu\text{m}$ contour map of the reflection nebula NGC 2247 overlaid on an optical image in grayscale. The contour levels are linear, starting at 50 mJy beam^{-1} with a step of 50 mJy beam^{-1} . The nebula is illuminated by HD 259431, which is close to a minimum in the dust emission. Two faint sub-millimeter sources, marked with black plus signs, are seen outside the nebula. The HPBW is shown in the bottom right corner.

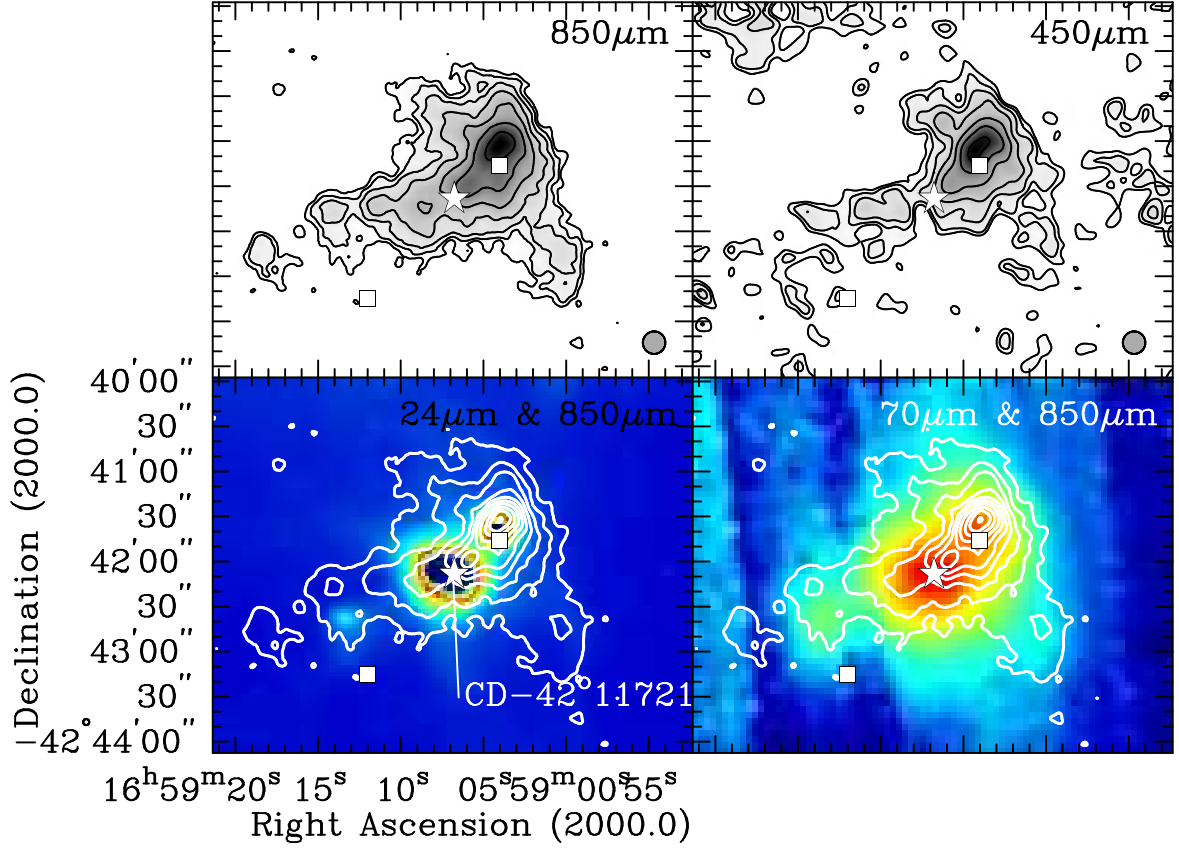


Fig. 30.— **Upper panels:** 850 and 450 μm SCUBA maps of the CD-42° 1172 field. The position of CD-42° 1172 is marked by a star symbol, and the two 13 cm radio sources (Thompson, Ugruhart & White 2004) are marked by filled squares. The contour levels are logarithmic. At 850 μm there are seven contour levels between 0.1 Jy beam $^{-1}$ and 1.58 Jy beam $^{-1}$, at 450 μm they go from 1 Jy beam $^{-1}$ to 15.8 Jy beam $^{-1}$. The SCUBA HPBW's are shown in the bottom right corner of each panel. **Lower panels:** False color images of 24 and 70 μm MIPS images overlaid with the same 850 μm contours as shown in the left upper panel. Note that the 24 μm image is saturated on CD-42° 1172 and the nebula surrounding it. The source to the northwest of the star is also saturated.

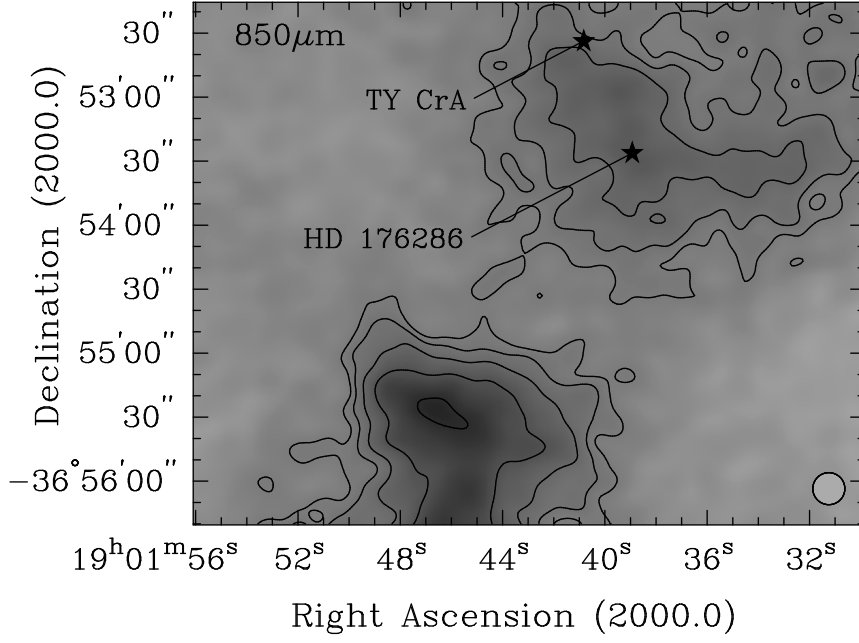


Fig. 31.— Sub-image of large SCUBA 850 μm scan map showing HD 176386 and TY CrA. Although both stars are definitely embedded in a dense dust cloud, neither of them are associated with any sub-millimeter continuum emission. The HPBW is shown in the bottom right corner.

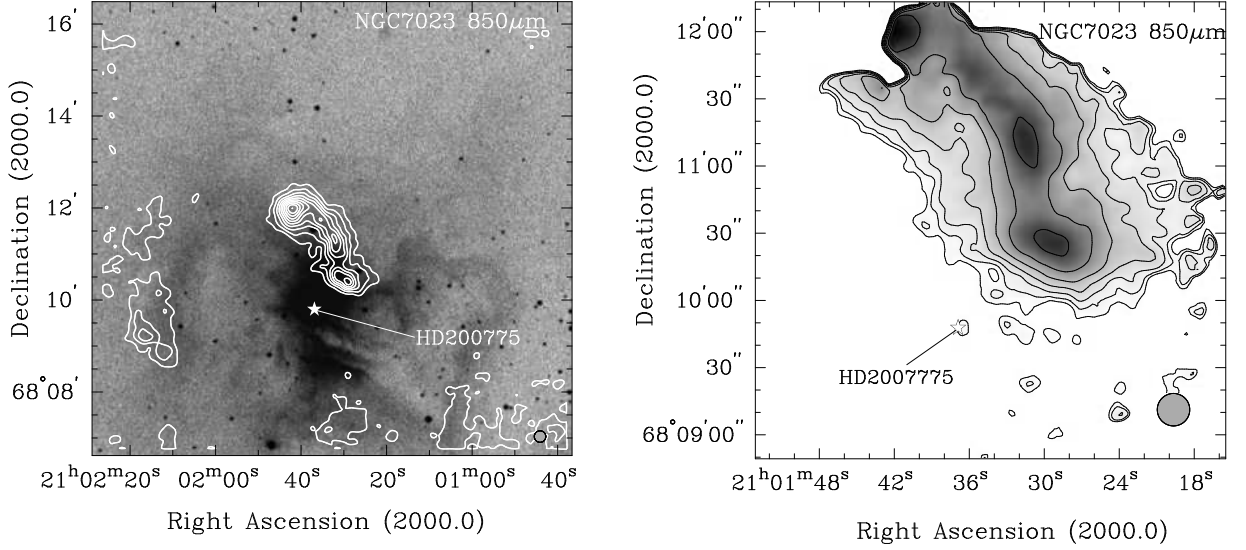


Fig. 32.— **Left panel:** Large 850 μm scan map of the reflection nebula NGC 7023 plotted with contours and overlaid on an optical image in gray scale. We applied a logarithmic stretch to the optical image to enhance the faint nebulosity. The contour levels are linear, starting at 40 mJy beam $^{-1}$ with ten contours up to the peak flux density of 712 mJy beam $^{-1}$. The HPBW is shown in the bottom right corner. **Right panel:** A much deeper 850 μm jiggle map with a 3- σ rms of 25 mJy beam $^{-1}$. The lowest contour in this map is at 25 mJy beam $^{-1}$. The rest of the contours are plotted logarithmically to the peak flux density, 530 mJy beam $^{-1}$. Even though HD 200775 falls inside a 3- σ contour, we consider it a non-detection, because it is not distinguishable from other noise features in the map. However, our observations are consistent with Okamoto et al. (2009), who detected HD 200775 with the SMA at 350 GHz (856 μm) with a flux density of 35 ± 5 mJy. The SCUBA HPBW is shown in the bottom right corner of the image.

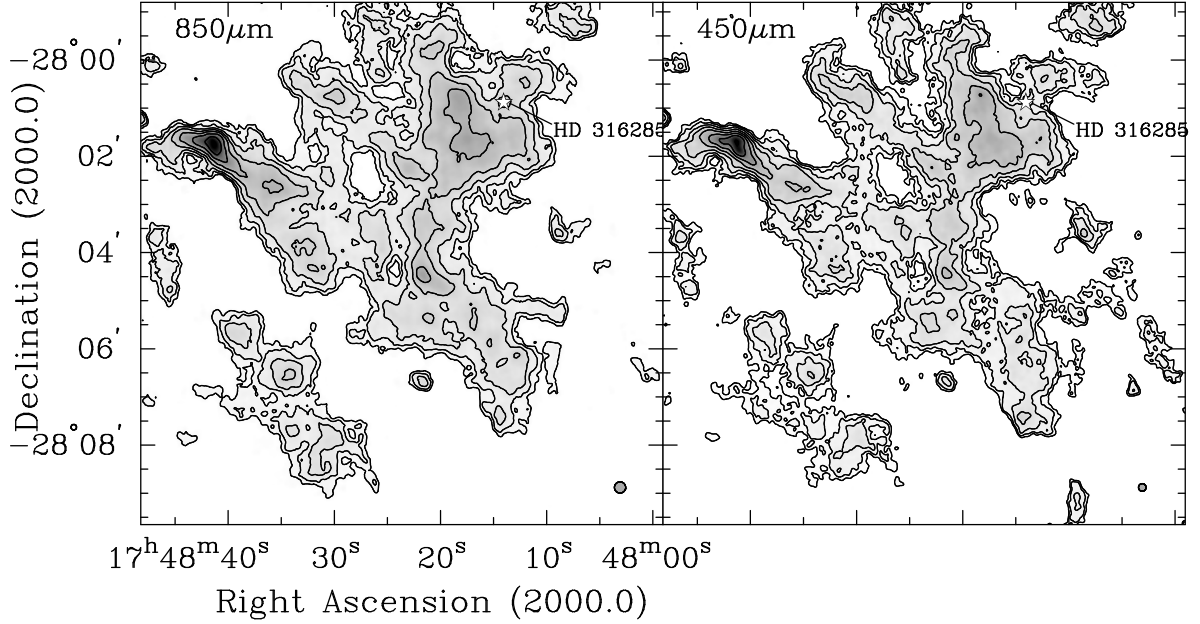


Fig. 33.— Large SCUBA scan maps at 850 and 450 μm in the direction of HD 316285. There is a faint peak at the position of the star at 850 μm (hidden by the star symbol), but not at 450 μm . The contours are logarithmic for both images. For the 850 μm image, we plot seven contour levels between the lowest contour, 200 mJy beam^{-1} , and the peak flux density, 3.16 Jy beam^{-1} . For 450 μm we plot eight contours between 1 Jy beam^{-1} and 25.1 Jy beam^{-1} . The HPBW is shown in the bottom right corner of each image.

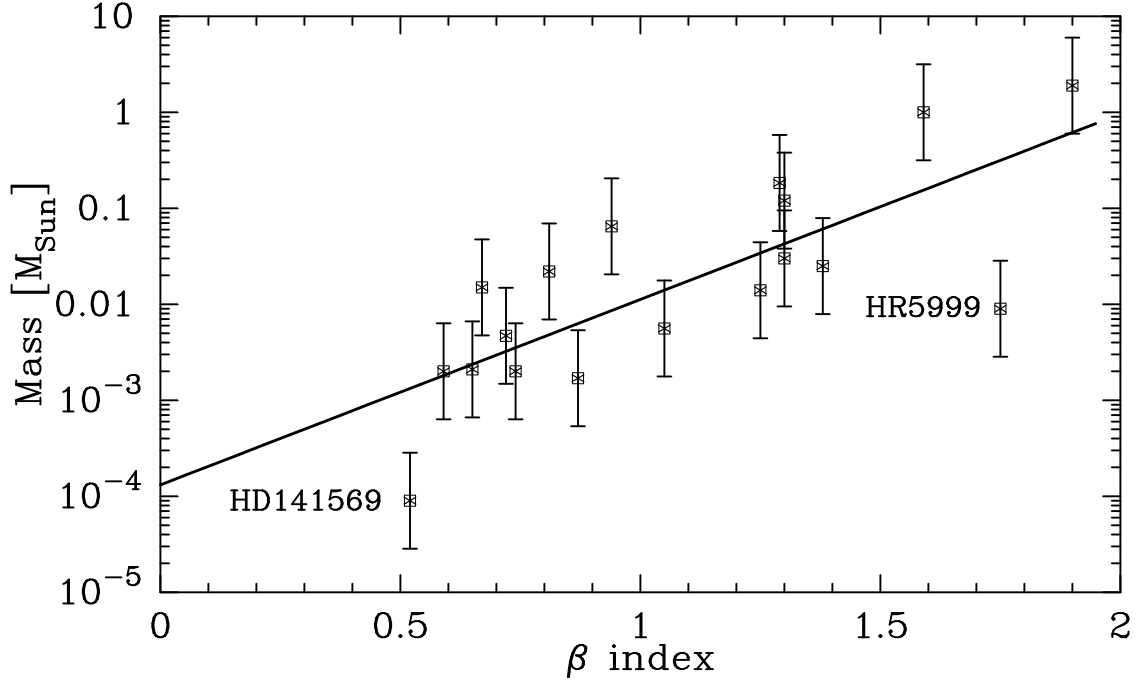


Fig. 34.— Disk mass as a function of dust emissivity, β . The error bars show a worst case uncertainty of a factor of two for disk mass. The errors for β are of the order of 0.1 – 0.2. The two extreme outliers, HD 141569 and HR 5999 are labeled in the Figure.